NASA/TM–2018-219829

A Summary of Results from Two Full-Scale Fokker F28 Fuselage Section Drop Tests

Justin D. Littell
Langley Research Center, Hampton, Virginia

May 2018

NASA STI Program . . . in Profile

Since its founding, NASA has been dedicated to the advancement of aeronautics and space science. The NASA scientific and technical information (STI) program plays a key part in helping NASA maintain this important role.

The NASA STI program operates under the auspices of the Agency Chief Information Officer. It collects, organizes, provides for archiving, and disseminates NASA's STI. The NASA STI program provides access to the NTRS Registered and its public interface, the NASA Technical Reports Server, thus providing one of the largest collections of aeronautical and space science STI in the world. Results are published in both non-NASA channels and by NASA in the NASA STI Report Series, which includes the following report types:

- TECHNICAL PUBLICATION. Reports of completed research or a major significant phase of research that present the results of NASA Programs and include extensive data or theoretical analysis. Includes compilations of significant scientific and technical data and information deemed to be of continuing reference value. NASA counter-part of peer-reviewed formal professional papers but has less stringent limitations on manuscript length and extent of graphic presentations.

- TECHNICAL MEMORANDUM. Scientific and technical findings that are preliminary or of specialized interest, e.g., quick release reports, working papers, and bibliographies that contain minimal annotation. Does not contain extensive analysis.

- CONTRACTOR REPORT. Scientific and technical findings by NASA-sponsored contractors and grantees.

- CONFERENCE PUBLICATION. Collected papers from scientific and technical conferences, symposia, seminars, or other meetings sponsored or co-sponsored by NASA.

- SPECIAL PUBLICATION. Scientific, technical, or historical information from NASA programs, projects, and missions, often concerned with subjects having substantial public interest.

- TECHNICAL TRANSLATION. English-language translations of foreign scientific and technical material pertinent to NASA's mission.

Specialized services also include organizing and publishing research results, distributing specialized research announcements and feeds, providing information desk and personal search support, and enabling data exchange services.

For more information about the NASA STI program, see the following:

- Access the NASA STI program home page at http://www.sti.nasa.gov

- E-mail your question to help@sti.nasa.gov

- Phone the NASA STI Information Desk at 757-864-9658

- Write to:
  NASA STI Information Desk
  Mail Stop 148
  NASA Langley Research Center
  Hampton, VA 23681-2199

NASA/TM–2018-219829

A Summary of Results from Two Full-Scale Fokker F28 Fuselage Section Drop Tests

Justin D. Littell
Langley Research Center, Hampton, Virginia

National Aeronautics and
Space Administration

Langley Research Center
Hampton, Virginia 23681-2199

May 2018

Available from:

NASA STI Program / Mail Stop 148
NASA Langley Research Center
Hampton, VA 23681-2199
Fax: 757-864-6500

Table of Contents

Table of Figures

Abstract

During 2017, two vertical drop tests were conducted on two partial sections removed from a Fokker F28 MK4000 aircraft as a part of a joint NASA / Federal Aviation Administration (FAA) effort to investigate the crashworthiness characteristics of Transport Category Aircraft, as defined by 14 Code of Federal Regulations, Part 25. The first test was a pure vertical drop test of a relatively uniform forward section, which included an underfloor area for luggage. The second test was a canted drop test onto a sloped surface of a portion of the fuselage representing the wingbox stiffened structure. In both tests, accelerometers were installed on the floor, seat track, luggage, and overhead bin to measure responses in the two airframe sections. In addition, ten Anthropomorphic Test Devices (ATDs, a.k.a. crash test dummies) were included in each test to measure the potential of onboard occupant injury. Self-contained data recorders, logging accelerations and rotational rates, were also used on the seat tracks and lower structure for evaluation as potential crash recording devices in future tests. Finally, the starboard side of each section was painted with a stochastic black and white speckle pattern for use in full field photogrammetric imaging techniques.

The results collected show notable differences in the Forward and Wingbox Section responses. The Forward Section floor accelerations showed a relatively uniform response of approximately 7 g throughout the impact event. This section exhibited large amounts of subfloor crushing, floor stiffener failures and seat deformation upon impact. These results are contrasted by the Wingbox Section accelerations, which showed large differences when comparing accelerations recorded from either the rear or the front portion of the section reaching peaks of 39 g in some locations. Additionally, the Wingbox Section test induced a forward motion caused from the rotation at impact. With the exception of the lower cavity, there was minimal deformation in the Wingbox Section, and ATD responses were consistently higher than those for the Forward Section.

A complete set of results are presented for the airframe, seat, ATD, overhead bin, and subfloor regions for each section. The ATD results are compared to current injury criteria, and determinations will be made on the likelihood of injury. Additional results for cargo-hold stored luggage are presented in an attempt to provide a component-level characterization for better understanding of under-floor loading. Finally, a discussion of the relevance of the results for a proposed airframe level crashworthiness guideline are presented.

Introduction

Through a collaborative agreement with the Federal Aviation Administration (FAA) and NASA Langley Research Center (LaRC), a research effort was undertaken to obtain data through a series of drop tests to support the development of airframe level crash requirements for transport category airplanes [1]. This research was conducted on two Fokker F28 MK4000 fuselage sections in 2017. The Fokker F28 MK4000 is a high performance twin-turbo fan narrow-body aircraft with seating in a triple configuration on the starboard side and a double configuration on the port side, capable of carrying up to 85 passengers on medium range routes. The original F28 aircraft was type certified by the FAA in 1969 with major operations in the US occurring up through the 1990s. The majority of the F28 fleet has been retired from service, with only a handful of still airworthy aircraft operated by African commercial carriers. NASA LaRC acquired a full F28 aircraft, along with 3 additional partial fuselage section test articles in the early 2000s timeframe.

Drop test of partial fuselage sections (commonly called "barrel drops" or "barrel section drops") have occurred for a variety of aircraft throughout the past 30 years. A set of drop tests were conducted in the 1980s by NASA LaRC for the preliminary acquisition of occupant, structural and seat loadings from Boeing 707 fuselage sections [2-4] in preparation for a full scale crash test, known as the Controlled Impact Demonstration (CID), which occurred in 1984 [5]. More recently, a series of barrel section drops for both Boeing 737 and Boeing 707 fuselages were conducted by the FAA. A subset of these were used to evaluate airframe interaction with auxiliary fuel tanks [6], but these tests also collected airframe, seat and occupant loads for the evaluation of various injury metrics [7]. The FAA used this information as a precursor for a series of vertical drop tests of full aircraft including an ATR42-300 [8], Metro III [9], Beechcraft 1900C [10], and a Shorts 3-30 [11]. All of these drop tests were conducted to investigate the structural response of the aircraft and occupant injury under severe but survivable conditions.

Test Setup

There were two untested barrel sections located at LaRC. Their positions as removed from the full F28 aircraft are highlighted in the schematic in Figure 1. The first section was a Forward Section, which consisted of 5 windows and 6 frames between Fuselage Stations (FS) 5305 and 7805. (For the Fokker 28 aircraft, these FS numbers were designated in units of centimeters). In this section, all of the interior paneling, overhead bins, floor and windows were removed. There was a functional cargo door on the starboard side of the section, but otherwise the section had a uniform cross section. The second section was a Wingbox Section, which consisted of 5 windows, 6 frames and two emergency exit doors between FS 9805 and 12405. As with the Forward Section, the interior paneling, overhead bins, floor and windows were removed. The emergency exits were functional prior to being used for testing. The wings were disconnected from the wingbox attachment points on either side.

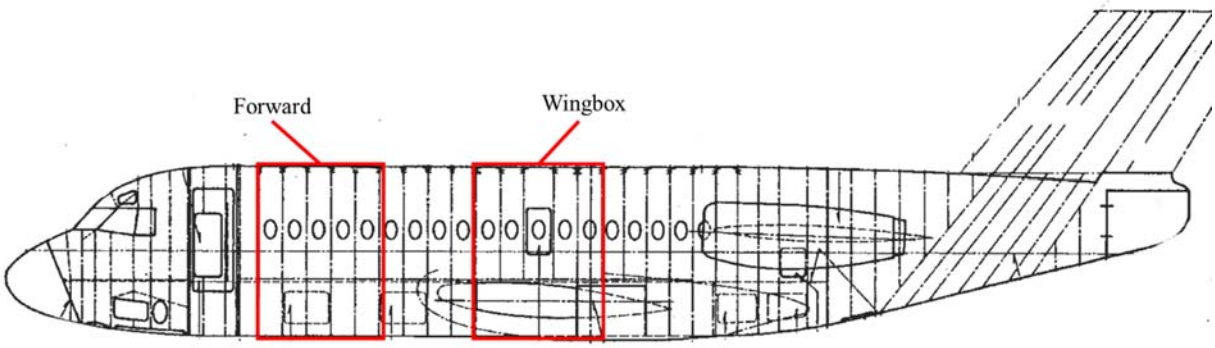

Figure 1 - Schematic of F28 section locations

Each section was approximately 9 ft in length and approximately 9 ft wide when measured at the floor level. The sections were of a semi-monocoque design, with skin-stringer-stiffener frame construction. Frame sections were spaced approximately 20 inches apart throughout each section, and the Forward Section floor was stiffened with lower stanchions. The Wingbox Section floor structure was supported by the wingbox itself. All electronic wiring was removed, and all fluids were drained. In the Wingbox Section, the existing mechanical linkages were cut at the ends of the section, but the mechanical components already present in the structure remained for the test. The underfloor wing truss structure was left unmodified. The unmodified sections are shown in Figure 2.


Figure 2 - Unmodified F28 test article sections. Forward (left), and Wingbox (right)

All tests were conducted at NASA LaRC's Landing and Impact Research Facility (LandIR), shown in Figure 3. LandIR is a 240-ft high, 400-ft long steel A-frame gantry structure built in 1965, and used to conduct full-scale crash testing, both under combined horizontal and vertical loading [12-13] or under purely vertical loading only [14] through a series of overhead cabling and release mechanisms.

Figure 3 - Landing and Impact Research Facility (LandIR)

In order to populate a fully instrumented test article from the unmodified sections, floor panels, seats, ATDs, overhead mass, and underfloor luggage were all installed into the sections. The original floor panels, which were in storage, were reused in testing. The floor panels were a sandwich composite structure, fabricated from either a fiberglass face sheet with Nomex® core, or aluminum face sheet with balsa wood core. Each floor panel was fit for a specific location on the floor, so the two types of floor designs were used at their correct positions during installation, with care taken to identify where each type of material was installed at which position. It is not clear why two different types of floor panel materials were used interchangeably in various locations. Each floor panel was fastened to the seat track flanges through a series of quarter turn fasteners along their edges.

Two rows of seats were installed in a triple-double configuration, with the triple seats installed on the starboard side of the section and the double seats installed on the port side. These seats were Code of Federal Regulations (CFR) § 25.562 [15] certified and were removed from an in-service Boeing 737 aircraft. However, all seats were of a triple configuration and needed modification in order to be used in testing. Figure 4 shows a schematic taken from the Fokker F28 Weight and Balance Manual [16] of the F28 seat configuration.

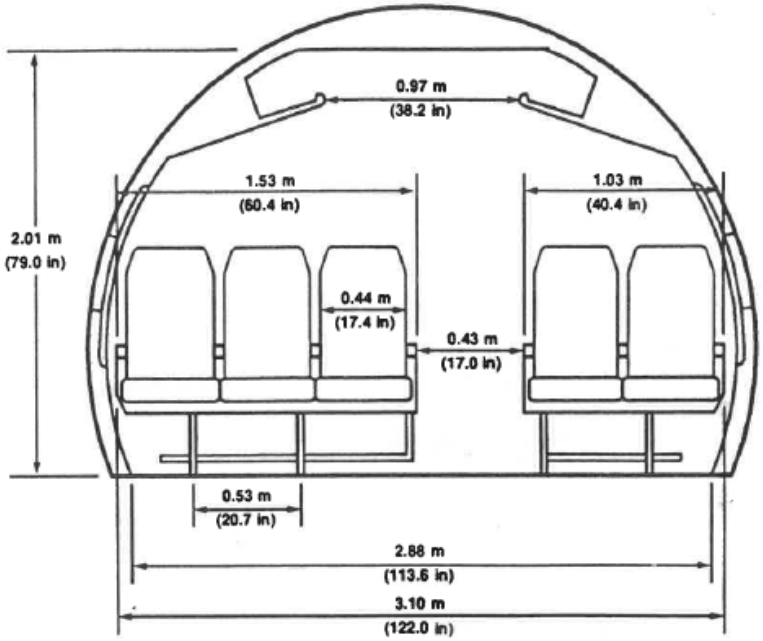

Figure 4 - Original F28 seating configuration from the F28 Weight and Balance Manual

Care was taken to adhere to the original F28 configuration as much as possible. The seat legs were reconfigured to interface with the seat track dimensions for the F28. For the triple seats located on the starboard side of the fuselage, this involved moving both of the seat legs outward to interface with the starboard side seat track spacing. For the double seats, the process involved removing the original window seat, and then re-spacing the seat legs inward to interface with the F28 port side seat track spacing. The original window seat was not used in testing, and the old middle seat became the window seat. For the remainder of this report, the old middle / new window seat will simply be referred to as the port side window seat. Figure 5 shows an illustration of the modifications made on both the starboard side triple seat and the port side double seat. Note that the aisle seat in the triple configuration was overhung up to 25 in after the modifications have been complete.

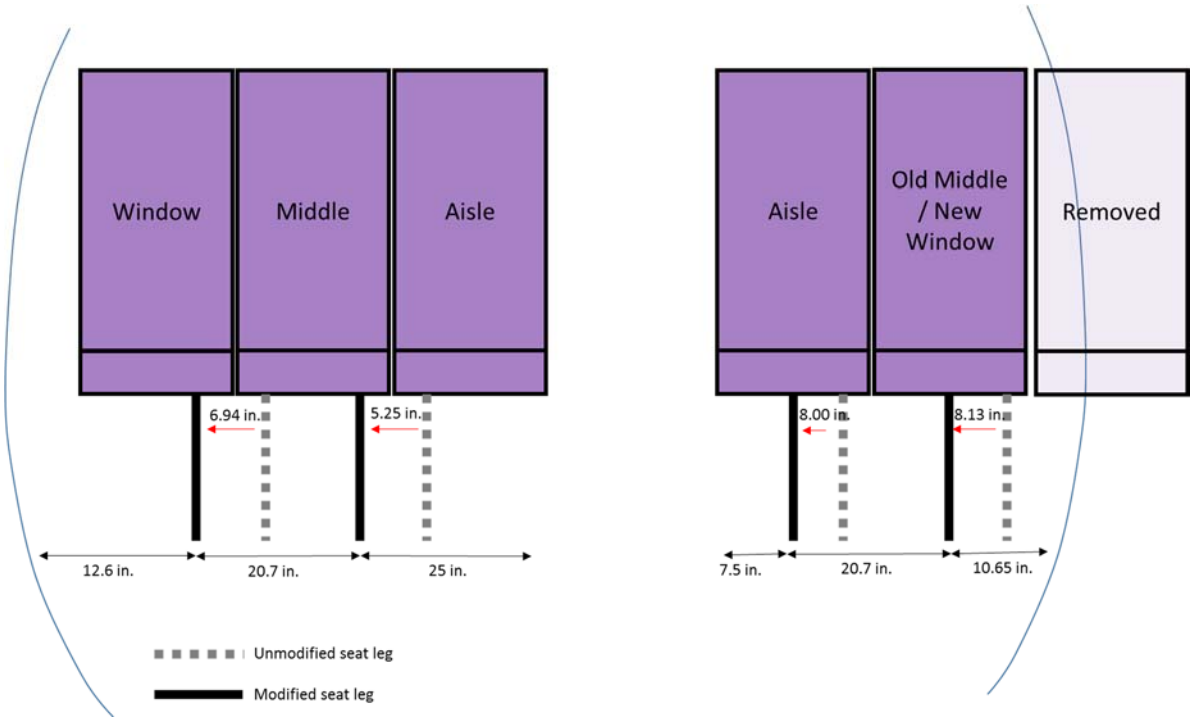

Figure 5 - Seat modification illustration

Figure 6 shows the unmodified and modified triple seat configuration, noting that the window seat is on the left side and the aisle seat is on the right side in both of the views. The modification and layout of the double seat is shown in Figure 7. The existing lap belts present in the seats were used to restrain all of the ATDs and were unmodified.

Figure 6 - Triple seat configuration for starboard side. Unmodified (left) and modified (right)

Figure 7 - Double seat configuration for port side. Unmodified triple (left) cut and modified into a double (right)

Underfloor luggage was included in the Forward Section test to accurately simulate a fully loaded fuselage condition. Packed luggage was acquired from the FAA, and the contents consisted of clothing, shoes, toiletries, and other expected items typically placed in packed luggage. Bags were loosely placed and stacked up to the required loading limit in the subfloor luggage compartment between the stanchions. This configuration approximated a packing sequence of three bags wide, four bags deep and three bags stacked high. The intention was to have some realistic nonuniformity in the luggage configuration due to the construction, size, and contents of the individual bags, as this would accurately replicate a real aircraft containing underfloor luggage. The compartment was held by a safety net on each end. The total weight of luggage included in the subfloor compartment was 922 lb. Figure 8 shows a close-up of the Forward Section luggage compartment. After the test, the luggage was discarded.

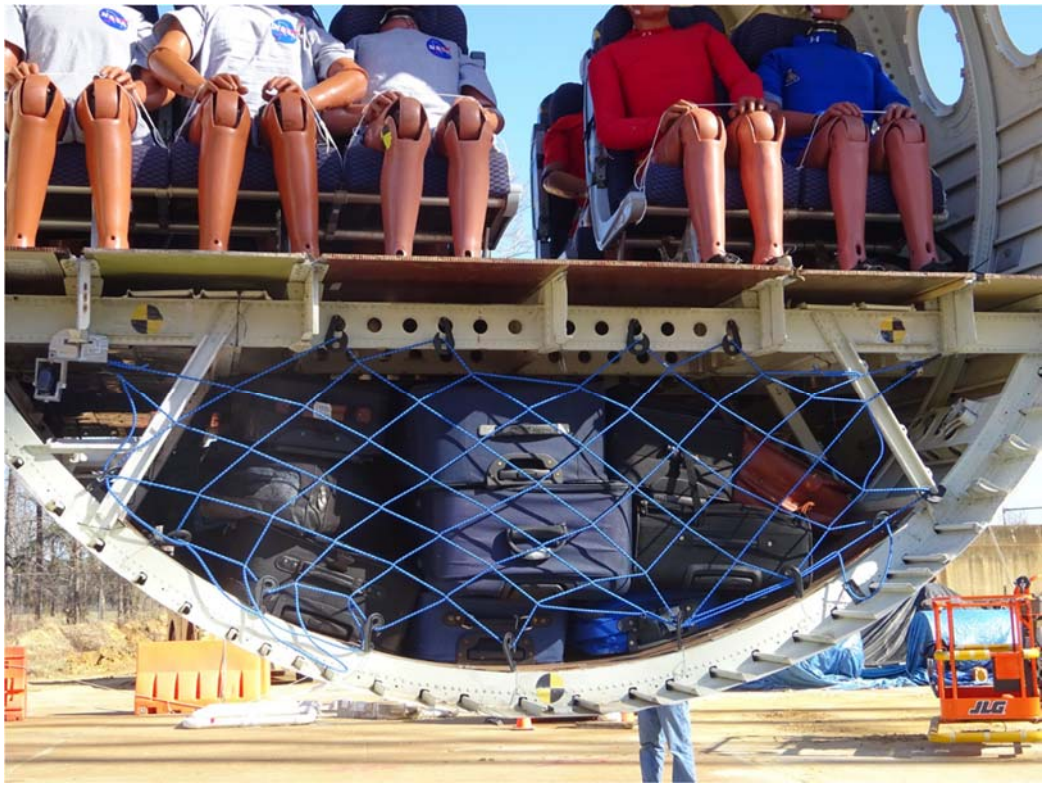

Figure 8 - Underfloor luggage configuration for the Forward Section test

Overhead compartments, called “hat racks” on the F28, were not available for use in the tests. Hat racks have similar functionality to overhead bins, but by lacking a door, have been replaced with overhead bins on current aircraft fleets, due to the possibility of stowed items coming loose during flight. The hat racks can be identified in Figure 4, shown at the top of the fuselage section, over the seats. The hat racks were instead simulated with ballast mass and aluminum c-channels. A section of aluminum c-channel was fastened to both sides of the interior four frames of each test article through links connecting to the three original overhead hat rack attachment locations. The links were sized such that the overall center of gravity (CG) position of the structure was 71.6 in above the floor and 25.25 in off of the fuselage centerline. These dimensions located the CG in the middle of the hat rack opening shown in Figure 4. Lead ballast, in the form of 25 lb weights was fastened to the three interior center spans of the c-channel, and the onboard cameras were attached to the underside of the c-channel. In total, the weight for each side was 116 lb, giving a running load of 33.2 lb/ft. Figure 9 shows the overhead mass configuration.

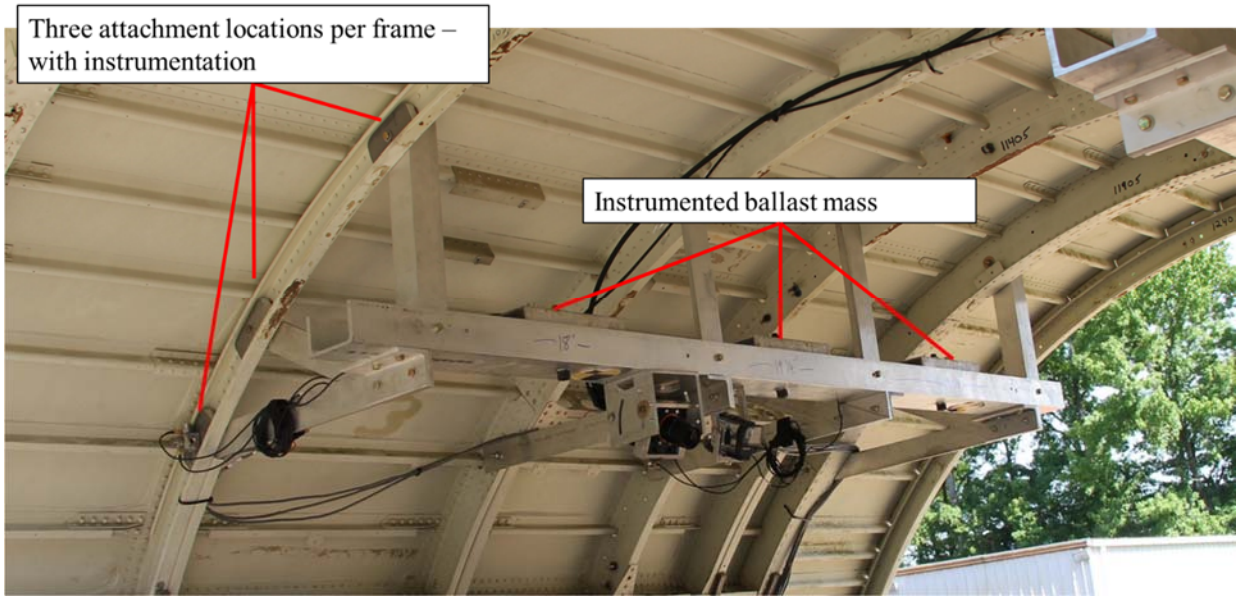

Figure 9 - Overhead mass configuration

In the Forward Section test, the rear row of seats was centered over FS 6805. The forward row of seats was positioned over FS 5805. In the Wingbox Section, the rear row of seats was centered over FS 11405 while the front row of seats was positioned over FS 10305. The seat pitch was 32 in between rows for both tests. All seats were placed in their most upright position, and all armrests were placed up as to not interfere with the ATD and ATD arm motion. Rear seat back monitors and corresponding electronics were removed for the tests. Aluminum plates were installed in their place to determine ATD head contact, should it occur during the test.

There were 10 ATDs seated in the 10 seats - supplied by both NASA LaRC and the FAA Civil Aerospace Medical Institute (CAMI). A combination of Hybrid II (H2), Hybrid III (H3) or FAA H3 [17] ATDs in different sizes ranging between a 110 lb - 5th percentile, a 170 lb - 50th percentile, and a 237 lb - 95th percentile. Each Hybrid III ATD was instrumented with head, chest and pelvic accelerometers, along with upper and lower neck and lumbar load cells. Each Hybrid II was instrumented with head, chest, pelvic accelerometers and a lumbar load cell only. Figure 10, left, shows the ATD make, size and in which seat it was positioned for both tests, noting that the setup for both tests was identical. Figure 10, right, shows an overhead view of the ATDs in their test configuration. This report will use the following nomenclature to identify the ATD along with its seat position as ATD #. For example, the ATD seated in seat 3 will be identified as ATD 3.

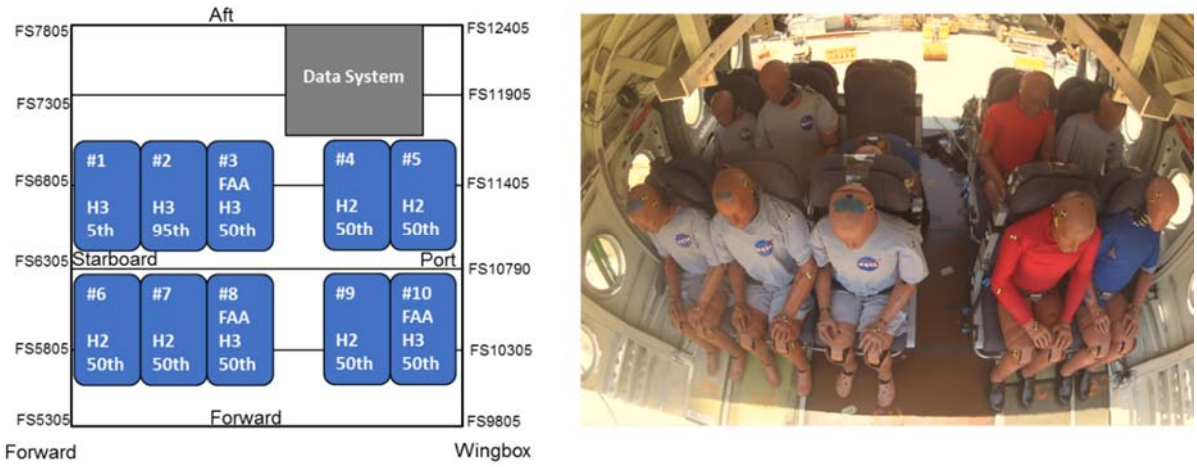

Figure 10 - Seat schematic (left) and picture of ATDs in test configuration (right)

Airframe data were collected via accelerometers placed in various locations throughout the test articles. Accelerometers were placed along the floor at the floor / frame junctions along both the port and starboard sides to measure floor accelerations. Small holes were drilled into the base of the seat legs for the placement of seat leg accelerometers used to measure seat base accelerations. Accelerometers were also mounted directly to the overhead lead ballast mass and at the c-channel attachment locations at the forward and aft frame attachments. These accelerometer locations were common to both test articles and example positions of these are shown in Figure 11.

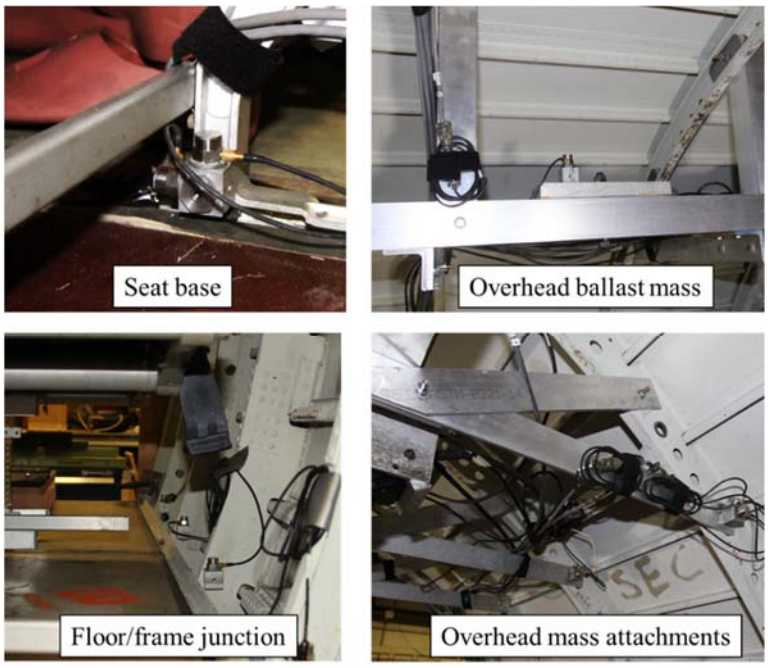

Figure 11 - Accelerometer locations. Seat base (top left), Overhead ballast mass (top right), Floor / frame junction (bottom left), and Overhead mass attachments (bottom right)

For the Forward Section test, additional accelerometers were placed near the lower stanchion/frame attachment points on both the port and starboard sides at FS 5805 and 6805 to measure underfloor accelerations. Since the Forward Section test was designed to be a purely vertical impact, accelerometers primarily measured vertical accelerations, with only a handful of accelerometers present to measure horizontal (forward / aft) accelerations, should a test anomaly occur. The Forward Section channel count was 145 total, which included the entirety of the airframe and ATD sensors.

Two additional crash data recorders (CDRs) were placed on the rear starboard side floor. Each of the CDRs was a standalone data logging unit whose physical dimensions measured approximately 3 in x 3 in x 1 in, and consisted of acceleration sensors in three axes, non-volatile memory, circuit board with computer USB connection, and a battery. Each was armed independent of all other sensors and triggered at impact via a sensed acceleration threshold. There were two types of CDRs – a blue unit with a 500-g range recording at 10 kHz, and a brown unit with a 6000-g range recording at 75 kHz. The CDRs were included as an evaluation for robustness for use as an alternative means of measuring acceleration through a portable measurement system. In the Forward Section test, an additional blue CDR was placed in one of the luggage bags to measure the acceleration of the luggage during the test event. Figure 12 shows two CDRs used in the Forward Section test.

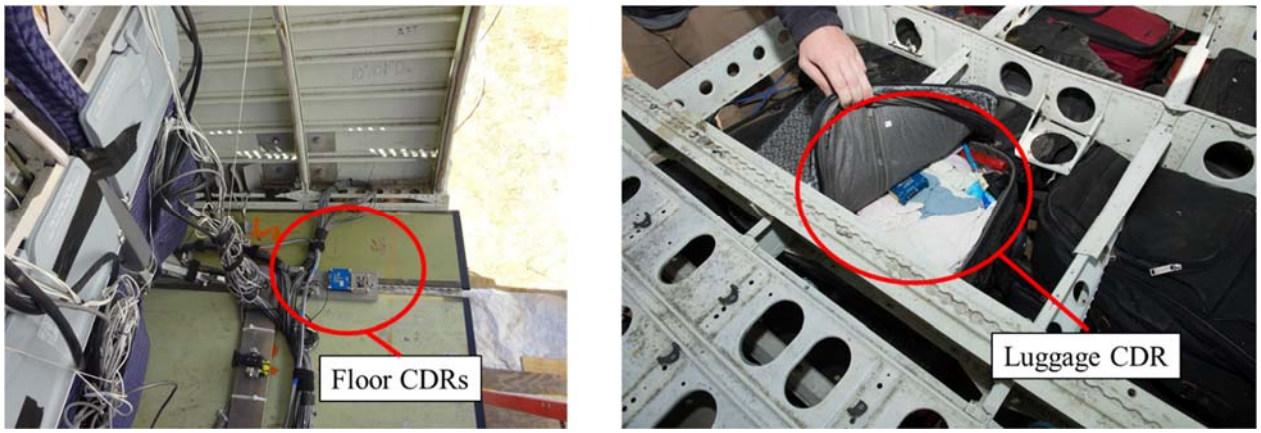

Figure 12 - Forward Section CDRs. Floor level (left) and luggage (right)

In the Wingbox Section test, it was expected that the test conditions would produce both vertical and horizontal accelerations, so accelerometers measuring horizontal accelerations were positioned both on the seat leg bases and at the frame / floor junction locations. Additional rotational rate sensors were placed both in the front and in the rear of the wingbox truss structure to measure rotation rate of the test article during the impact. Similar to the Forward Section, a plate containing both blue and brown CDR, along with DAS sensors measuring vertical and horizontal accelerations were attached to the starboard window seat track to give a second data point to evaluate these measurement systems. Since there was no luggage compartment on the Wingbox Section, a blue CDR was placed instead at the base of the lower cavity. Figure 13 shows the CDRs in the Wingbox Section.

Figure 13 – Wingbox Section CDRs. Floor level (left) and lower cavity (right)

The majority of the airframe and occupant data were collected via an onboard ruggedized data acquisition system (DAS). The DAS was situated on a pallet located at the rear port side of the test articles, mounted to the port side seat track rails. It consisted of three 64-channel data collection racks, battery, power distribution box, and time code generator mounted on a rigid aluminum plate. Data were collected at a sampling rate of 10 kHz and triggered via a start trigger initiated in the LandIR control room. Additionally, ATD 7 had its own internal data acquisition system that was being evaluated for use in this and future test series. For this ATD, a separate arming and triggering mechanism was used for data collection, and was also controlled from the LandIR control room. All of the standalone CDRs for both tests were armed pre-test and triggered upon reaching a predetermined acceleration level threshold at impact. All airframe and occupant data were filtered in accordance to guidelines specified by SAE J-211 [18], unless noted.

External high speed cameras were placed around the perimeter of the test area. Most recorded the test events at resolution of 2 megapixels (MP) at a speed of 1 kHz, however there were two photogrammetric cameras used for full field Digital Image Correlation (DIC) [19]. These cameras recorded at a resolution of 4 MP and speed of 500 Hz. The starboard side of each test article was painted with a black and white stochastic pattern for the acquisition of DIC results. The DIC results will be a subject of a separate report. Two high speed onboard cameras were mounted to the overhead hat rack bin ballast, and viewed all of the ATDs either on the double or triple sides. Additional onboard high definition (HD) cameras were mounted at various locations of interest for each test article. For the Forward Section, camera locations included underfloor cargo area. For the Wingbox Section, camera locations included inside the subfloor wingbox truss structure and in the lower cavity below the wingbox truss structure near the bottom skin. Additional HD and ultra-high definition (4k) cameras were placed on the ground and perimeter of the test area. A series of photogrammetric yellow and black “bowtie” targets were applied to specific areas along the forward and port sides of the test articles for aid in determining the impact conditions during the tests.

The Forward Section test article weight was 4,465 lb. This weight included 814 lb for the empty section, 922 lb of underfloor luggage, 232 lb of overhead hat rack bin ballast and 2,496 lb for the floors, ATDs, seats and DAS. The CG was located at FS 6524, which was 1.3 in forward of the geometrical center and 0.75 in starboard of the geometrical center of the section. The vertical CG position was not measured. Figure 14 shows the fully instrumented section, prior to test.

Figure 14 - Forward Section test article

The Wingbox Section test article weight was 5,182 lb. This weight included 2,454 lb for the empty section, 232 lb of overhead hat rack bin ballast and 2,496 lb for the weight of the floors, ATD's, seats and DAS. The CG was located 2.1 in forward and 1.4 in starboard of the geometrical center of the section. The vertical CG position was not measured. Figure 15 shows the fully instrumented section, just prior to test.

Figure 15 - Wingbox Section test article

For each test, the test article was lifted into position via a combination of the LandIR overhead cables. The test articles were lifted though four soft straps located near the four corners of each test article. In the Forward Section test, they were attached to locally reinforced attachments above the windows at approximately FS 5305 for the forward straps and at approximately FS 7305 for the aft straps. The straps were attached to the original wing attachment fastener locations for both the forward and aft lifting points for the Wingbox Section test. The required nose down pitch in the Wingbox Section test was achieved by using different vertical locations on the wing attachment fastener pattern. Test articles were released via a release hook operated by personnel in the LandIR control room.

The nominal impact velocities for both tests were expected to be 30 ft/s onto a bed of soil. The Forward Section was expected to impact at a nominal pitch angle of zero degrees, corresponding to a purely vertical flat impact. The Wingbox Section was intended to impact pitched at a 4-degree nose down angle as measured on the floor, impacting onto a 10-degree forward sloping soil bed. The differences in the contact angle allowed for the rear portion of the Wingbox Section to rotate about the rear impact point, inducing a locally perceived forward velocity into the ATDs during the rotation, giving a two-dimensional loading condition. Figure 16 shows the test articles at their respective drop positions, just prior to release.

Figure 16 - Forward Section (left) and Wingbox Section (right) at release position

Forward Section Structural Response Results

The Forward Section test occurred on March 23, 2017. The Forward Section impacted the soil surface at a velocity of 28.9 ft/s using data obtained through both the forward and port side photogrammetry bowtie targets. The photogrammetric data also showed the Forward Section with a 1.3-degree nose down pitch and a 0.7-degree starboard downward roll at impact. A forward high speed camera was capable of capturing the fuselage horizontal deformation, or "ovalization" of the test article at impact by measuring the change in distance between targets located on the port and starboard side of FS 5305 during the impact. A time history of the ovalization of the fuselage is shown in Figure 17, with the data locations identified.

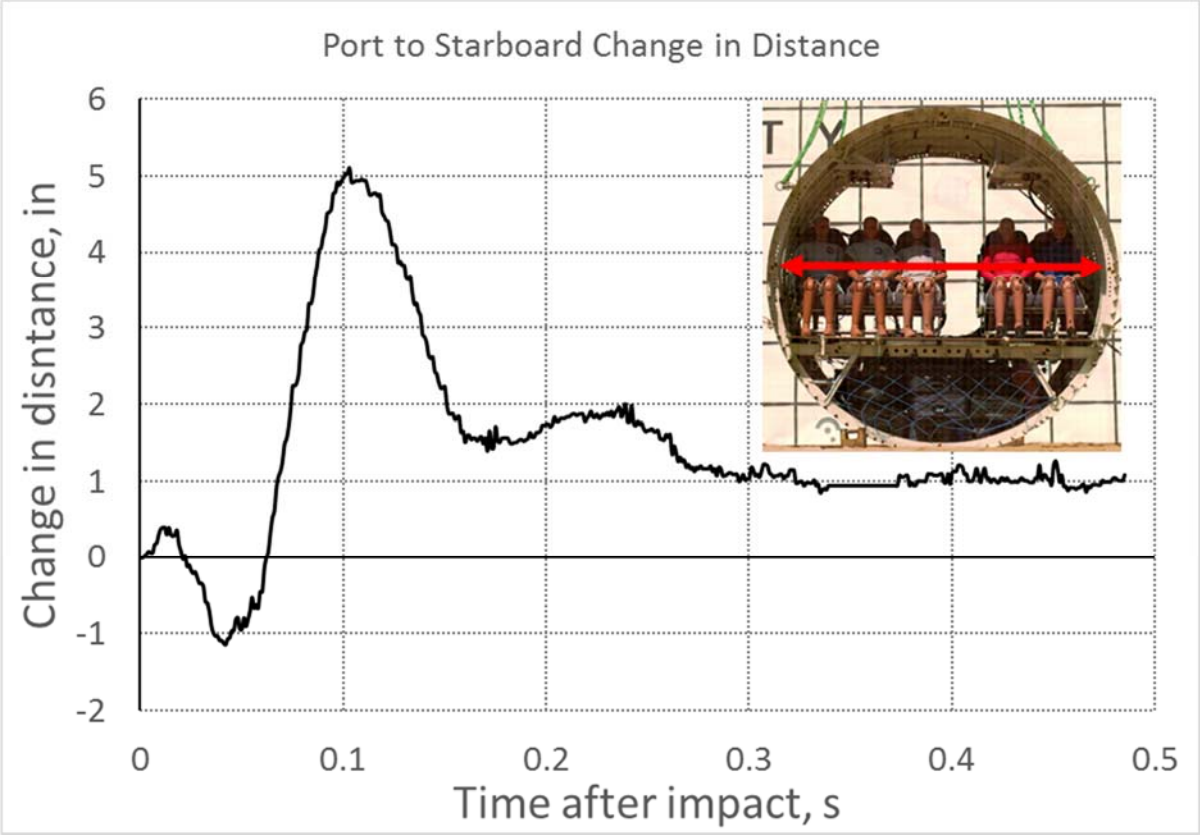

Figure 17 - Forward Section ovalization

The negative values shown before 0.06 s were a result of the inward motion of the port and starboard targets, which indicated an initial vertical ovalization of the fuselage at impact. This vertical ovalization was a result of the floor bending, which pulled the side walls of the fuselage inward. After the initial vertical ovalization, the sides of the fuselage deformed outward to a maximum value of 5.1 in at 0.103 s after impact. The late time history in Figure 17 showed that the fuselage sustained a permanent deformation of approximately 1 inch post-test. The test sequence as captured from the forward viewing high speed camera is shown in Figure 18, with notable events highlighted. Note that the initial floor bending can be seen in the upper right image.

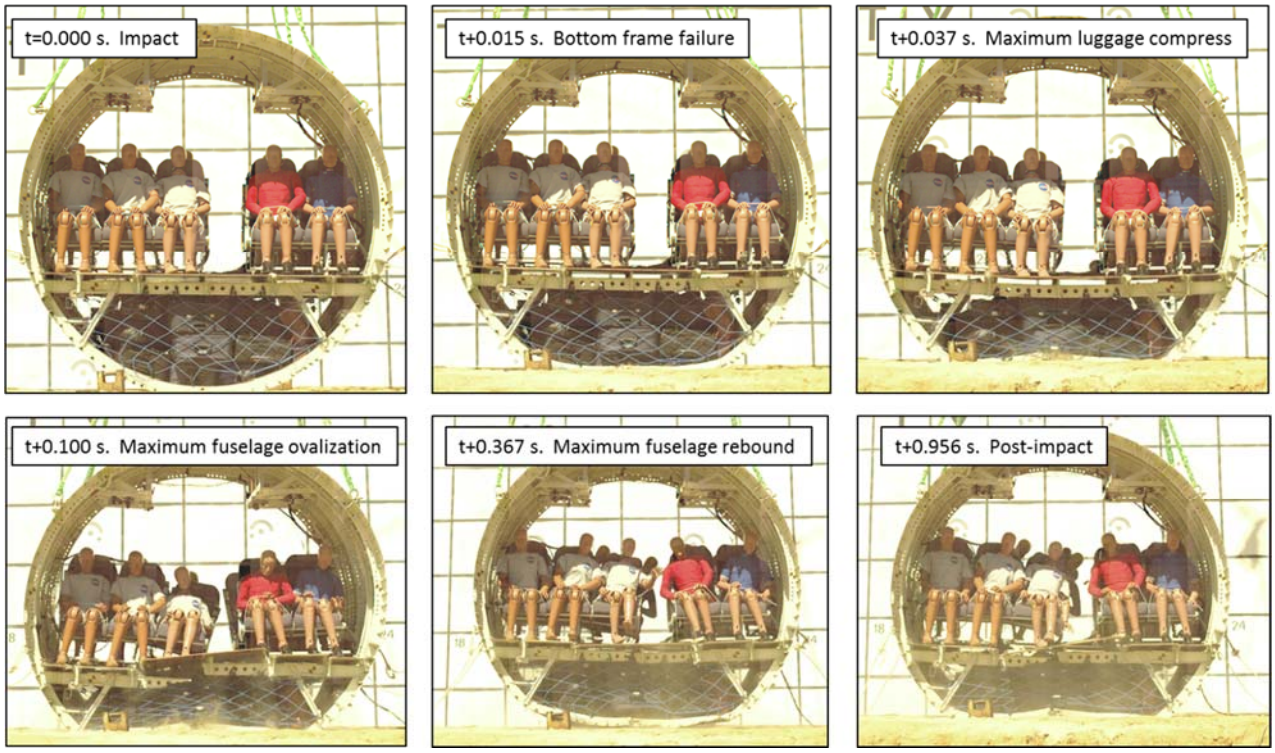

Figure 18 - Sequence of events for Forward Section test

The upper left image shows the test article at impact where first ground contact was made. This time was also the datum time used for the ovalization calculation. The upper middle image shows the first visible failure in the test article, which occurred at FS 5305 at the bottom skin / soil impact location. The upper right image shows where subfloor luggage underwent its maximum compression. This particular time was noted because it affected both the airframe and ATD responses. The lower left image shows the fuselage at 0.100 s after impact, which was where the maximum lateral ovalization occurred. This event was important due to its effect on the ATD response, described later in this section. The lower middle image shows the fuselage at the time where it underwent a small rebound. Finally, the lower right image shows the last acquired frame of the high speed camera almost one second after the impact event. This frame was beyond the time the major events occurred during the impact, even though the ceasing of all onboard motion after the test did not occur until a full 2.5 seconds after impact. Between these two times, there was additional gentle rocking back and forth of the fuselage due to the dynamics in the still attached, but slack, lifting straps.

Post-test inspections of the airframe showed failures in all of the floor support lateral stiffeners. However they were non-uniform, and did not follow a discernable pattern. A diagram highlighting complete failures of floor support stiffeners, depicted by red dash, is shown in Figure 19. The numbered items only depict where a stiffener completely separated in half. Much of the other floor support structure buckled, bent, and partially tore as well, but, for clarity, are not labeled in Figure 19.

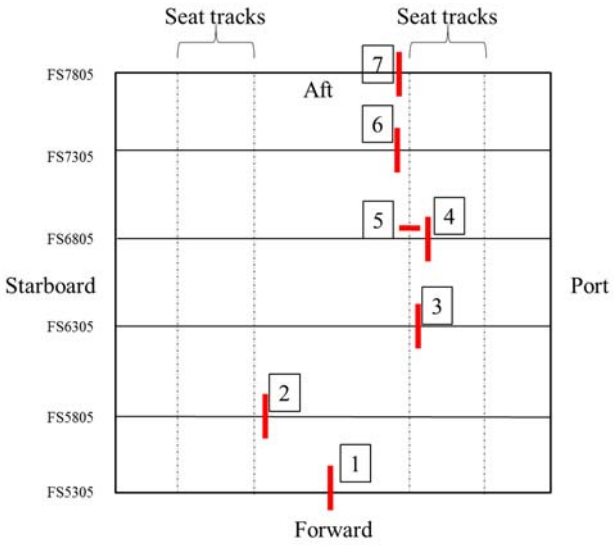

Figure 19 - Failure locations in the floor support structure and seat tracks

The failure pattern in the floor support structure at first appeared to be random and did not correlate to either a particular seating position or a place of overall stiffness discontinuity leading to high stress concentration (i.e. the cargo door). Upon closer inspection; however, it was determined that many of the specific failure locations were instead caused by the luggage interaction with the specific floor stiffener locations throughout the impact. The onboard and ground cameras were able to capture some of the exterior failures, but they were not able to cover all of the interior failures due to blockage of the failure from the luggage, floor, or both. Post-test inspections provided guidance in failure initiation and propagation for the interior members. The first interior failure inspected post-test was at location #2. A picture of failure in location #2 from Figure 19 is shown in Figure 20. Note that this failure was only visible once the floor and seats were removed.

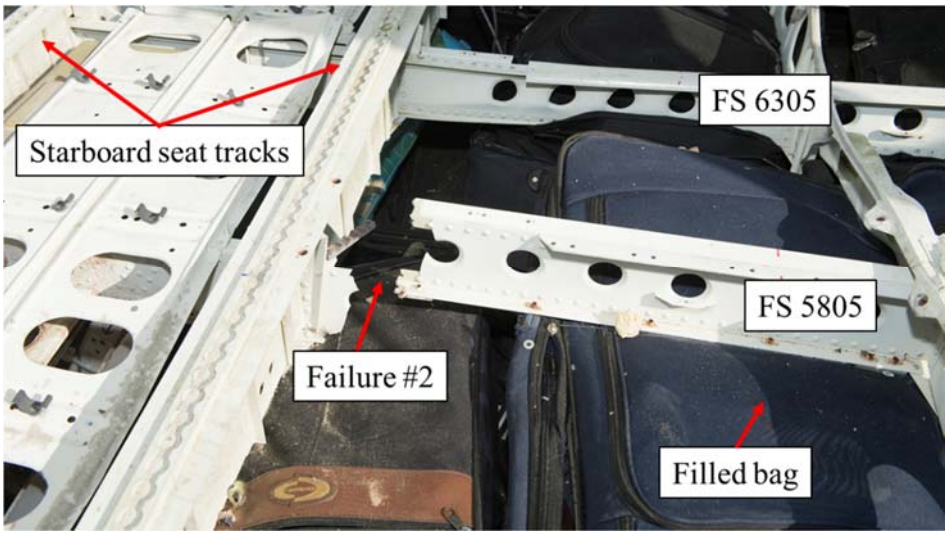

Figure 20 - Failure of FS 5805 at location #2

A detailed inspection at failure location #2 revealed a probable cause. Inboard of the starboard seat tracks, there was a fully filled dark blue bag located at the top of the underfloor luggage stack centered underneath FS 5805. To the left of the fully filled blue bag was a second black-with-brown-striped bag, stacked at a lower height than the fully filled blue bag. The difference in height was either from the black and brown striped bag not being completely filled or simply from being stacked on top of slightly shorter bags. At impact and during the maximum luggage rebound, the upward bearing of only the blue bag against FS 5805 the highest in the stack, caused the failure to occur near the seat track junction which was an area of differing localized stiffness. After the failure had occurred, the bag itself provided a surface for which FS 5805 to rest. Additionally, it is important to note that the blue bag was centered along FS 5805 and did not extend under either FS 5305, which is not shown, or FS 6305, which is shown in Figure 20. Had this bag extended into the area underneath FS 6305, it is conceivable that FS 6305 would have failed in a similar fashion. Similarly, Failures #3, #4 and #5 occurred adjacent to each other and are shown next in Figure 21.

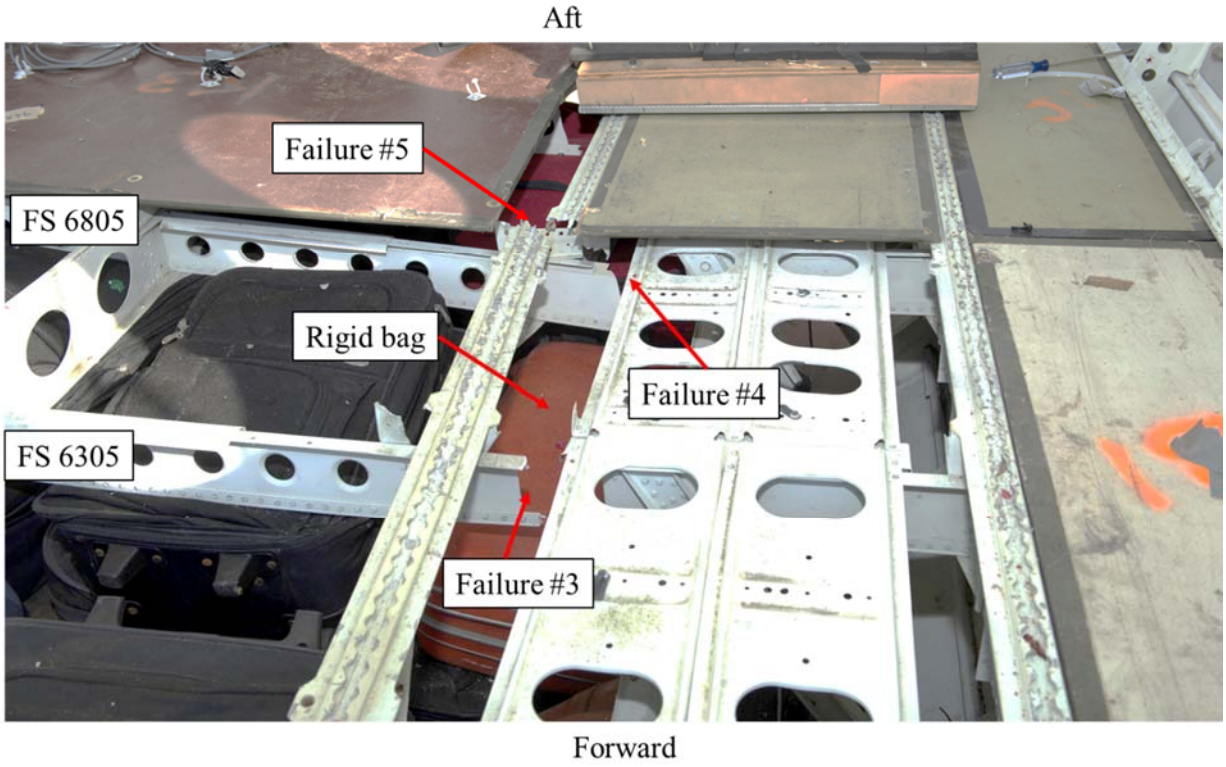

Figure 21 - Failure locations #3, #4 and #5

The root cause for the failure in FS 6305 (failure #3), FS 6805 (failure #4), and the inboard port seat track (failure #5) was attributed to the rigid brown bag underneath this area of the floor. The bag was (unintentionally) positioned such that it was centered between FS 6305 and FS 6805 at slightly outboard of the port inner seat track position. The impact and more importantly the rebound of this bag against these areas were the prime causes for the failures in these locations. The failures at FS 6305 and FS 6805 occurred at almost identical locations, which were immediately outboard of the inner seat track and positioned directly over the bag. The reason for the failure of the seat track (failure #5) was not as straightforward.

However, a combination of the failure of the two adjacent frame sections (failures #3 and #4), the added loading from the rear row double seat inboard leg attachment directly over FS 6805, and the added localized rigidity in the adjacent rear structure due to the DAS pallet attachment just aft of the seat track failure location is suspected.

Similarly, failures in locations #6 and #7 occurred due to the luggage interaction with the lateral support stiffeners inboard of the seat tracks near the rear of the fuselage section. The failures occurred inboard of the seat tracks due to the presence of the DAS pallet effectively rigidizing the area between the seat tracks at its attachments.

After the underfloor failures were thoroughly documented and photographed, the underfloor luggage was carefully removed to aid in the examination of the lower cavity and bottom skin areas of the test article. There were several failures in the lower section that are commonly seen both in previous testing, but also in in-service accident data. The first was the failure of the frame sections along the centerline at the very base of the fuselage. These failures were tensile failures at the inner end of the frame section, and were caused by the ovalization of the test article in the bottom skin region. The second prominent failure was the crushing of the frame sections immediately inboard of the lower-stanchion-to-subfloor attachment locations. This crush was caused both by subfloor deformation from the under floor luggage loading along with the outward motion of the frames themselves during the ovalization. These two failures are depicted in Figure 22.

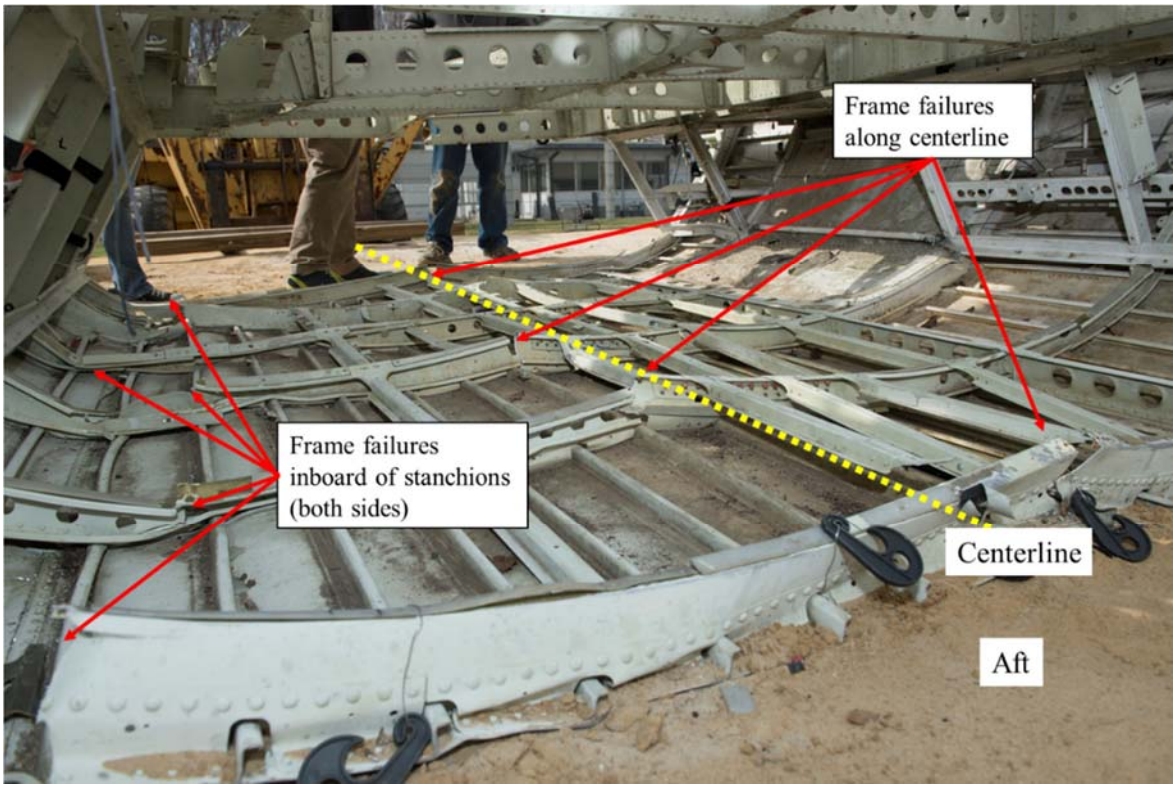

Figure 22 - Lower cavity failure locations

The upper portion of the fuselage section above the floor level was undamaged. The overhead ballast attachment points did not show any signs of deformation or fastener tear out and the ceiling was intact. The major deformations in the test occurred where the major items of mass such as the luggage and seats interacted with the lower support structure to cause deformation and failures.

The acceleration data at the starboard floor / frame junction locations were first examined to determine airframe response, and is shown in Figure 23. The data showed the fuselage section exhibited a nearly uniform response, which provided the first indication that the test was a (nearly) pure vertical drop, but also the fuselage, at least for the starboard side at the floor / frame junctions, reacted uniformly during the impact event. The different colored data series are representative of the response at the different FS locations on the section, which are defined by the starred locations in the legend in Figure 23.

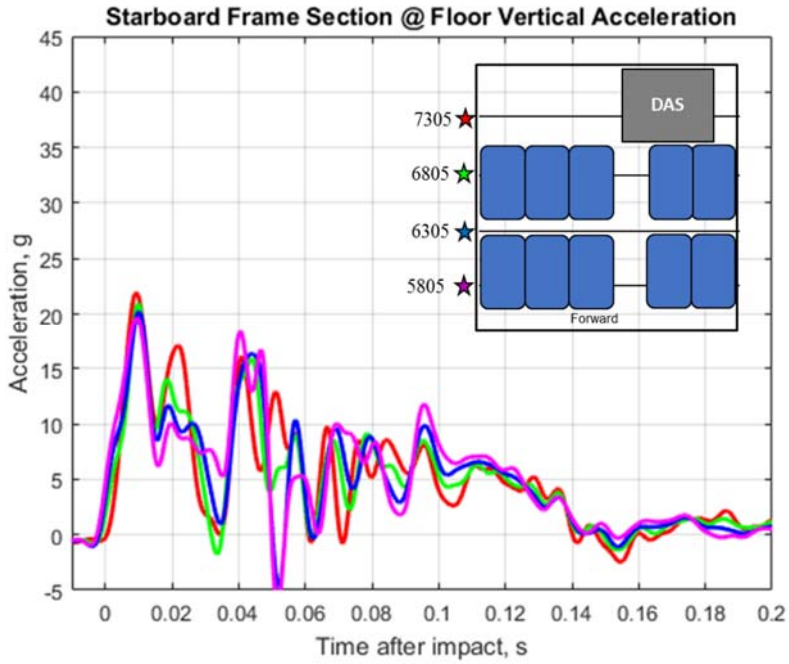

Figure 23 - Starboard floor / frame accelerations from Forward Section test

The accelerations reached initial peak values ranging between 19.7 g to 21.9 g, depending on location, which occurred approximately 0.010 s after initial ground contact. A large valley occurred at 0.033 s after impact, which was at the same approximate time as the change in the fuselage ovalization measurement shown in Figure 17, and, additionally, the same approximate time of maximum luggage compression, shown in Figure 18. The acceleration exhibited oscillatory motion through the major portion of the impact event. The overall shape of the acceleration data could be approximated as an acute trapezoid, having a rise time of 0.015 s, a plateau until 0.120 s, and a fall time of 0.031 s. Average accelerations were computed using the plateau region starting at 0.015 s and ending at 0.120 s. The average values of 7.2 g, 6.8 g, 6.8 g, and 6.9 g were obtained for FS 5805, FS 6305, FS 6805, and FS 7305, respectively.

Acceleration results for the port side of the airframe are next shown in Figure 24. Although there was a large amount of noise in the accelerometer located at FS 6805, the general shape in the data matched the

starboard side results. The cause of the noise is unknown at present and was only seen at this particular location. Thus, the large oscillations produced between 0.035 s and 0.070 s were based on some type of localized motion, and not representative of the test article as a whole. Additionally, the sensor at FS 6305 failed and did not record data, which may have been due to the localized phenomena recorded in the sensor at FS 6805. If the local oscillations are neglected, the acceleration time histories for all three locations resembled a trapezoid in shape, with a duration of approximately 0.086 s for FS 7305 and FS 6805, and a duration of 0.103 s for FS 5805. The end points of the plateau were measured between the times in which the acceleration response crossed the zero-g mark after impact. The initial peak accelerations were 19.4 g, 25.3 g and 26.4 g when examining the response from FS 7335, FS 6805 and FS 5805 respectively. The peak increased going from aft to forward in the test article, primarily due to the slight pitch down impact condition obtained from the photogrammetric results. When averaging the acceleration values between the end points in the plateau, values of 9.8 g, 9.7 g, and 9.6 g were obtained for FS 5805, FS 6805, and FS 7305, respectively. These numbers are slightly higher than the port side accelerations, and are potentially due to the small amount of starboard roll at impact.

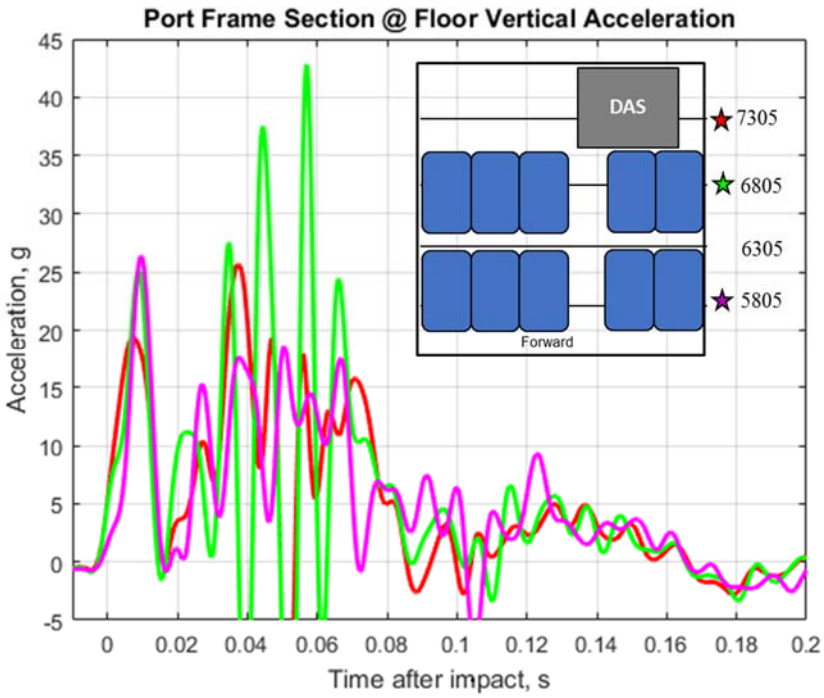

Figure 24 – Port floor / frame accelerations from Forward Section test

Seat accelerations were next measured on the floor of the base of each seat leg for both the double and triple seats. The seat base accelerations were an important measurement to obtain in order to determine the exact loading characteristics that were being input into the seated ATDs during the impact. The rear seat base accelerations are first plotted in Figure 25, noting that the color in the figure corresponds to the particular seat leg. For example, the red curve is the response on the triple seat, measured at the outboard seat leg position and the blue curve represents the response on the double seat, measured at the inboard set leg position.

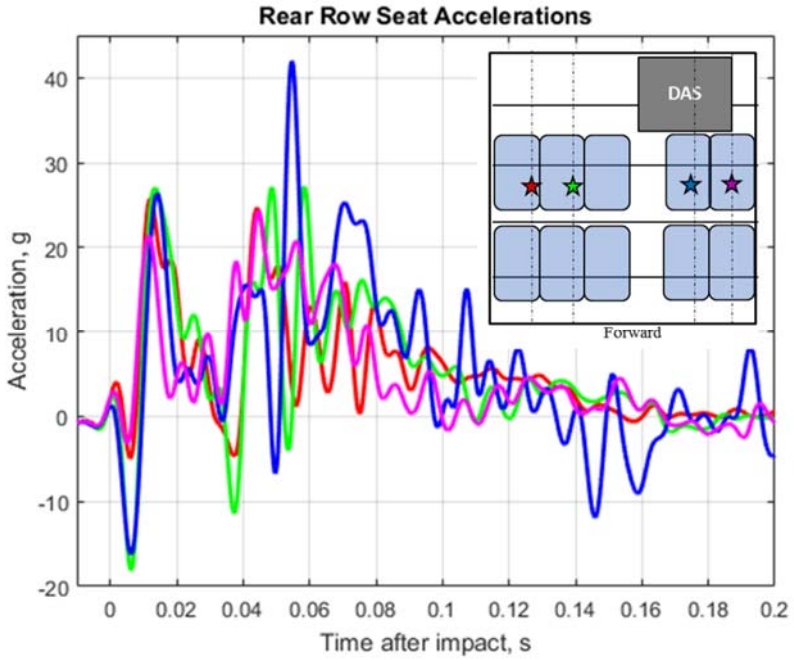

Figure 25 - Rear row seat accelerations from Forward Section test

An initial negative peak acceleration at 0.006 s occurred in all seat leg positions immediately after test article impact. The negative peaks, which reached a maximum of 18.0 g at the triple inboard seat leg position, was caused by the floor bending at impact. All seat leg accelerations then measured a positive peak of between 21.4 g and 27.0 g, between 0.012 s and 0.014 s after initial test article impact. However, when examining the acceleration pulses in their entirety, all seat leg positions exhibited similar characteristics in shape, which was approximated as triangular with vertex around the 0.060 s mark. The total pulse durations were similar for all seat leg positions, lasting between 0.134 s at the double inboard seat leg position to 0.166 s at the triple inboard seat leg position. The forward row seat accelerations are plotted next in Figure 26.

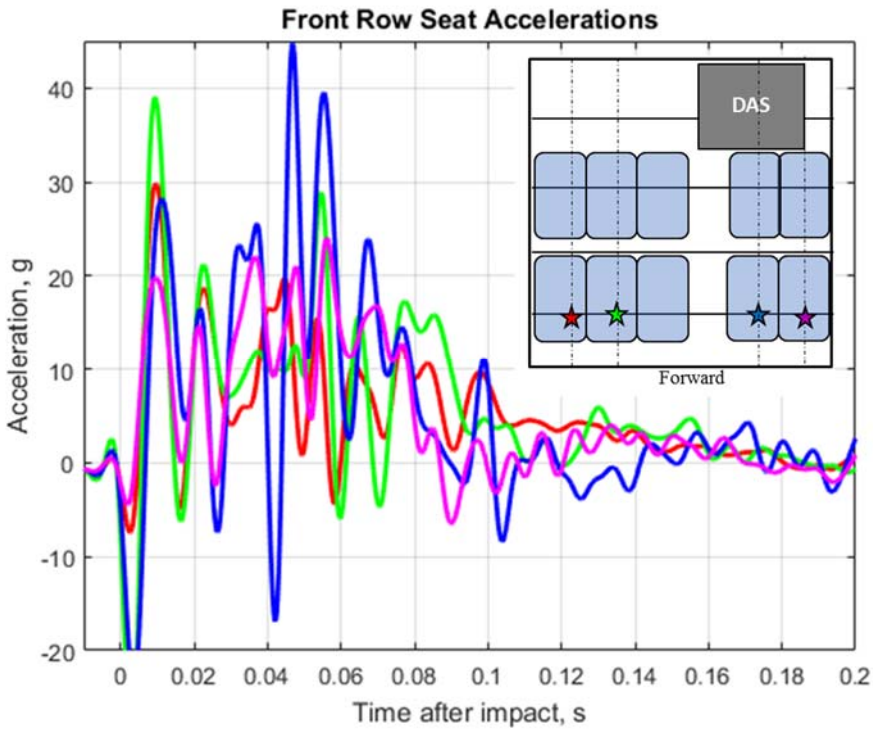

Figure 26 - Front row seat accelerations from Forward Section test

The front row seat leg responses exhibited the same general trends as the rear seat leg response results. The same initial negative peak in acceleration was also present, but occurred at an earlier time in the response at approximately 0.003 s after initial impact. The peaks were highest on the inboard locations and were consistent with the largest floor deformations occurring on the middle of the fuselage. The downward pitch angle was determined to be the cause of the time differences. The downward pitch angle caused the forward portion of the test article, corresponding to the forward row of seats, to impact first. The responses then showed positive peak accelerations between 19.8 g at the double outboard location to 39.0 g at the triple inboard location. Large oscillations were present in the double inboard seat leg location, which occurred between 0.040 s and 0.072 s after impact. The generalized shape for all responses were considered either triangular or trapezoidal, depending on how the data were interpreted. If assuming a trapezoid, the average acceleration values ranged between 9.7 g at the triple outboard seat leg location to 15.5 g at the double inboard seat leg location, when examining the data starting after the initial dip at 0.007 s lasting through 0.080 s. For either shape, the durations ranged between 0.087 s at the double outboard set leg location to almost 0.180 s at the triple outboard seat leg location.

Hat rack bin ballast attachment accelerations were next examined for the determination of the response in the overhead structures. Two out of the four attachment locations were instrumented on both the port and starboard sides. These locations, along with the corresponding acceleration data are depicted in Figure 27.

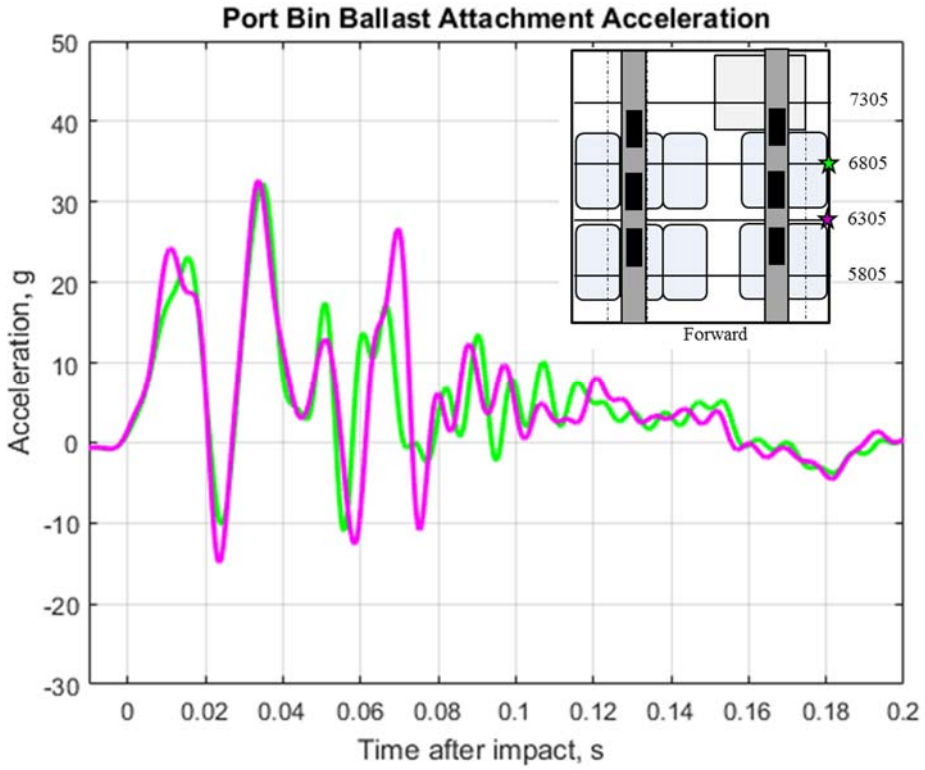

Figure 27 - Port side bin attachment accelerations from Forward Section test

Large oscillations were present in the hat rack bin ballast attachment locations, both at FS 6305 and FS 6805. There was no discernable shape for the first 0.080 s due to the oscillatory nature of the signals, and the signals were similar for the both locations. The oscillations tapered off to a sustained average acceleration 4.1 g and 4.3 g for FS 6305 and FS 6805 respectively, between 0.080 s and 0.160 s after impact, which was at the end of the loading in the attachment locations. The response was due to the large amount of mass being cantilevered off these attachment points, and the structural response of the test article, which did not deform at the upper attachment locations. The accelerations on two of the three bin masses are plotted in Figure 28.

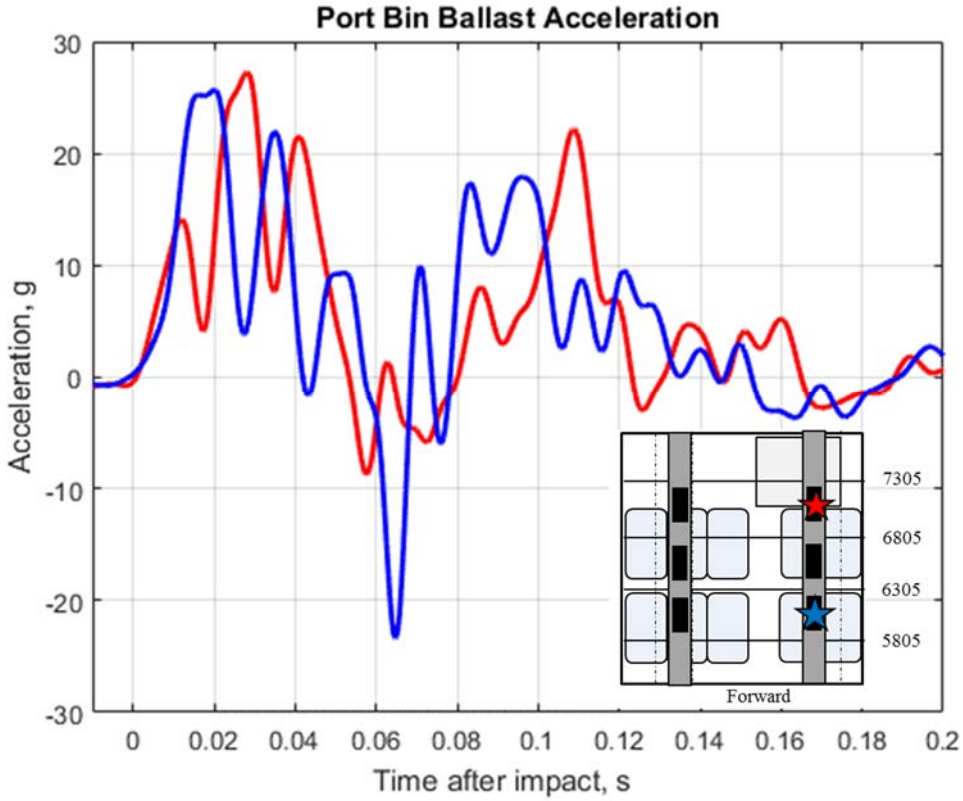

Figure 28 - Port side bin ballast accelerations from Forward Section test

The rear ballast mass, located between FS 6805 and 7305 is plotted in red, while the forward ballast mass, located between FS 5805 and 6305, is plotted in blue in Figure 28. Similar responses were measured for both masses that included an initial peak acceleration reaching 25.7 g in the forward ballast and 27.1 g in the rear. The forward ballast produced a large negative acceleration afterward, reaching 23.1 g, while the rear ballast reached a minimum of only 8.6 g. Both curves contained a noticeable sinusoidal shape with an overall frequency of approximately 11 Hz. The sinusoidal response was a result of the mass movement off the cantilever attachment points. The measured peak accelerations multiplied by the total overhead mass gave a maximum dynamic load of 3,143.6 lb which acted on the bin attachment points at their respective frame section locations. Both the starboard side bin ballast and bin attachment accelerations were of similar magnitude, shape and duration in nature.

The results from the CDRs were examined and compared to measurements obtained by the onboard DAS system. The CDRs along with an adjacent DAS accelerometer were rigidly mounted to the starboard outer seat rail at FS 7305. The location of the CDRs, along with the data obtained, is presented in Figure 29.

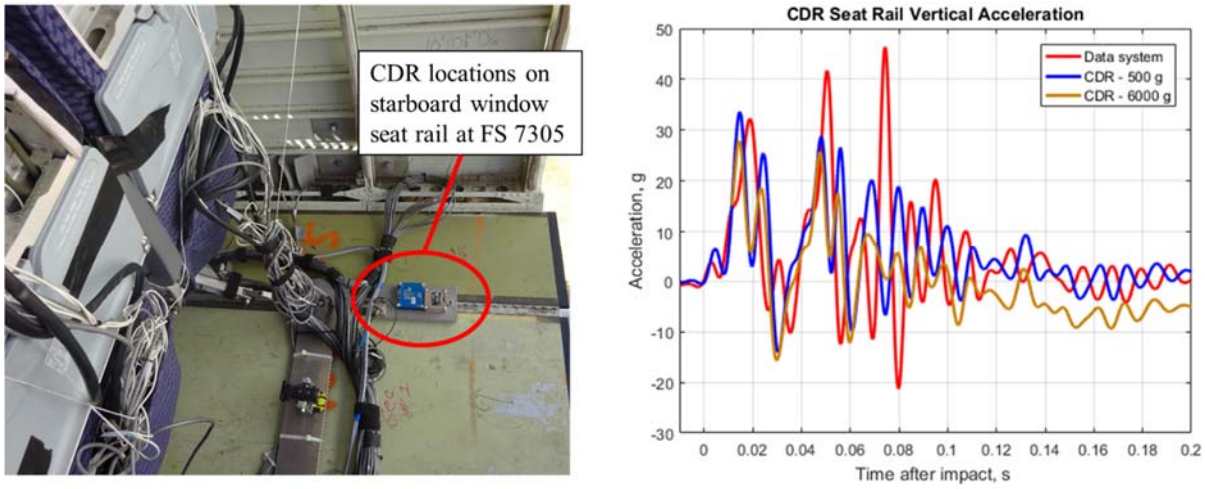

Figure 29 - CDR seat rail acceleration for Forward Section test

The red curve in Figure 29 is the accelerometer attached to the DAS, while the blue curve is the blue 500-g CDR, and the brown curve is the brown 6000-g CDR. All curves were in good agreement. The DAS data exhibited a first peak value of 32.2 g approximately 0.019 s after initial impact. The blue CDR exhibited a peak of 33.5 g and the brown CDR exhibited a peak of 27.8 g. Since the CDRs were not time-synchronized with the DAS or camera systems, analysis on the timing could not be completed and the curves were arbitrarily time shifted by using manual offsets, so timing information was not heavily scrutinized. Where possible, the DAS timing information was used to identify important event markers. After the initial peak value, all three curves showed a localized minimum in the acceleration at 0.030 s, then showed a second peak at approximately 0.051 s. All three curves decreased until the zero-g mark was reached, which occurred sometime after 0.100 s. The brown CDR initially showed a small offset from the blue CDR and the DAS as evidenced by the first peak value, but settled out to an approximate negative 6-g offset after 0.100 s. The 6-g offset was 0.1% of the brown CDR's full scale range, and was in the same range as the sensitivity in the sensor itself. The range on the brown CDR was simply too high to accurately capture the data at these comparatively low levels – which is an important point to note. The blue CDR, however, performed well as evidenced by its pulse peak values, duration and general shape matching the DAS data very well.

Finally, with confidence gained from the results of the blue CDR data, the data from the luggage CDR were examined. As noted previously with regard to the failure initiation and propagation, the luggage played a large role in the overall structural response of the test article. The compression and rebound of the luggage at impact interacted with the lower floor structure and created a distinct failure pattern in the seat track and floor supports. After the luggage was removed from the fuselage lower cavity post-test, the CDR located in one of the bags was removed and the recorded data were downloaded. The vertical acceleration data are plotted in Figure 30.

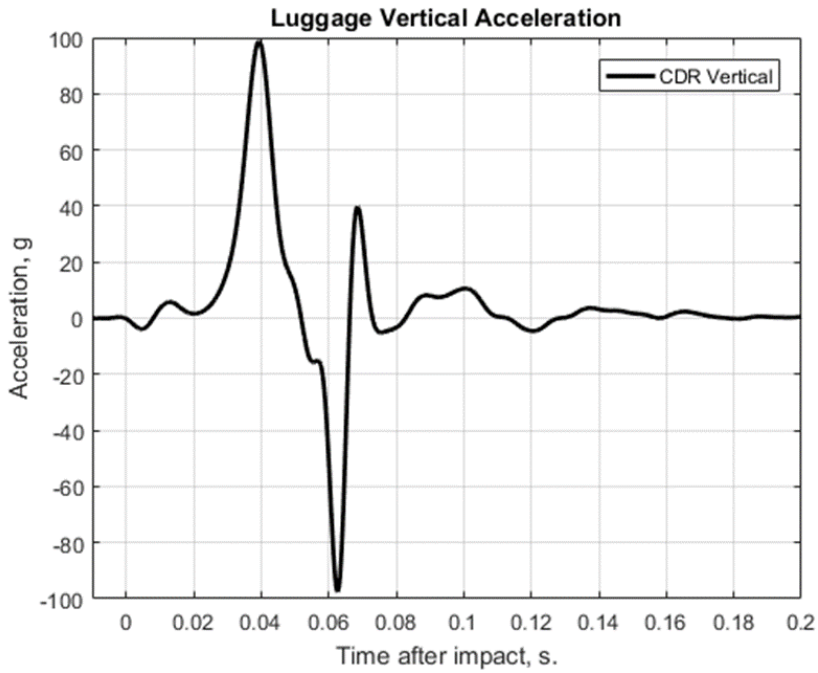

Figure 30 - Forward Section luggage vertical acceleration

The CDR measured two distinct peaks in the luggage response; the first at 0.040 s after impact and the second (in the negative direction) at 0.063 s after impact. These two events were the result of the luggage interaction with the soil (event #1) and the luggage rebound into the floor support lateral stiffeners (event #2). Three images were taken from the camera focused on the rear portion of the Forward Section. This camera was able to view the bag containing the CDR so correlation of the event data and video was possible. Figure 31 shows the image series of the luggage response using the two peak times identified from Figure 30, with the bag containing the CDR circled.

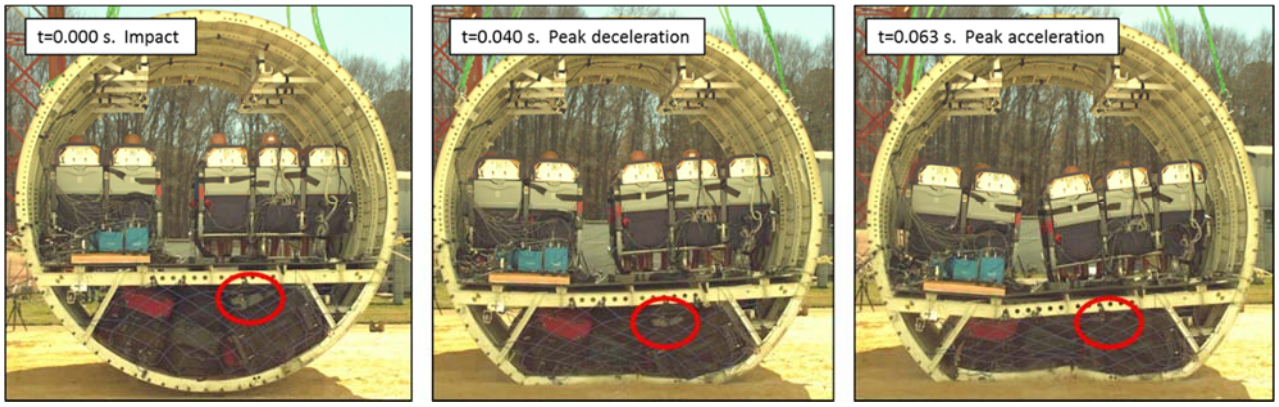

Figure 31 - Luggage response image series

The first positive acceleration peak of 98 g shown in the data was the maximum deceleration due to the compression of the luggage including the particular bag containing the CDR at impact. The high spike at 0.040 s resembles a compaction portion of a reponse curve from typical materials that exhibit compaction such as foams or honeycombs. This timing also agreed within a few milliseconds to the image series obtained from of the forward view of the section, as shown the top right image in Figure 18. The second acceleration, shown as a negative 96.6 g value in Figure 30, was a result of the luggage rebound after maximum compression, acting as a bearing surface for the floor support lateral stiffeners to react against as they continued their downward motion through the impact event. This was also likely around the time in which the failures occurred in the floor support lateral stiffeners.

The luggage response was deemed such an important part of the test that additional component level tests on the luggage were undertaken for the acquisition of luggage material properties. These tests are described in the *Component Level Luggage Test Results* section of this report.

Soil measurements were taken around the impact site. The soil used for testing is known as Gantry Unwashed Sand which is a silty sand (SM) using the Unified Soil Classification System [20]. It was built into 2-ft tall horizontal surface at the impact site. The strength and stiffness properties of the soil were measured approximately 1 hour before the test occurred. The soil moisture content was sampled at three locations and an average of 11.4% was measured at the time of the test. The California Bearing Ratio (CBR) [21] was also measured and is shown in Figure 32.

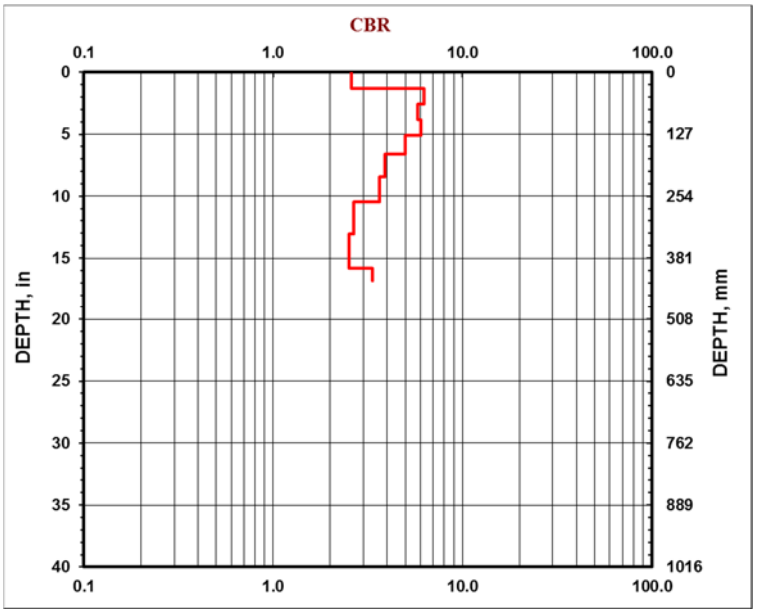

Figure 32 - California Bearing Ratio for soil in Forward Section test

The CBR can be thought of a measure of the stiffness as a function of the depth of the soil. There was initially a large jump from the top surface going to approximately 2 in down into the soil, which was the difference between the top layer of lose soil and the initial compacted layer underneath. From there, the stiffness steadily decreased throughout the depth until a depth of 15 in was reached. After this the soil began to stiffen, as evidenced by the curve moving to the right in Figure 32. However, the readings were

halted at this depth so no further analysis was completed, since this depth was well below the indentation made by the test article.

The soil indentation was measured once the test article was removed from the test area. Since the majority of the deformation was in the fuselage itself, a large indentation was not made in the soil. Only ripples in the soil were created from the stringers located on the bottom skin. Indentations ranging from 0.25 in to approximately 1.5 in were measured at locations around the impact site. As shown in the CBR measurements, it was also at this depth that the soil showed a jump in stiffness, so the deformations were primarily contained to the outermost layer of loose soil. Figure 33 shows the impact area with the outline of the fuselage footprint highlighted.

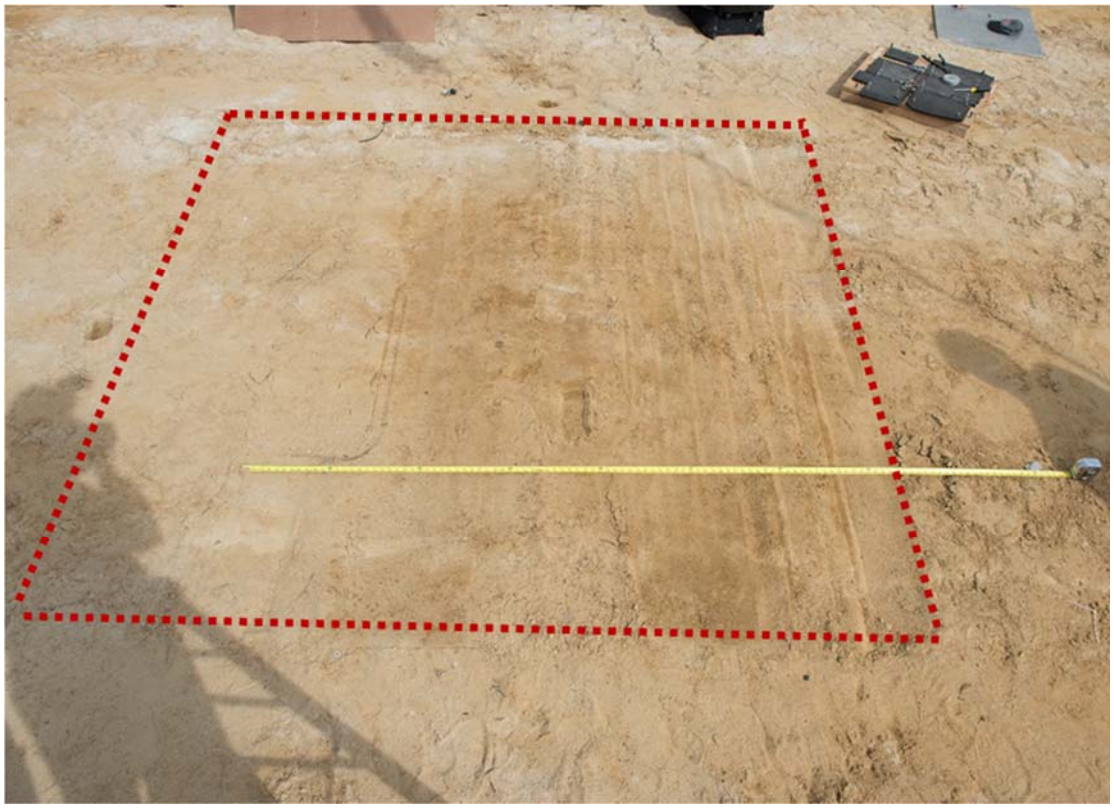

Figure 33 - Forward Section soil indentation results with test article outline

After the examination of the airframe deformation and responses, responses of the occupants were next evaluated to determine the magnitude of loads and likelyhood of injury. Figure 34 shows the front row of occupants post-test. The ATD seated in seat 8 was leaning into the aisle, restricting any potential egress. The ATDs seated in seats 7 and 9 were also leaning toward the aisle. The outboard ATDs seated in seats 6 and 10 were upright. The inward lean in most ATDs was due to the fuselage floor supports failing primarily inboard of the lower stanchions, causing the weight of the ATDs and seats to sag onto the underfloor luggage.

Figure 34 - Forward Section front row ATDs (Seats 6 through 10)

A view of the rear row ATDs is shown in a pieced together composite view in Figure 35. A composite view was the only available view for the rear row ATDs since the section needed to be partially disassembled to examine the rear row in detail. In the rear row, the post-test ATD positions were similar to the front row. ATD 3 was leaning into the aisle, almost making contact with the ATD 4. The large amount of deformation in seat 3 was also noticeable, which included the headrest separating from the seat frame. The 95th percentile ATD 2 also showed a lean toward the center; however, ATDs 1 and 4 remained upright, while ATD 5 actually showed an outward lean toward the outside of the test article.

Figure 35 - Forward Section rear row ATDs (Seats 1 through 5)

The ATD data were next examined and the probability of injury determined. The occupant lumbar data were first examined. Figure 36 shows the time histories on the left, and the peak value measured on the right.

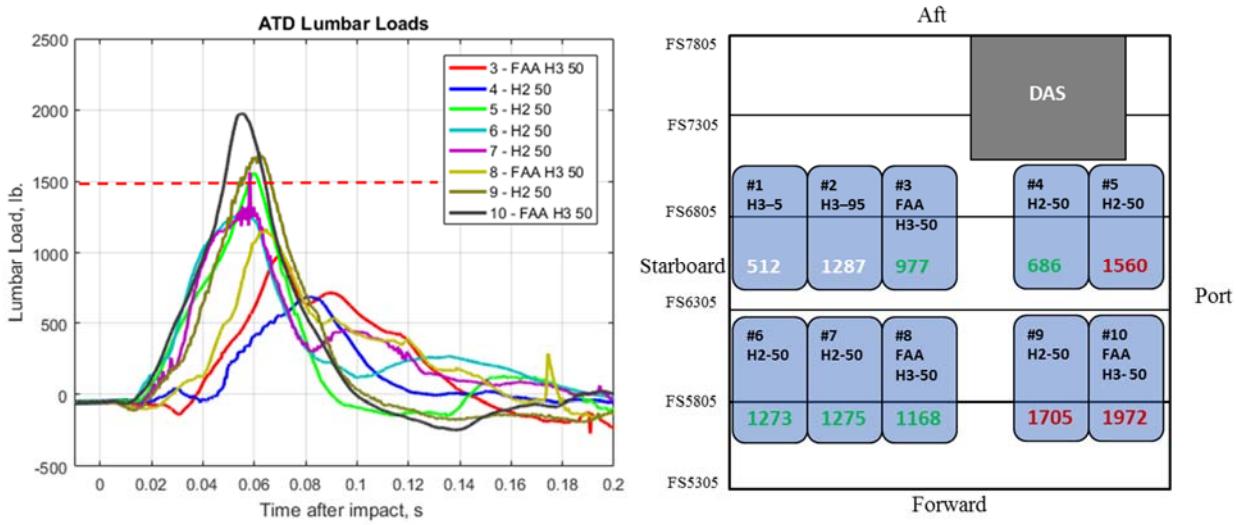

Figure 36 - Forward Section ATD lumbar load time history (left) and highlighted peak values (right)

The time histories of the ATD lumbar loads fell into two distinct shapes for the 8 ATDs plotted in Figure 36. ATDs 1 and 2 are not plotted on the chart and the peak value is included in the illustration for comparative purposes only. These two ATDs were included in the test to obtain data points for non-typical sized ATDs, but were not evaluated for injury because there are no current lumbar load injury criteria for these sized ATDs. The 50th percentile ATDs experienced environments that produced lumbar loads both above and below the 1,500 lb limit as specified by 14 CFR § 25.562 [15], which is depicted by the red dashed line in Figure 36, left.

There were three ATDs that exhibited lower peak values and a longer pulse duration. ATDs 3, 4, and 8 measured the lowest peak values, with load time history from ATD 4 different from the others. The difference was attributed to the failures in the floor supports located underneath ATD 4. Due to the failure of the floor members below ATD 4, there was an inadequate surface in which to react the occupant loads. This ATD (and its seat) sunk further into the floor than any other of the ATDs in the test, which was confirmed by examining the onboard video.

ATDs 3 and 8 exhibited marginally lower lumbar load results due to their position in the cantilevered portion of the triple seat configuration. The absence of a reaction device such as a seat leg or other surface caused these loads to be lower on average, and deformations in the horizontal seat pan support tubes to be the greatest out of all the seats.

Head accelerations were next examined for the determination of head injury. The ATDs seated in the rear row are plotted on the left and the ATDs seated in the front row are plotted on the right in Figure 37.

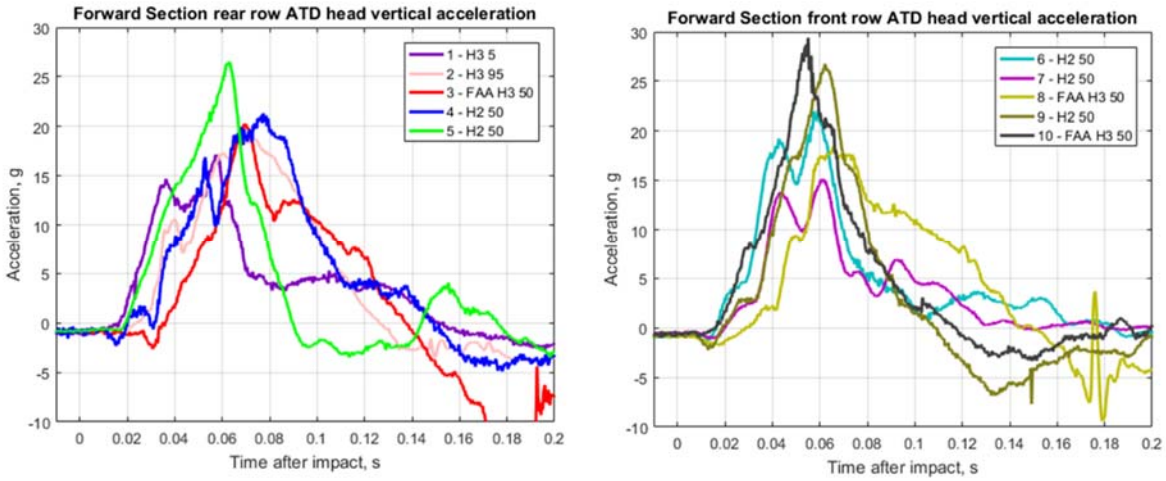

Figure 37 - Forward Section ATD head vertical acceleration. Rear row (left) and front row (right)

The head vertical acceleration peak values measured by the ATDs were less than 30 g for all ATDs and for some ATDs, less than 20 g. The maximum head acceleration was recorded in ATD 10 at 28.5 g, while and the second highest acceleration was recorded in ATD 5 at 26.4 g. Both of these seats were the window seat in the double seat configuration. The acceleration in ATD 5 had the shortest duration at 0.090 s, and exhibited a triangular pulse shape. All other pulse durations ranged between 0.109 s and 0.183 s. The head accelerations from both the vertical and horizontal directions were used in computations of Head Injury Criteria (HIC). HIC, as defined in the Federal Motor Vehicle Safety Standards (FMVSS) No. 208 [22], is a way of evaluating the acceleration data obtained from an ATD during a crash test and equating it to the probability of skull fracture. The equation is:

$$HIC = \max\left(\frac{1}{t_2 - t_1}\int_{t_1}^{t_2} a(t) * dt\right)^{2.5} * (t_2 - t_1)$$

The variable a(t) is the root-sum-square of the head acceleration time history obtained from the test, which has moving end points of t_1 and t_2. This report will use a 36 millisecond moving window and a limit of 1000 for a 50th percentile ATD. The HIC value of 1000 gives the probability of a skull fracture (Abbreviated Injury Scale $\geq$ 2) at 48% [23] and is used as a limit in 14 CFR § 25.562 [15]. Table 1 shows the results for all of the ATDs in the test.

Table 1 - Forward Section test ATD HIC values

ATD Type - Size	Seat #	HIC Value
H3 – 5	1	28.3*
H3 – 95	2	58.5*
FAA H3 – 50	3	39.4
H2 – 50	4	59.1
H2 – 50	5	55.9
H2 – 50	6	45.6
H2 – 50	7	15.9
FAA H3 – 50	8	34.6
H2 – 50	9	68.4
FAA H3 - 50	10	60.5
*For reference only		

The lack of a high spike in the acceleration time histories indicated that the ATD heads did not strike the seat back or other surfaces. Consequently, all HIC values were well below the established limits with a low probability of injury. Finally, pelvic acceleration was examined on each of the ATDs. Figure 38 shows the results from the rear row ATDs on the left and the front row ATDs on the right.

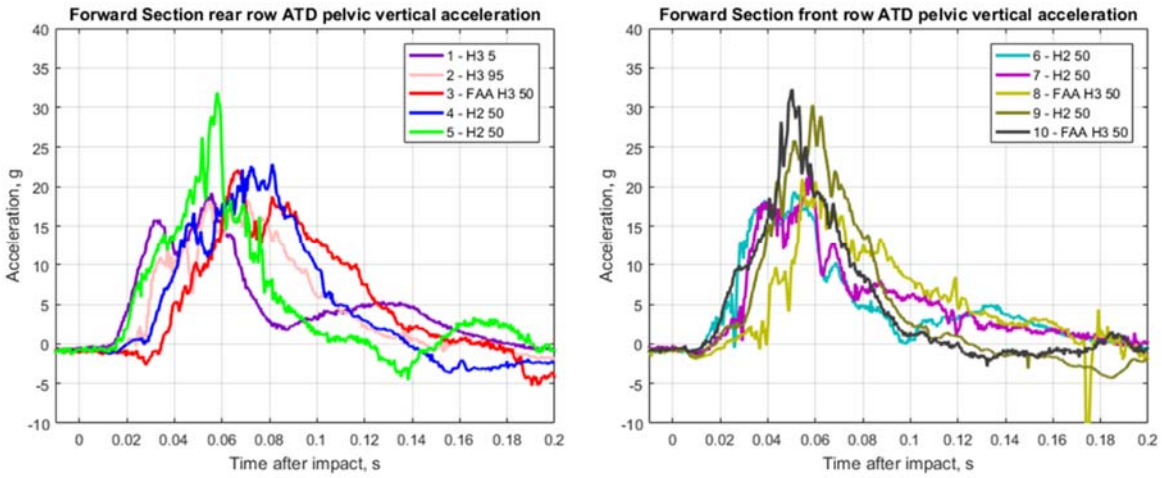

Figure 38 - Forward Section ATD pelvic vertical acceleration. Rear row (left) and front row (right)

The pelvic responses, while not required for specific injury criteria in 14 CFR § 25.562, were examined as a check to the lumbar loading since the physical locations in which the pelvic measurements were taken were close to the load cell used for the lumbar load measurement. Ideally, the two shapes of the curves should be similar and trends resulting from higher and lower magnitudes of peak values should be in general agreement. The highest pelvic accelerations for the rear row were recorded in ATD 5. The peak acceleration of 31.6 g, occurred 0.58 s after impact, and prior to the peak values from the rest of the seats in the rear row. Similarly, ATD 1 exhibited the fastest onset rate of acceleration, which showed an initial localized peak of 15.7 g occurring 0.032 s after impact, and the ATD 3 showed the slowest onset rate, with its acceleration reaching a peak of 21.9 g at 0.068 s after impact. Similarly, the front row ATD pelvic data

were compared to the lumbar load data. ATDs 9 and 10 showed the largest magnitude of accelerations of 29.8 g and 32.3 g. These were the two highest values of pelvic acceleration for all of the ATDs, and corresponded to the two highest values of lumbar load.

After removal of the ATDs, the seats were examined for permanent deformation. Both the front and rear triple seats are shown in Figure 39. Both seats exhibited similar post-test deformation shapes.

Figure 39 - Post-test triple seats. Rear (left) and front (right)

The maximum seat deformation occurred on both overhung seats - seats 3 and 8. Both seat frame rear tubes deformed to a maximum of approximately 4.5 in in the vertical direction when measured at the aisle armrest location, and the luggage guard buckled at the aisle seat rear attachment location, leading to a crack in the material. The middle and window seats and seat leg structure were undamaged for both of the triple seats. The double seats appeared undamaged when conducting post-test inspections. Figure 40 shows the underside of the triple seat in the rear row, noting the bent rear seat frame tube and the cracked luggage guard.

Figure 40 - Post-test rear triple aisle seat deformation (seat 3)

Component Level Luggage Test Results

The luggage interaction with the floor has been previously identified as an item of interest for determining fuselage response. To acquire material property data on the luggage, two component-level dynamic impact tests were performed on the luggage components only. Two tests were conducted using a 50-ft drop tower located at LandIR. Each test consisted of filled bags, picked at random out of a set of old luggage, randomly stacked at a configuration of two bags wide and three bags tall at the base of a drop tower. For each test, both the cloth style and the rigid style bags were included and stacked at random to achieve a "global" average luggage response. The bags were compressed via an instrumented 620-lb falling mass guided down the tower by a series of rails. Figure 41 shows the test setup for the luggage compression test.

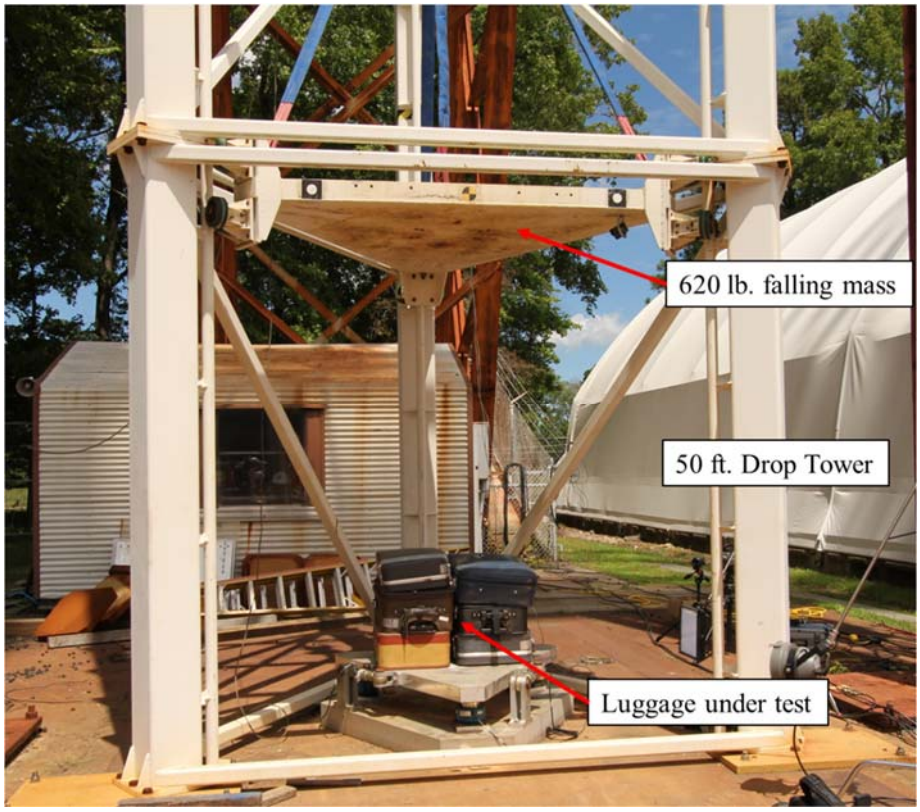

Figure 41 - Luggage component test setup

The first test was conducted with the impact velocity of the falling mass at 18 ft/s. The total luggage weight was 128.6 lb. A pre- and post-test picture is shown in Figure 42. Post-test inspections revealed that the impact shattered the rigid bags; however, left the soft bags mostly intact. The items inside were not examined for damage.

Figure 42 - Luggage test 1 pre- (left) and post-test (right)

The acceleration vs. time response as measured on the instrumented falling mass is shown in Figure 43. All luggage acceleration data from both tests were filtered at a Butterworth 4-pole low-pass filter with cutoff frequency of 300 Hz. The acceleration response could be interpreted as either a triangle or a trapezoid shape with duration of 0.127 s. The acceleration reached a peak of 13.3 g, which occurred 0.060 s after impact. If assuming a trapezoid shape, then the average acceleration on the plateau was 11.9 g when using the initial and final peaks at 0.060 s and 0.078 s as endpoints.

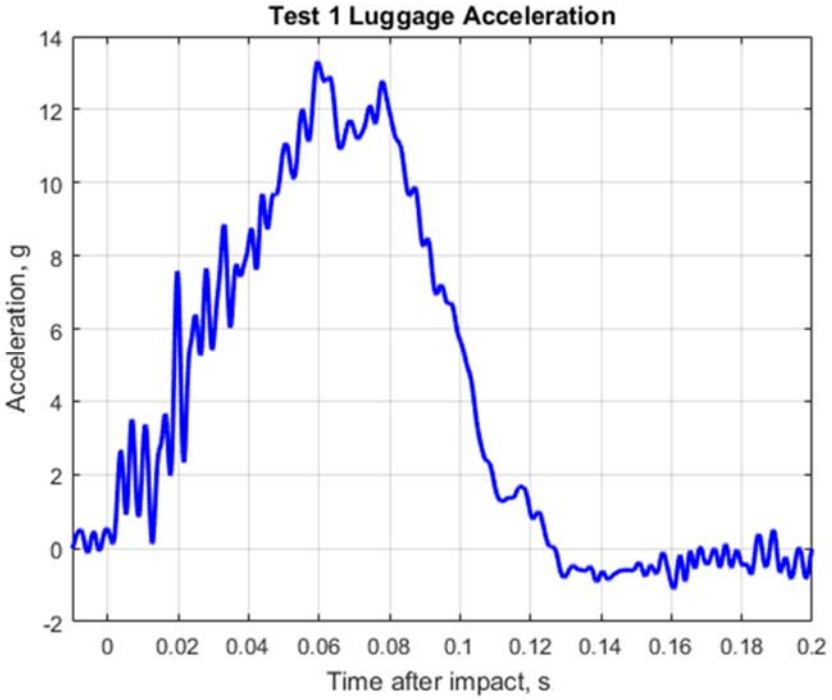

Figure 43 - Test 1 luggage acceleration

The acceleration data were then converted into crush stress vs. relative deflection data to achieve a result similar to a material property stiffness curve. Individual bag dimensions were measured and then averaged to obtain an average bag size. This average was used in the bag footprint area calculations, with the footprint being twice the average measured width multiplied by the average length. The total height was found by multiplying the average bag height times three. The acceleration was double integrated and then divided by the total height to achieve relative deflection and the acceleration was multiplied by the drop mass weight and then divided by the footprint area to achieve crush stress. The data for test 1 is plotted in Figure 44.

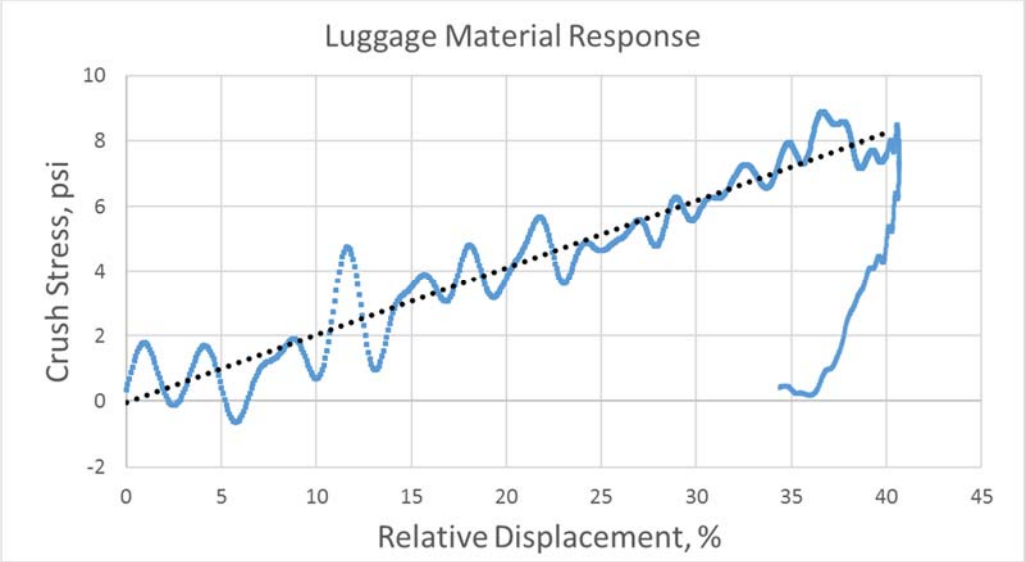

Figure 44 - Luggage response

A linear trend line was fit to the loading portion of the curve in an effort to smooth out the large amounts of oscillations and noise leading up to approximately 40%. The slope of this trend line was 20.7 psi. There was no plateau in the curve, presumably caused by the lack of residual available kinetic energy needed to further crush the bags after the initial loading region of the curve was reached. Test 2 added additional kinetic energy into the luggage in an attempt to reach the sustained crush region portion of the crush curve.

Test 2 was conducted in a similar fashion as test 1. Six different bags were used; however the methodology in developing the crush curve was the same. In test 2; however, impact velocity was 24.5 ft/s, which was an increase of the initial kinetic energy at impact by 85%. The total luggage weight for test 2 was 147.4 lb. Figure 45 shows a pre- and post-test picture of test 2.

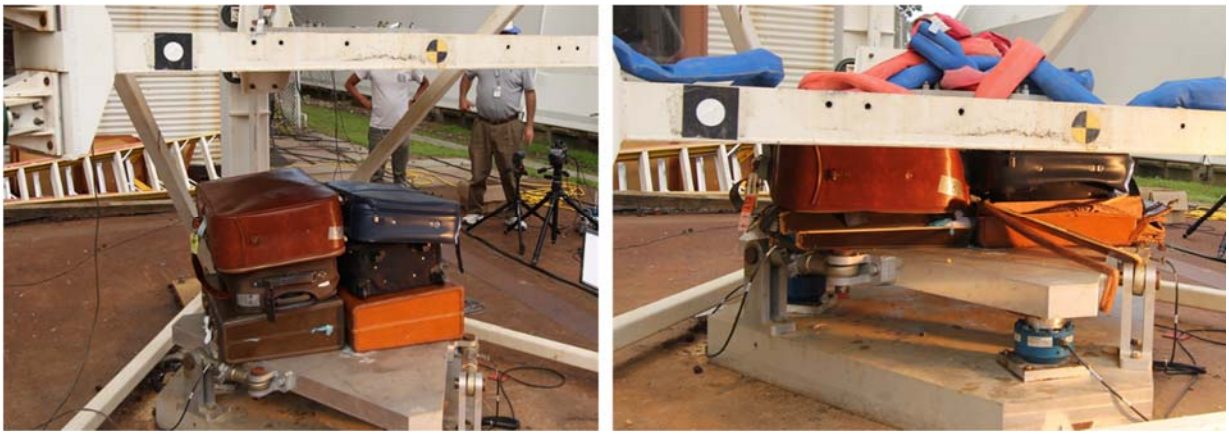

Figure 45 - Luggage test 2 pre- (left) and post-test (right)

The acceleration data are shown in Figure 46. Large amounts of oscillations were present in the data through the first 0.020 s of contact, which was the amount of time taken for the impact mass to fully engage the tops of the different sized bags. Once fully engaged, the acceleration averaged 10.6 g between 0.020 s and 0.070 s. The final acceleration reached a peak value of 19.4 g at 0.079 s after initial contact, which was at the point where maximum crush displacement of the impact mass occurred. After the maximum acceleration, the impact mass rebounded, and the luggage unloaded.

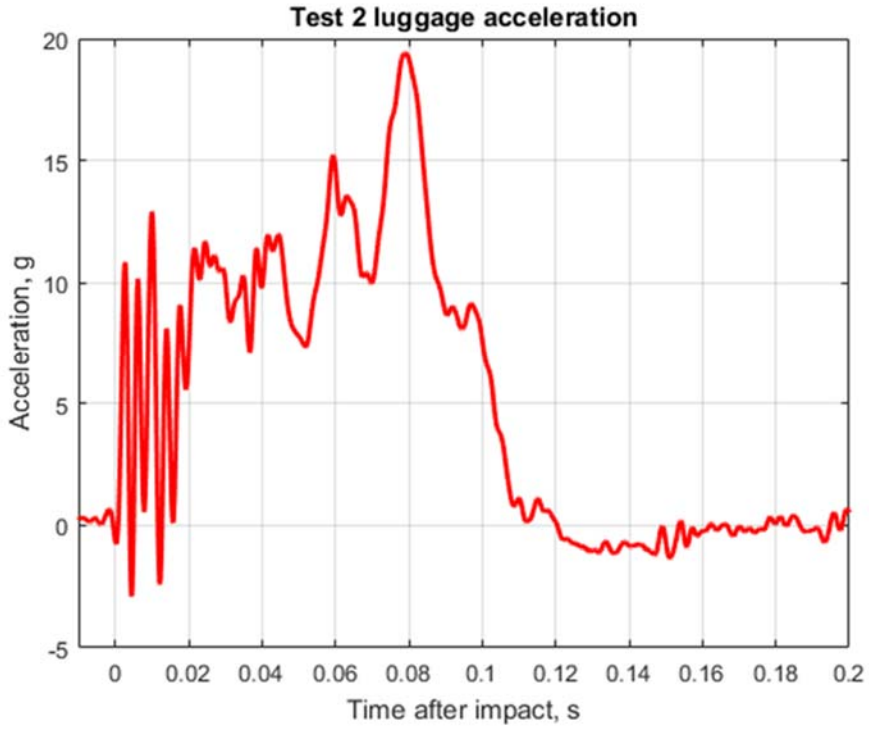

Figure 46 - Test 2 luggage acceleration

The crush stress vs relative displacement is plotted in Figure 47. An exact curve fit was difficult to determine when examining the data, first due to large oscillations at the beginning of the data, but also due to the potential for a beginning of material compaction toward the end. One interpretation resolved a linear slope of 8.0 psi up until 22.7% of relative displacement, then a plateau of 5.55 psi until 48.8% of relative displacement, then compaction until 57.1% of relative displacement. A second interpretation was also able to characterize the response as an elastic-plastic material behavior, starting with a linear slope of 8.0 psi until 22.7% relative displacement, and then a linear slope of 9.1 psi in the plastic regime. There are additional interpretations that are also valid.

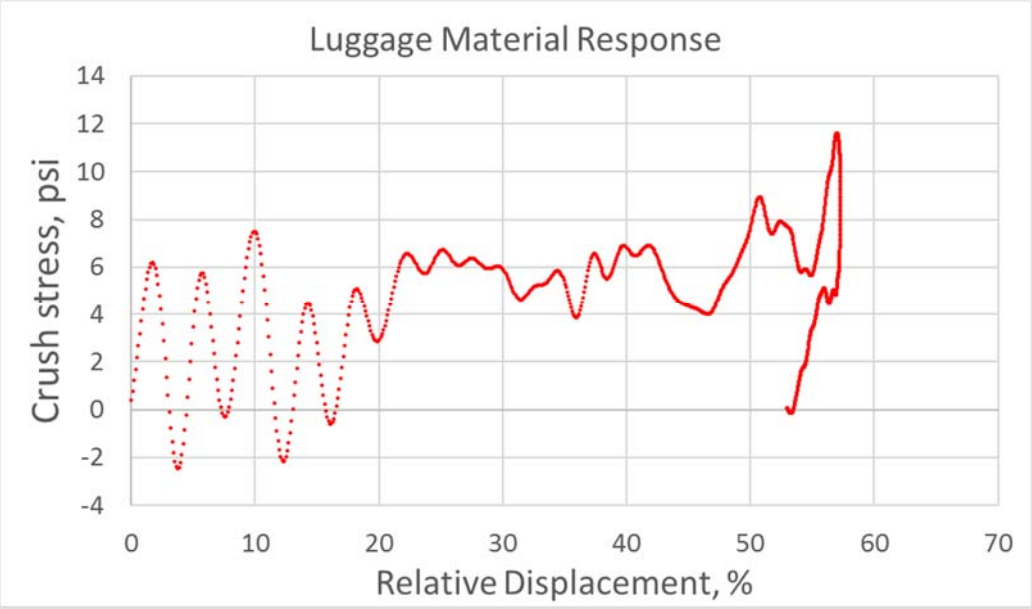

Figure 47 - Luggage response

Wingbox Section Structural Response Results

The Wingbox Section test occurred on June 29, 2017. An image series as captured from the front high speed camera is shown in Figure 48, with notable events highlighted.

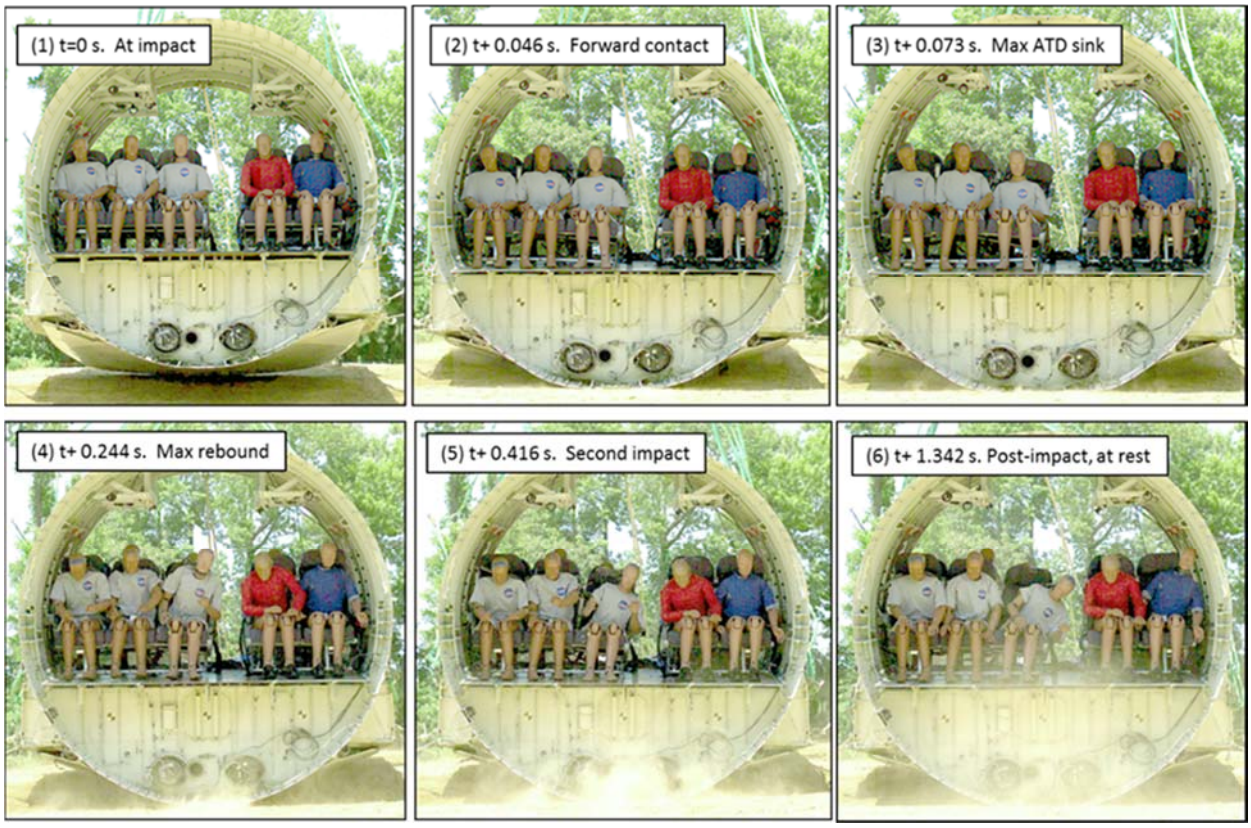

Figure 48 - Sequence of test events for the Wingbox Section test, forward view

The initial contact of the aft portion of the test article onto the sloped soil surface was considered the initial impact, and is depicted in the top left image of Figure 48. Between impact and t+0.046 s, the test article rotated about the rear impact point, terminating with the forward portion of the test article initiating ground contact at t+0.046 s, which is depicted in the top middle image. No sliding between impact at t+0.046 s was evident from the videos, so the horizontal acceleration between these two times was presumed to be from the test article rotation only. The next notable time occurred when the onboard ATDs experienced their maximum downward vertical motion, also known as their maximum sink position, occurring at t+0.073 s. The test article and ATDs appeared to exhibit uniform motion between t+0.073 s and t+0.244 s, until both test article and ATDs rebounded to their maximum unloaded positions. There was a second impact of the test article that occurred at t+0.416 s. During the second impact, the test article uniformly contacted the soil surface without rotational motion. The test article came to rest shortly thereafter. A final position of the test article is depicted in the lower right portion of Figure 48, and shows the test article at rest at a time well beyond where the final motion occurred during the test. An additional side view image

sequence is also presented to illustrate the fuselage motion and especially the fuselage rotation during the impact event, shown in Figure 49.

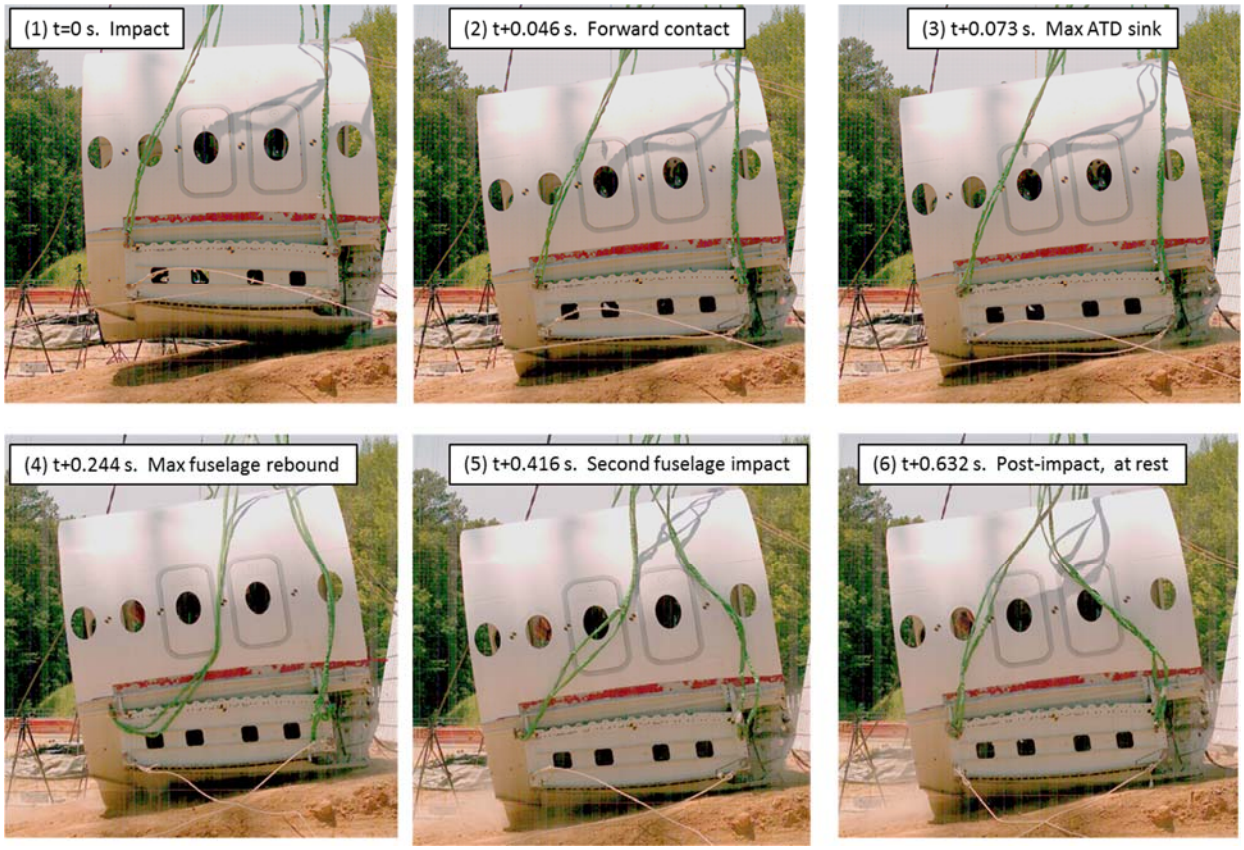

Figure 49 - Sequence of test events for the Wingbox Section test, port side view

The image sequence presented in Figure 49 depicts the motion of the Wingbox Section from the port side and corresponds to discrete times highlighted in Figure 48. The initial contact with the rear portion of the fuselage is shown in the upper left image. A gap underneath the forward portion of the section is also shown in this image. In the top middle image, the gap has closed due to the rotation about the rear portion of the fuselage. The top right image shows the section at ATD maximum sink, and is included for reference since the ATDs were not visible in the port side camera. At t+0.244 s, maximum upward rebound occurred in the test article, and the bottom middle image shows the second contact, occurring at t+0.416 s. The bottom right image shows the final frame of captured video from the camera after all of the major impact events have occurred.

The velocity results were resolved from a series of four black and yellow bowtie targets placed between the window openings at mid-cabin height. The target data showed the aft portion of the test article impacted the soil surface first at a pitch as determined from the floor of 2.9 degrees nose down with a vertical velocity of 29.5 ft/s. The pitch down in combination with the sloped soil created induced local vertical and horizontal velocities. The four velocity traces were translated into the test article local coordinate system using calculations based on the pitch angle time history, and are shown in Figure 50, noting that positive

horizontal velocity indicated motion of the test article forward, and positive vertical velocity indicated motion of the test article downward. The velocities were smoothed using a 5-point moving average, however no filtering was used. The individual velocity curves obtained from each target followed the same general trends, so the data were taken as a whole with individual traces averaged together for reporting overall values. The numbered vertical red bars correspond to several image times shown in Figure 48 and Figure 49.

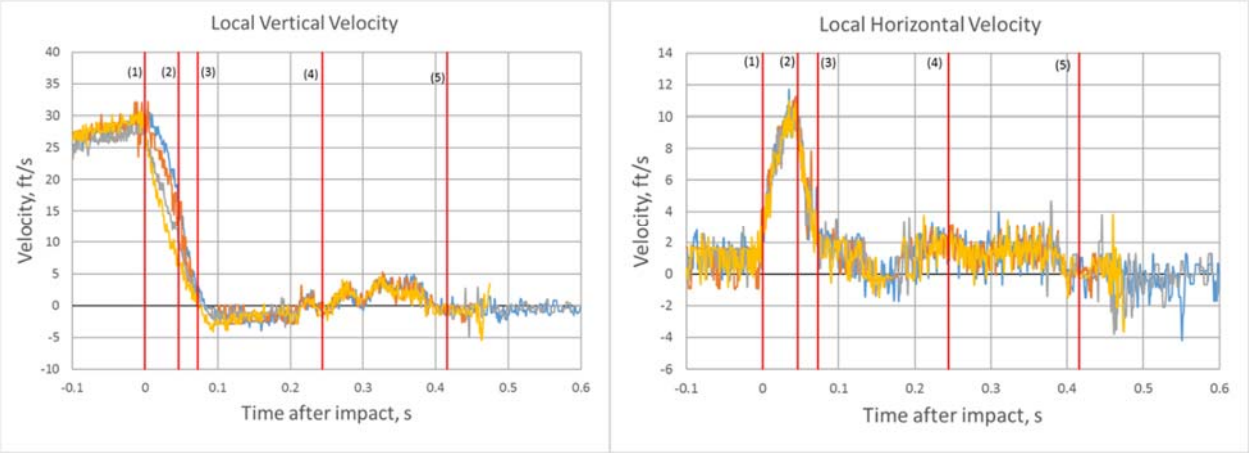

Figure 50 - Velocity time histories for Wingbox Section test. Vertical (left) and horizontal (right)

The local vertical velocity was 29.1 ft/s downward and the local horizontal velocity 1.1 ft/s forward at initial impact, which is designated by line 1. The rotation of the test article after impact caused the local horizontal velocity to reach 9.6 ft/s in the horizontal direction, which occurred immediately before forward test article contact at 0.046 s, designated by line 2. Both the horizontal and vertical velocities approached zero at the maximum ATD sink at 0.073 s. During the rebound (between lines 3 and 4), the vertical velocity averaged 1.6 ft/s in the upward direction ending at 0.244 s after impact. The second impact occurred with a forward velocity of 1.3 ft/s and a vertical velocity of 1.5 ft/s, which is noted in the data between lines 4 and 5. After the second impact, the motion stopped, noted by a zero velocity after line 5, and the test article came to rest. The rotation rate of the section is next plotted in Figure 51.

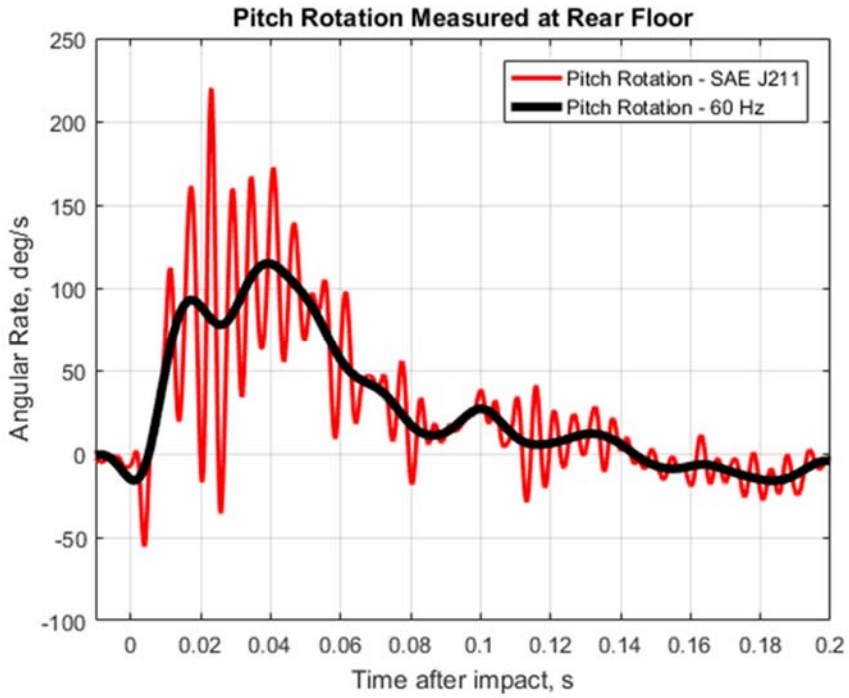

Figure 51 - Rotational rate for Wingbox Section test

Although the rotational rate was filtered in accordance to SAE J211, it still showed a large amount of oscillation. Thus, an additional curve that was filtered using a lower Butterworth 4-pole 60 Hz lowpass filter was also examined. This curve shows a rise after impact until 92.6 deg/s was reached at 0.017 s, then a gradual dip at 0.026 s until the pitch rotation reached a maximum value of 114.7 deg/s at 0.039 s. As noted by the images in Figure 49, the main portion of the rotation that occurs during the test was between impact and 0.046 s after impact, where forward contact is made. There was additional rotational motion due to the ATD sink until 0.073 s after impact. The data obtained from the rotational rate sensor correlated these results.

Other than the aft lower cavity region, the test article did not show noticeable signs of structural damage. The wingbox truss structure appeared to be undamaged, and the seat tracks did not show signs of fracture or tearing. Similar to the Forward Section, the structure above the floor did not appear damaged. Additionally, all four emergency exit doors opened nominally post-test, which indicationed no permanent deformation or warpage around the door frames. Figure 52 shows the doors pre-test and the openings post-test on the port side of the test article.

Figure 52 - Wingbox Section port emergency exit doors pre- (left) and removed post-test (right)

Figure 53 shows a close-up view of the aft lower cavity pre- and post-test. The entirety of the fuselage deformation during the impact event occurred in the lower cavity vicinity. The lower cavity section was located below the wingbox truss structure supported by a series of vertical stiffeners between the lower wingbox truss structure and the bottom skin.

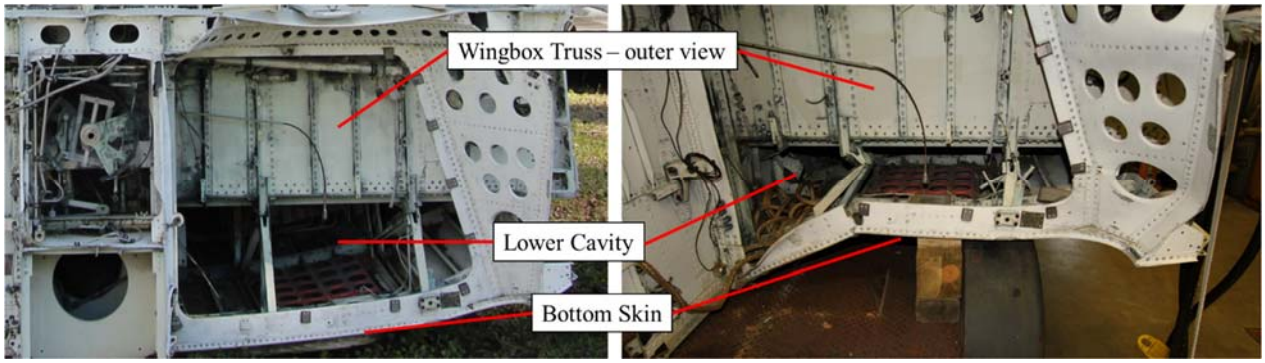

Figure 53 - Wingbox lower cavity pre- (left) and post-test (right)

Additional images were taken from an onboard camera mounted inside the Wingbox truss structure. Figure 54 shows a still image from a video taken from the camera post-test, which verified that the truss structure did not exhibit deformation or failure during the test.

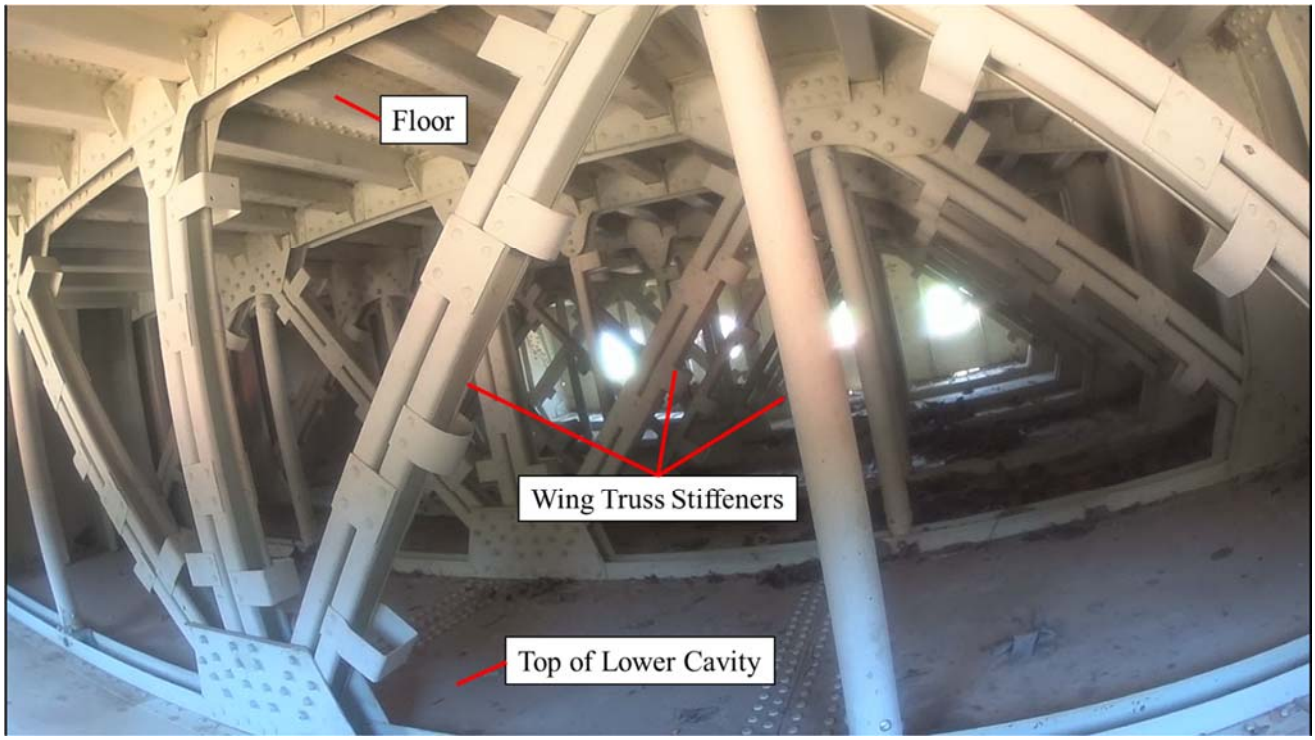

Figure 54 - Wingbox Section truss structure post-test

The soil moisture content was sampled at three locations and had an average of 8.4% at the time of the test. CBR measurements were also taken at three locations around the impact point. The CBR data showed a high bearing capacity at and near the surface of the soil, with a gradual decrease as the depth was increased. It reached a minimum at approximately 12 in depth, and then began to increase again. The trends were similar to the general trends obtained from the Forward Section soil, which were expected since the same soil was used. However the CBR surface results were higher and the moisture content was lower than the measurements taken in the Forward Section test. The differences were due to the Wingbox Test being conducted in the summer where the temperature was much higher. The higher temperature led to the evaporation of the surface moisture, which caused the soil to dry out and exhibit a stiffer response at the surface. The results of the location near the forward impact point are shown in Figure 55.

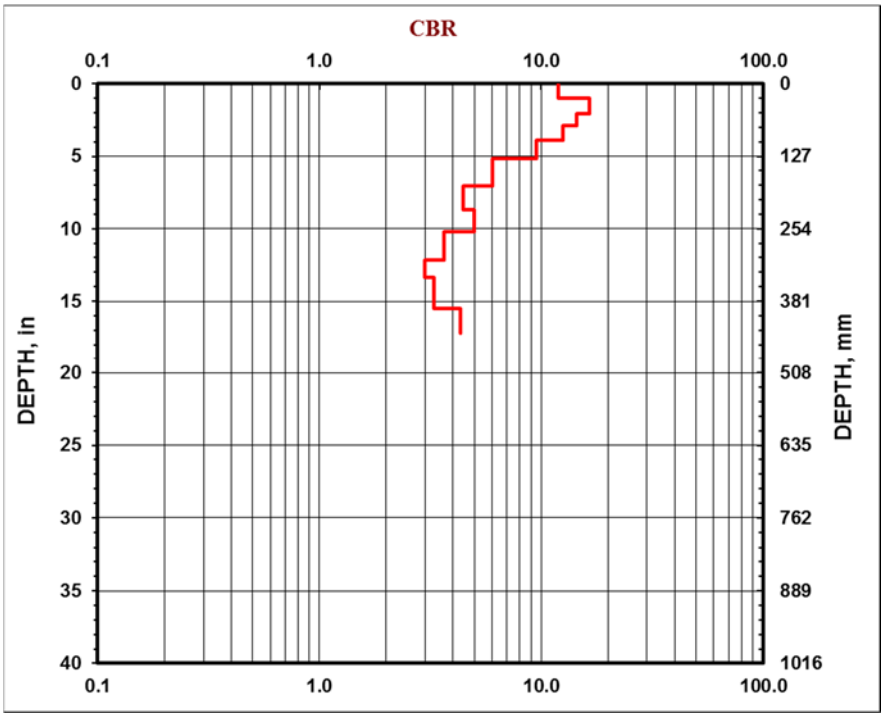

Figure 55 - California Bearing Ratio for soil in Wingbox Section test

The impact caused a distinct impression in the soil. Specifically, the impression exhibited two distinct parallel vertical lines with the deepest penetration occurring near the aft of the test article and gradually becoming shallower when moving toward the front. The parallel lines were created by vertical stiffeners located at the bottom of the test article, approximately 9 in outboard from the test article's geometric centerline. Since the aft portion of the test article impacted first, the rear features, including the vertical stiffeners, made the deepest impression in the soil surface. Generally, the rest of the soil mound was undeformed due to the impact. Figure 56 shows the indentation of the soil surface from the test. The two vertical indentations are noted, and the top of the image is toward the aft end of the section.

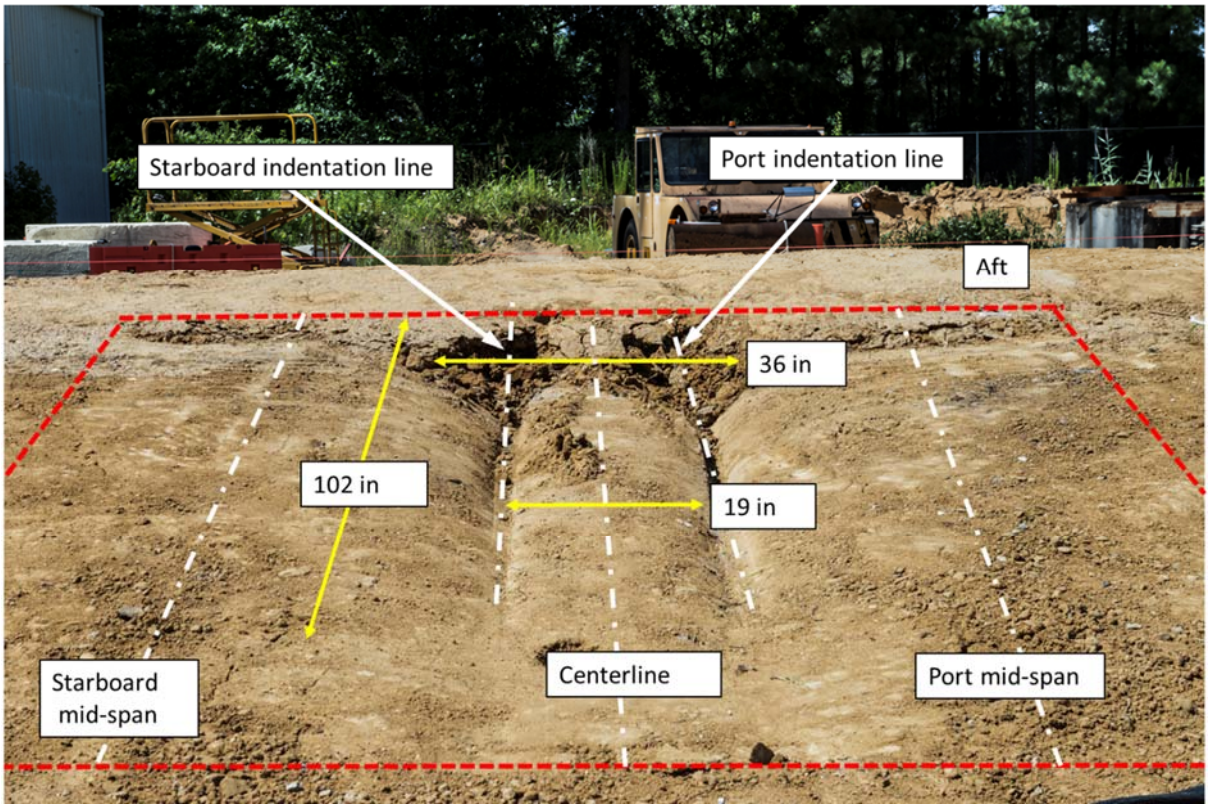

Figure 56 - Wingbox Section soil indentation results with test article outline

Penetration measurements were taken at three locations in the crater, depicted in Figure 56. Measurements for the starboard indentation line, which is the vertical line on the left in Figure 56, the middle between the indentation lines, and the port indentation line, which is shown to the right in Figure 56 were taken and the results are shown in Table 2.

Table 2 - Wingbox Section crater depth measurements

Position from aft (in)	Starboard indentation depth (in)	Centerline depth (in)	Port indentation depth (in)
15	7.0	4.25	7.25
22	8.0	4.0	7.0
37	8.0	4.0	8.0
47	6.0	3.25	7.5
62	6.0	2.5	6.0
76	4.75	2.75	5.25
102	3.0	3.0	3.0

The soil crater measurement data marked differences between the vertical stiffener and bottom span locations. In the aft impact location, vertical stiffener penetration was 7 in deep on the starboard side and

7.25 in deep on the port side, while the location of the mid-spans corresponding to the lower cavity locations of the test article lightly penetrated the soil. The differences were notable because accelerations obtained at the different measured locations were able to provide a local loading profile. Using the aft subfloor accelerometer for the vertical stiffener accelerations and the CDR for the lower cavity accelerations, the acceleration data were compared. Figure 57, left, shows the locations of both accelerometers in the post-test damaged view to contrast the difference in their locations. The data obtained are shown in Figure 57, right. The data were not time synchronized so manual shifting was implemented on the CDR data to give a more direct comparison. The data in Figure 57 are filtered using a Channel Frequency Class (CFC) 60 low-pass filter for visualization.

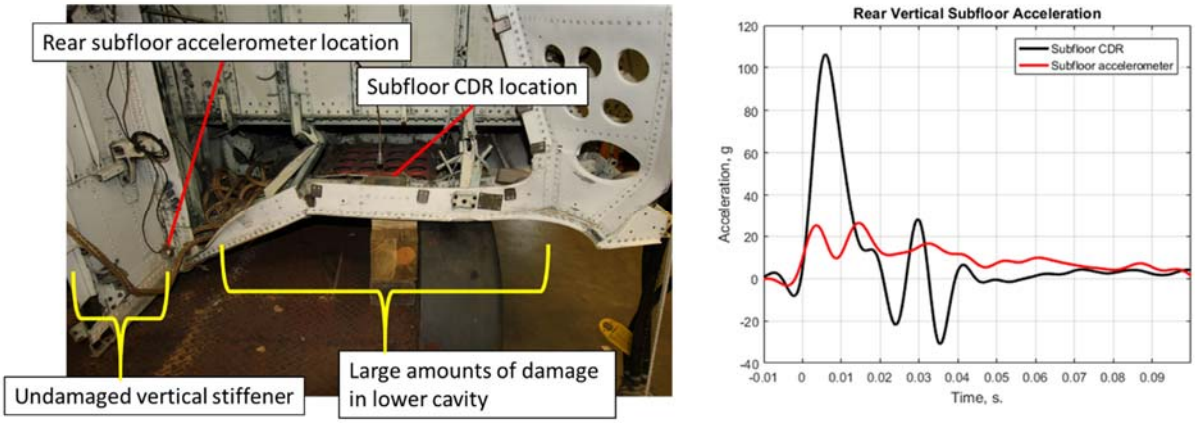

Figure 57 - Wingbox Section aft lower sensor locations (left) and acceleration results (right)

The filtered CDR data showed a triangular shaped pulse with a peak acceleration of approximately 106 g and duration of approximately 0.021 s, if using the first data point for which the acceleration trace crossed the zero-g mark after maximum. In contrast, the subfloor accelerometer located on the vertical stiffener produced accelerations that more closely matched the results from the airframe floor accelerometers. The vertical stiffener remained undamaged during the impact, but produced the deepest soil crater where penetration occurred, shown in Figure 56, in a controlled manner throughout the initial rotation, front impact, and through ATD max sink. The soil penetration, along with the rotation, limited the peak magnitude of 26.0 g, with a duration of 0.100 s.

Figure 58 shows an image series of the aft lower cavity crushing illustrating the differences in deformation at the two locations where the sensors were mounted. Note that the horizontal lines in the images were artifacts of the camera sensor not related to the test, test setup, or results, and ignored when interpreting the images.

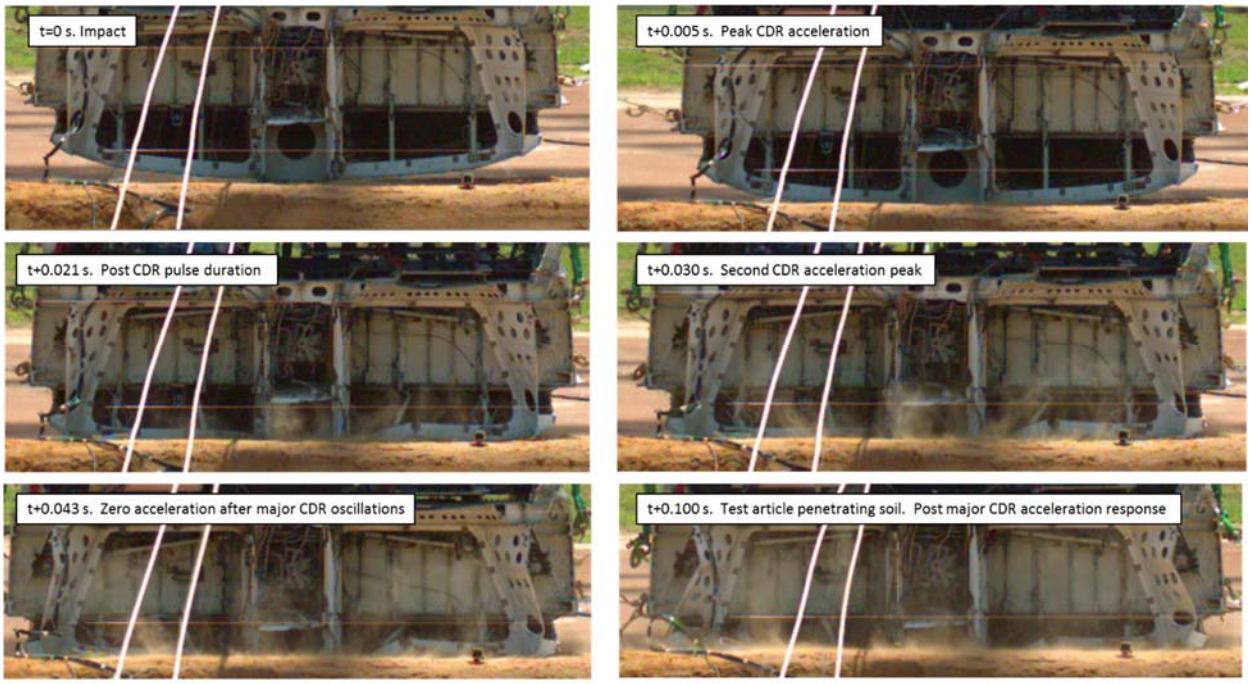

Figure 58 - Aft lower cavity deformation image series

The initial contact between the aft portion of the test article and the soil surface is shown in the upper left image in Figure 58. The peak CDR acceleration, shown in the upper right, was 106 g and occurred 0.005 s after initial contact. Between impact and this time, there was not any noticeable deformation in the lower cavity occurring. The impact shape and magnitude of the acceleration response were a result of contact between the bottom skin's large surface area and soil. It was only after the 106-g peak that the lower cavity deformation initiated. The CDR pulse shape crossed the first zero-g mark at 0.021 s, shown in the middle left image, and after 0.021 s the lower cavity deformation continued to occur. The oscillation in the CDR data was from the flexing of the panel where the CDR was mounted during the failure of the lower cavity, shown in the middle right and lower left images. After 0.100 s, the major acceleration pulses for both the data logger and the accelerometer on the vertical stiffener have concluded.

Local horizontal accelerations for the sensors mounted at the floor level of the Wingbox Section are next plotted in Figure 59 for the starboard side and Figure 60 for the port side.

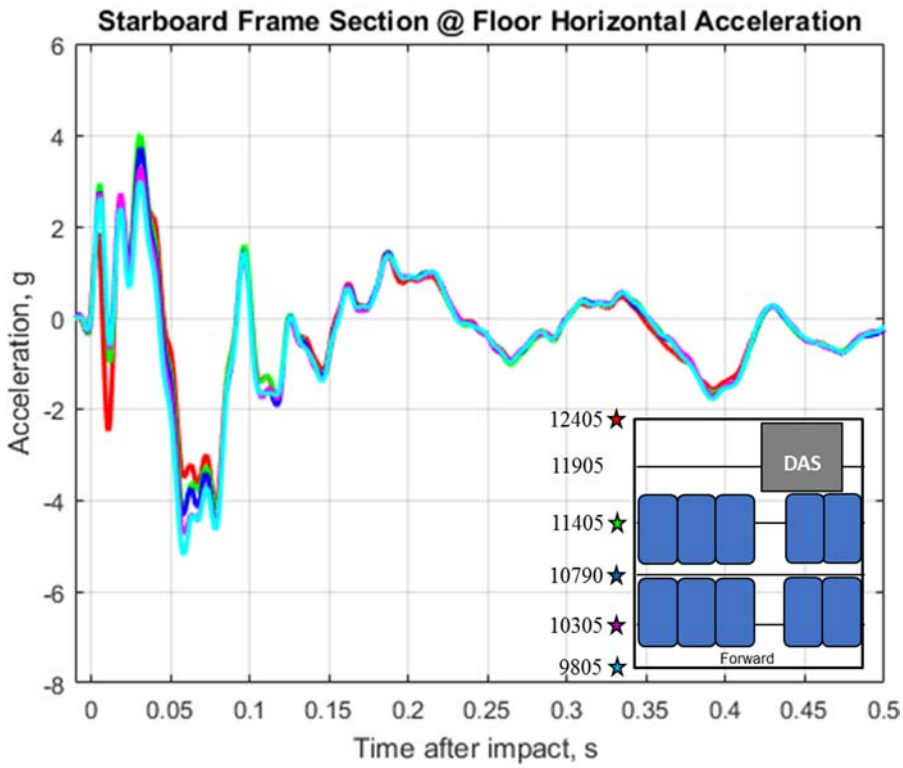

Figure 59 - Starboard floor / frame horizontal accelerations from Wingbox Section

Horizontal acceleration results obtained from all accelerometers closely matched each other throughout most of the impact event, with minor differences in some of the initial peak (both positive and negative) values that occurred before 0.100 s. Positive acceleration peaks of 4.0 g occurred at FS 11405 during the test article rotation up until initial forward impact, which occurred at 0.046 s. After forward impact, the acceleration reached negative values which ranged between 4.1 g at FS 12405 to 5.2 g on at FS 9805 approximately 0.058 s after impact. The large negative accelerations were a result of the restriction of further fuselage tip over due to the interaction with the soil impact surface immediately after the initial rotation. The rebound of the fuselage occurred between 0.073 s and 0.244 s after impact, corresponding to positive acceleration recorded by the accelerometers at all locations toward a maximum of approximately 1.4 g at 0.192 s after impact, which was in the middle of the rebound event. The horizontal accelerations reached a value of 1.7 g at 0.393 s, approximately when the second impact occurred. After the second impact, there were no additional notable acceleration events. The horizontal accelerations on the port side of the fuselage were next examined, and are shown in Figure 60.

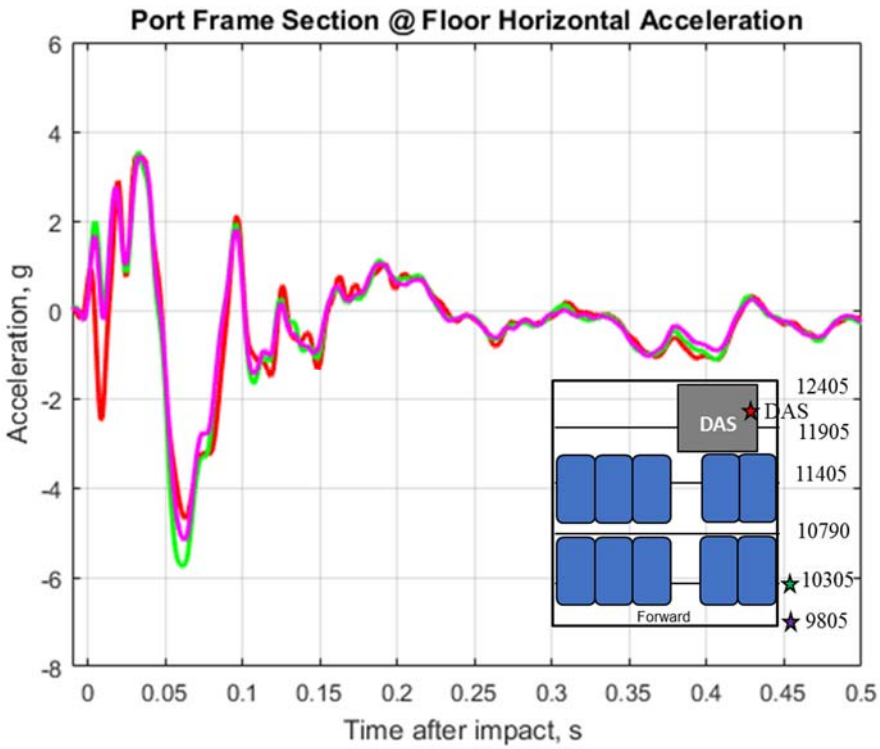

Figure 60 - Port floor / frame horizontal accelerations from Wingbox Section

The accelerometer at FS 11405 did not function during the test, so an accelerometer on the DAS plate, near FS 12405, was used in its place. Acceleration traces for all accelerometers closely matched throughout the impact event, with minor differences in the negative peaks occurring at 0.064 s. Positive acceleration peaks of 3.5 g occurred during the test article rotation up until initial forward impact at 0.046 s. The acceleration traces went negative, reaching between -4.7 g on the DAS plate to -5.7 g on FS 10305 until they crossed the zero-g mark again at 0.084 s after initial impact. The general shapes of the acceleration curves were similar to the accelerations measured on the starboard side of the fuselage, and were caused by the same factors acting on the starboard side. The rebound of the fuselage occurred between 0.073 s and 0.244 s after impact, and this rebound caused positive accelerations measured by all accelerometers, with almost identical response traces. After a localized maximum at 0.118 s, there were no other significant events recorded by the port side accelerometers.

The starboard vertical accelerations at the floor / frame junctions are shown in Figure 61. In general, the pulses were trapezoidal shaped, having a total duration of approximately 0.100 to 0.120 s, and an average plateau value of between 9.8 g and 12.2 g for times between 0.02 s and 0.05 s after impact. An initial peak occurred at approximately 0.008 s after initial test article / soil contact. The peak values were greatest at the aft of the test article and decayed as the location moved toward the front. The highest peak of approximately 39.0 g occurred at FS 12405, which was followed by a peak of 26.3 g at FS 11405. The accelerations decayed with no discernable peaks exhibited after 0.08 s after impact.

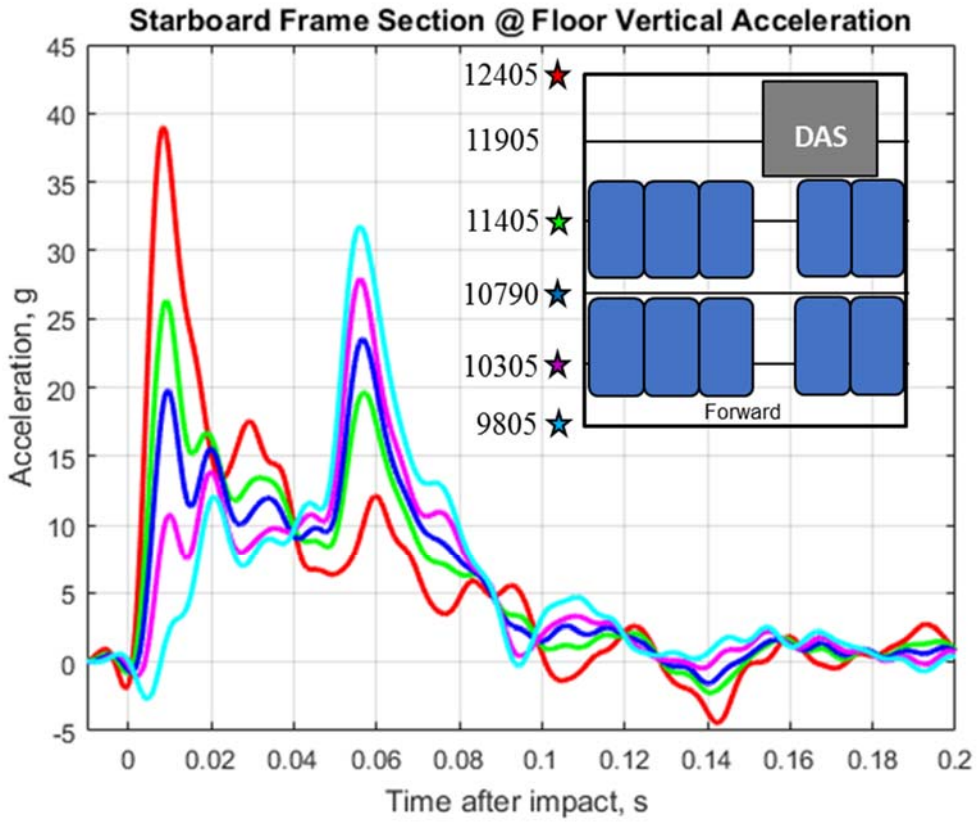

Figure 61 - Starboard floor / frame vertical accelerations from Wingbox Section

The second peak occurred approximately 0.055 s after impact, which was shortly after the time the forward portion of the test article made contact with the soil surface due to the rotation of the test article at impact. In contrast to the trend observed in the initial peak values for the response, the greatest magnitude in the second peak occurred in locations at the front of the test article. Specifically, the highest magnitude peak occurred at FS 9805, which exhibited an acceleration magnitude of approximately 31.7 g, and decreased rearward until a peak of only 12.1 g was observed at FS 12405. The acceleration data on the port side of the airframe were next examined, and plotted in Figure 62.

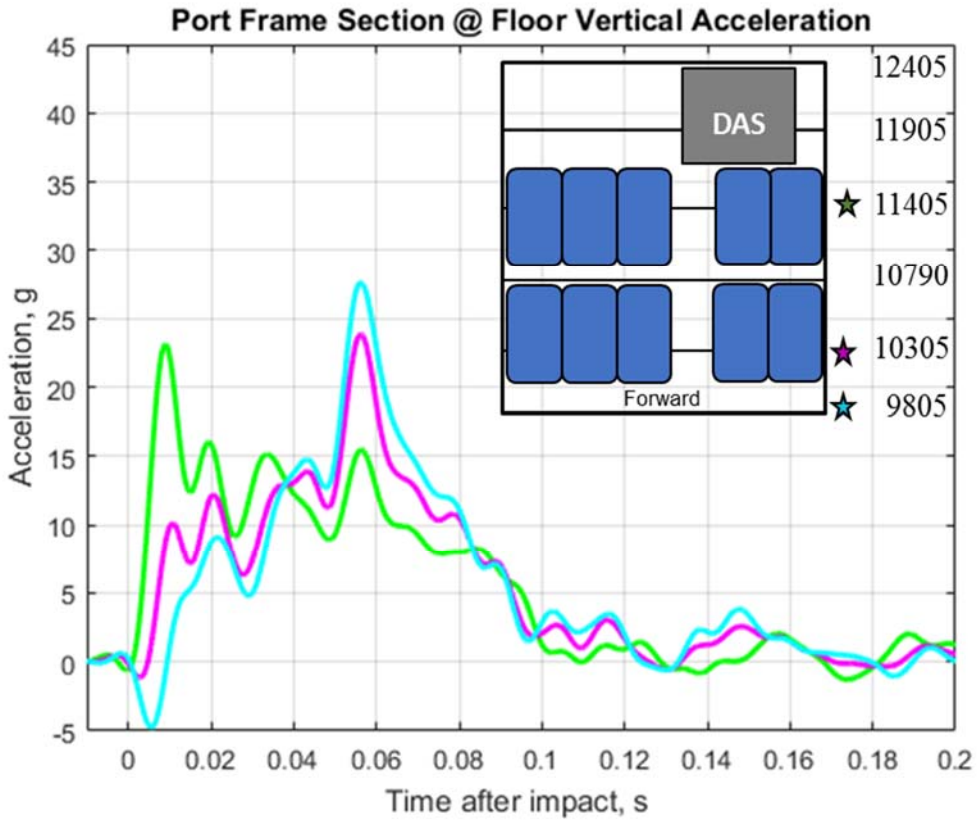

Figure 62 - Port floor / frame accelerations from Wingbox Section

Although the port side of the Wingbox Section was not as heavily instrumented as the starboard side, the data collected from the instrumented locations closely mimicked the response from the starboard side. The acceleration data obtained from FS 11405 showed an initial peak occurring at the beginning of the response, with a peak value of 23.1 g occurring at 0.009 s after initial contact. This value was close to the 26.3 g peak recorded on the starboard side at this location. Similar to the starboard data, both FS 10305 and FS 9805 did not show an initial peak at the beginning of the response. The peak acceleration at these locations occurred at the end of the response, similar to the starboard side behavior. Peak values of 27.6 g, 23.8 g, and 15.5 g were measured for FS 9805, FS 10305, and FS 11405 respectively, which occurred at 0.060 s after impact. These values corresponded to values of 31.7 g, 27.8 g, and 19.7 g at the same locations on the starboard side. The average values computed between 0.020 s and 0.05 s after impact were 12.0 g, 11.0 g, and 10.4 g at FS 11405, FS 10305, and FS 9805, respectively. These values were similar to the values obtained on the starboard side. The overall response at the floor locations for both the starboard and port sides were in general agreement, with only slightly higher peak acceleration values occurring at the end of the response on the port side. The acceleration results at the seat bases were next examined. The rear row vertical seat acceleration is first plotted in Figure 63.

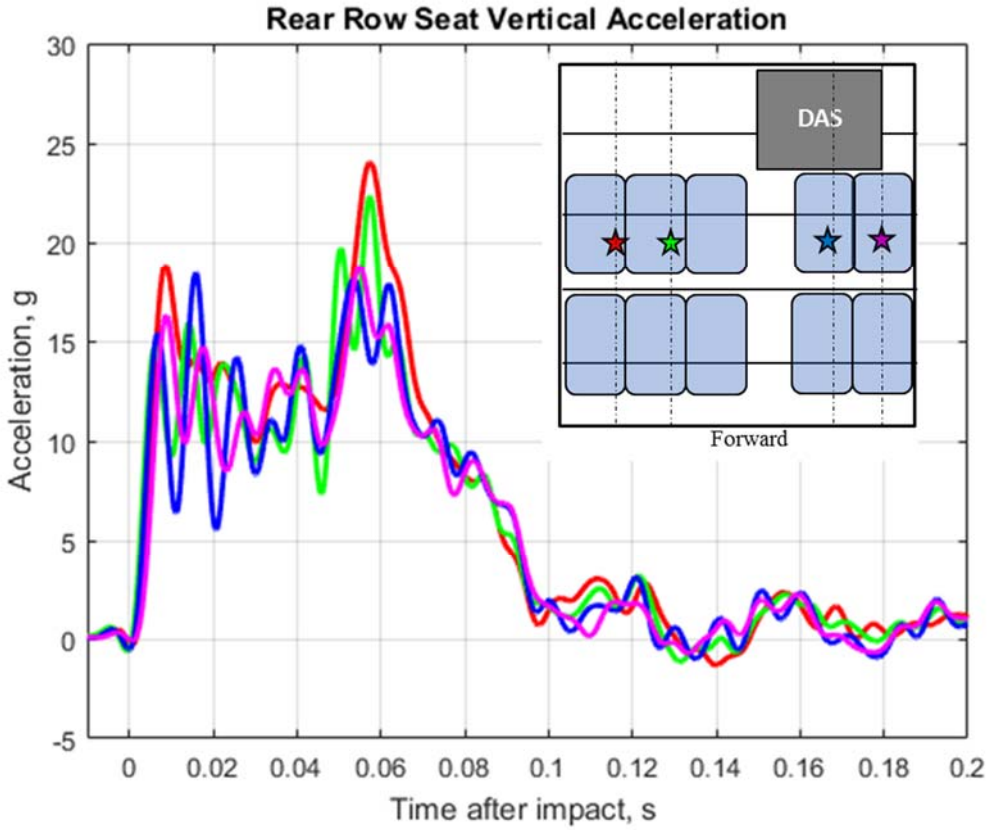

Figure 63 - Rear row seat vertical accelerations from Wingbox Section

All of the rear row seat leg accelerations exhibited a trapezoidal shaped pulse response. A small initial peak appeared at the beginning of the response with a well defined peak at the end. For the triple outer measurement location, the peak at the end of the response reached a value of 24.1 g, which was the highest for all locations measured. If assuming a trapezoidal shaped response, accelerations averaged between 0.010 and 0.046 s were 11.5 g, 12.8 g, 11.2 g, and 11.8 g for the triple outer, triple inner, double inner and double outer seat leg base locations, respectively. The response duration was approximately 0.097 s for all locations measured. The front row vertical seat acceleration data are next plotted in Figure 64.

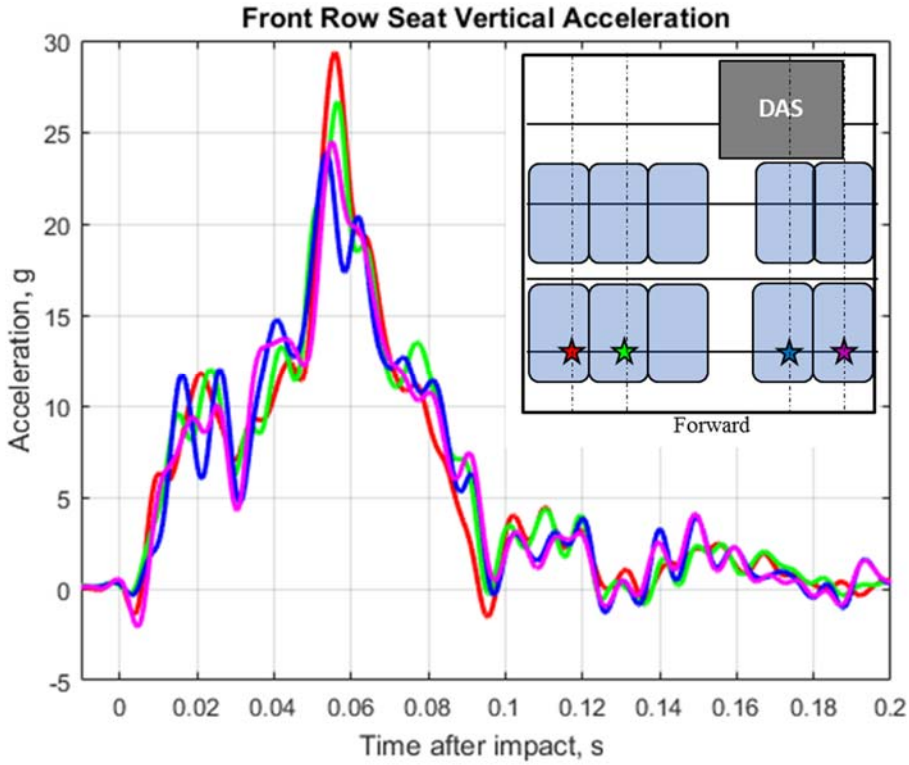

Figure 64 - Front row seat vertical accelerations from Wingbox Section

The seat leg vertical acceleration responses for the front row of seats did not exhibit the same response as the rear row. The four seat leg locations exhibited nearly uniform responses, with the only major difference being their peak accelerations at 0.055 s after impact. The acceleration data ranged between 23.8 g on the double inboard seat leg, to 29.3 g on the triple outboard seat leg. Since these seats were located approximately over FS 10305, the timing in which the peak occurred was in general agreement with the timing of the floor / frame acceleration data at FS 10305. The duration of all responses was approximately 0.095 s, which was in general agreement with the rear row results.

The horizontal accelerations from the rear seat location are next shown in Figure 65. The general trend matched the trend in the floor / frame horizontal acceleration data, as shown in Figure 59 and Figure 60. There was an initial oscillation that occurred for the first 0.02 s after impact, leading to an initial peak of 4.6 g from the port side outboard seat base accelerometer, in blue. A minimum acceleration of 6.5 g was recorded on the port side outboard accelerometer. Note that the port side inboard seat base accelerometer measured the maximum positive acceleration, which occurred at 0.032 s after impact, while the port side outboard seat base accelerometer measured the maximum negative acceleration that occurred at 0.064 s after impact. All four responses followed the same shape, and differences in the maximum negative accelerations were in the range of 2-3 g. This did not affect the overall response significantly since the total magnitude of the response was less than 8 g, which is depicted in the limits of the chart. The results suggested minor differences between the side of the section and the middle. Other than slight differences in maximum values, the acceleration curves generally matched both in magnitude and shape.

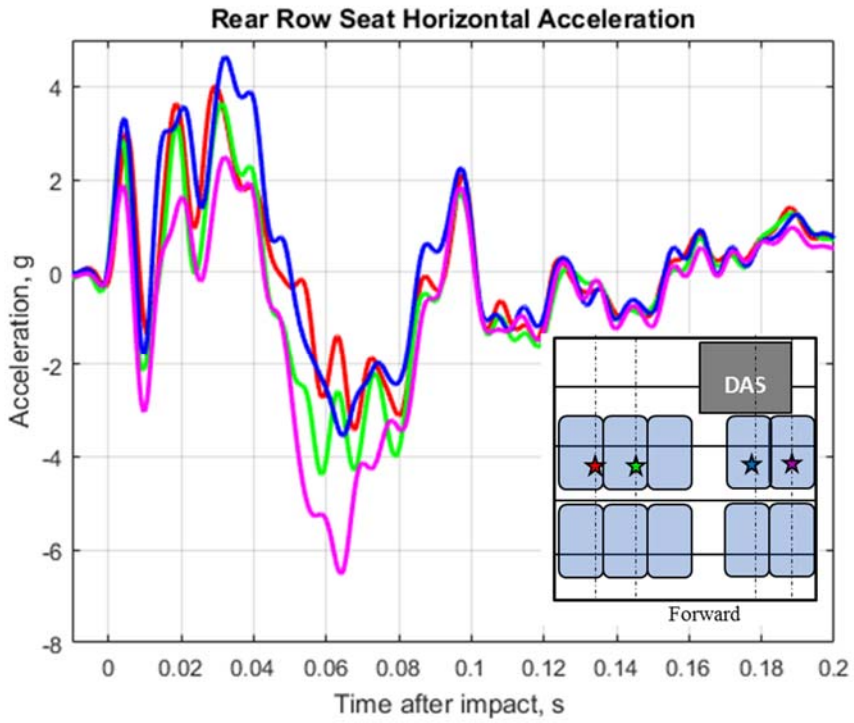

Figure 65 - Rear row seat horizontal accelerations from Wingbox Section

As shown in Figure 66, the horizontal accelerations recorded in the forward seats matched the trends seen both in the rear seats and also in the floor / frame accelerations. An initial oscillation was present for the first 0.030 s after impact. A maximum of 3.6 g occurred at 0.031 s after impact in the triple outboard accelerometer location; however, the responses were similar for all locations at this time. All accelerations then trended negative, leading to maximum negative accelerations of 5.8 g and 5.9 g at the double outer and inner seat leg locations. The triple side accelerations measured maximums of 4.7 g. These accelerations were both less than those on the double side, but also a slightly different shape resembling a trapezoid between 0.04 s and 0.10 s. Other than the noted differences, the acceleration curves generally matched both in magnitude and shape.

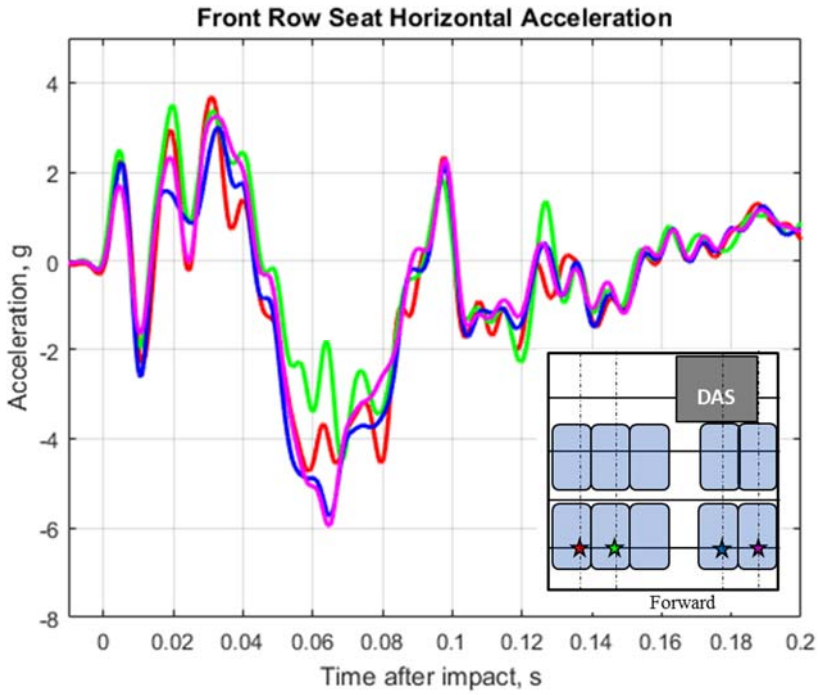

Figure 66 - Front row seat horizontal accelerations from Wingbox Section

The results from the CDRs on the floor were next examined. The acquired CDR data were compared with measurements obtained from an adjacent accelerometer similar to what was examined in the Forward Section. However, unlike the Forward Section test, the brown CDR did not trigger and did not collect impact data. This faulty triggering was caused by the sensor's threshold trigger limit being set too high by mistake, and was noted for future testing. However, data was obtained from the blue CDR and is presented in Figure 67, which shows both the horizontal and vertical direction results.

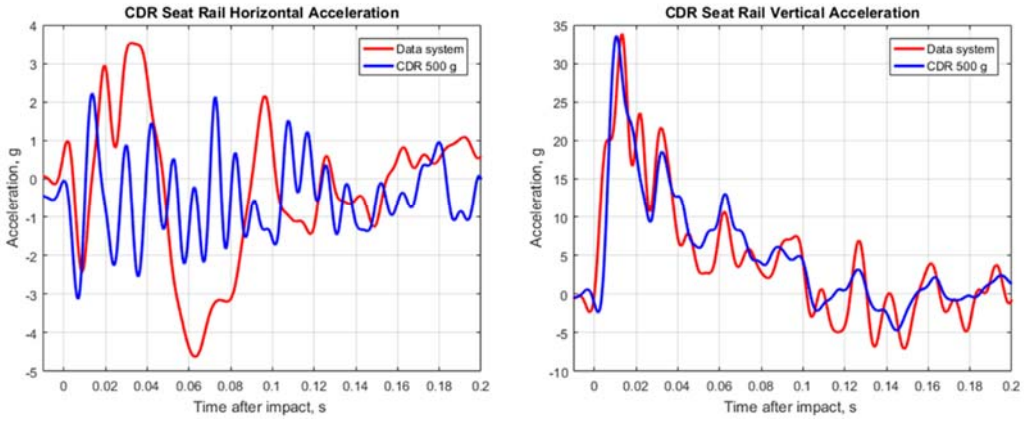

Figure 67 - CDR seat rail acceleration for Wingbox Section test. Forward direction (left) and vertical direction (right)

The results from the CDRs showed good agreement in the vertical direction and less than ideal agreement in the forward direction. In the forward direction, both curves exhibited initial negative peak values immediately after impact that were similar in magnitude and time. The DAS acceleration measured 2.4 g and the CDR measured 3.1 g. After the initial spike, the curves deviated. The data system measured positive acceleration between 0.014 s and 0.048 s reaching a second negative peak of 4.6 g. In contrast, the CDR showed oscillations with no defined curve shape. However, in the vertical direction, the two measurements matched well. In the vertical direction, both the CDR and data system show peaks at 0.013 s after impact, which ranged between 33.6 g on the CDR and 33.8 g for the data system. As with the Forward Section test, the CDRs were not synchronized to the data system or cameras, so a manual time shift was implemented, in this case using the peak value timing information as reference. After the initial peak, both of the vertical measurements decayed toward the zero-g mark, and crossed it at 0.101 s for the data system and 0.104 s for CDR. The difference of only 0.003 s is remarkable.

The hat rack bin ballast results displayed the same trends as the floor level accelerations, and are shown in Figure 68. The aft-most attachment location at FS 11405 measured an initial peak of 28.5 g, and then settled into an average acceleration of 12.1 g when the data were averaged between 0.020 s and 0.060 s after impact. In contrast, the forward-most attachment location at FS 10305 exhibited a peak of 30.3 g near the end of the plateau region of the response. However, averaged data over the same 0.020 s and 0.060 s plateau region gave a response of 12.6 g.

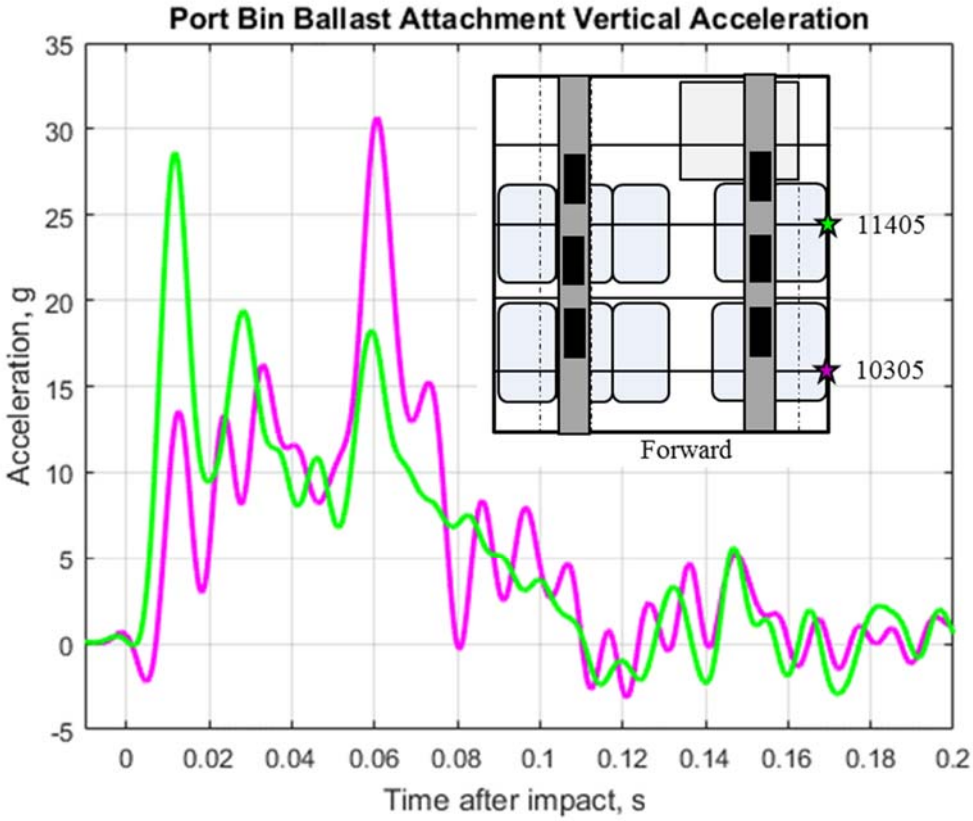

Figure 68 - Overhead bin attachment location vertical accelerations

As Figure 69 shows, accelerations recorded on the hat rack bin ballast mass were of higher magnitude than either the bin attachment or floor accelerations. They also did not exhibit a trapezoidal pulse, but an oscillatory response of between 26.6 and 27.2 Hz for all instrumented ballast locations on both the port and starboard sides centered about zero g. The oscillations were a result of the ballast masses and c-channels swaying at the end of the cantilever attachment arms post impact. The accelerations also followed the general trend seen in other portions of the data, in which aft locations show an initial peak due to aft ground contact, while the forward locations show the peak after forward ground contact. The magnitudes for the peaks were 45.9 g for the FS 11405 location, and 47.3 g for the FS 10305 location. Finally, the oscillation frequency in the ballast mass was approximately 2.5 times higher than the Forward Section oscillation frequency. From a structural standpoint, the higher frequency would indicate a stiffer response at impact.

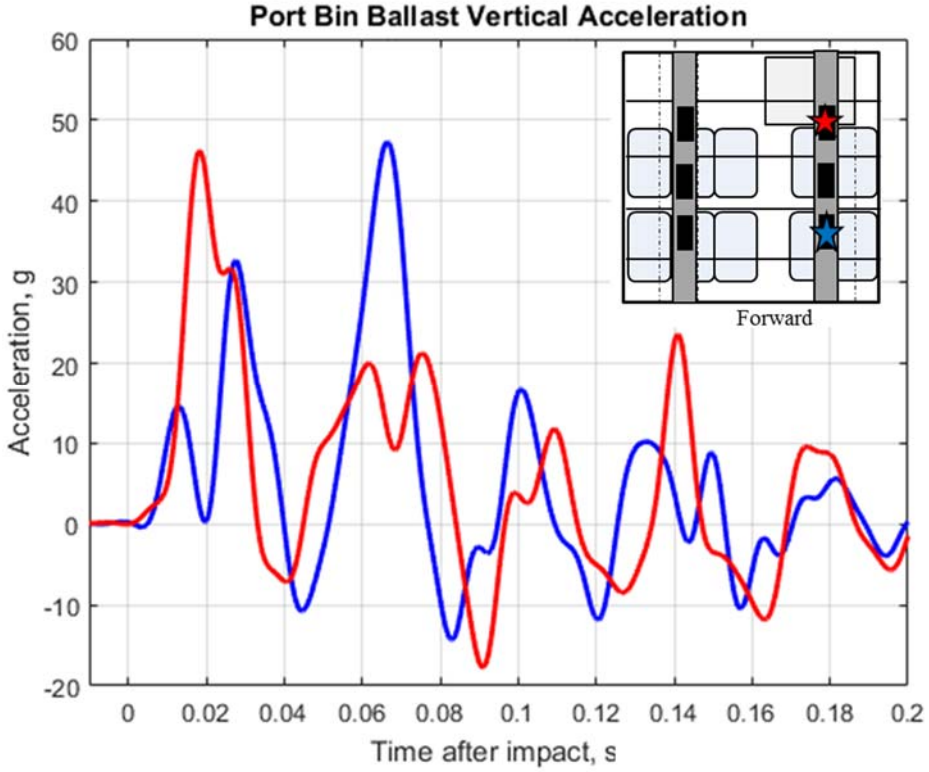

Figure 69 - Port side bin ballast accelerations from Wingbox Section

ATD data were next examined. Nine of the ATDs were seated upright with their hands on their knees, in an identical position to that of the Forward Section test. ATD 3 was unique in that it was positioned in the "brace" position, configured by leaning its chest forward, and positioning its head such that it was nearly touching the seat #8 seat back. Its arms were down at its side resting below its knees with the hands located near its shins. Figure 70 shows a view of ATD 3, positioned in the brace position, just prior to impact.

Figure 70 - ATD 3 in the brace position

On overhead view of the post-test configuration for the ATDs is shown in Figure 71. ATDs 1, 4, 6, 7 and 9 all appeared to be leaning directly forward. ATD 3 appeared to be in the same position as prior to the test. ATDs 5 and 10 were leaning both backward and sideways, toward the window, in a similar position that was observed for the Forward Section test. Finally, ATD 8 appeared to be leaning purely sideways, into the aisle.

Figure 71 - Wingbox Section post-test ATD positions

After capturing the post-test ATD positioning, the ATD data were examined and the probability of injury was determined. The first occupant data examined were the ATD lumbar loads. Figure 72 shows the time histories on the left, and the peak values on the right.

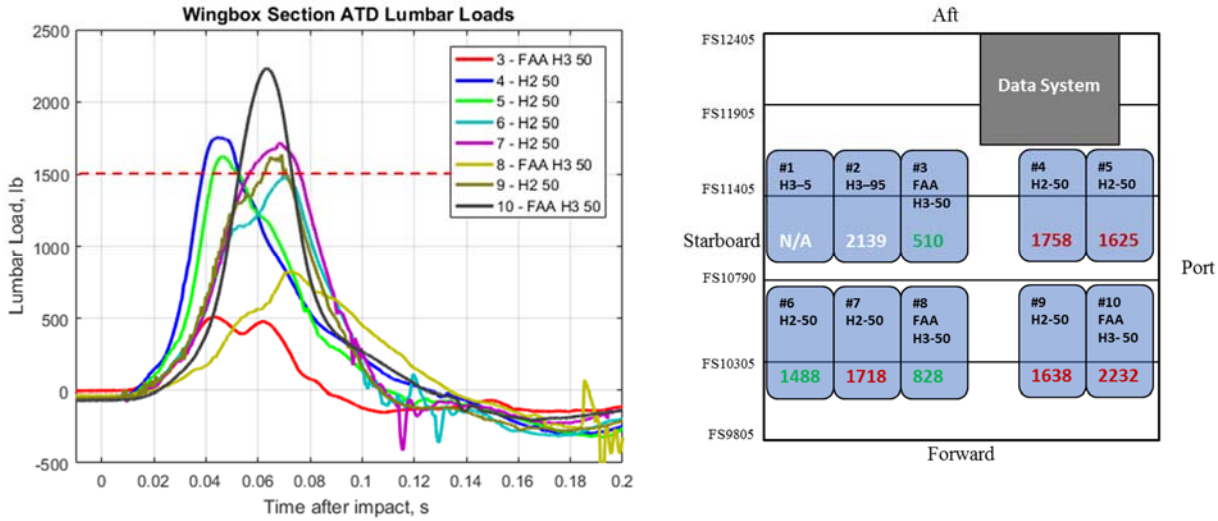

Figure 72 - Wingbox Section ATD lumbar load time history (left) and highlighted peak values (right)

The Wingbox Section test resulted in higher lumbar loads for 6 of the ATDs as compared to the Forward Section test. The exceptions were ATDs 3 and 8, which were seated in the cantilever seats on the triple side. However, in addition to being seated in the cantilever seat, ATD 3 was positioned in the brace position and not directly upright. Both resultant peak load and the overall pulse shape in this ATD were much less than the other ATDs because of this positioning change. ATD 8 saw a lumbar load approximately 300 lb less than in the Forward Section test due its location in the cantilever seat only. The lower lumbar value result for ATD 8 was caused by additional deformation of the seat itself, since the specific accelerations were actually higher in the seat leg in this test. Finally, the results from non-standard sized ATDs are shown in Figure 72, right. The 95th percentile ATD seated in seat 2 showed a significant increase in load in the Wingbox Section test, however data were not collected for the 5th percentile ATD seated in seat 1.

Head vertical accelerations were next examined for the determination of head injury. The ATDs seated in the rear row are plotted on the left and the ATDs seated in the front row are plotted on the right and are shown in Figure 73.

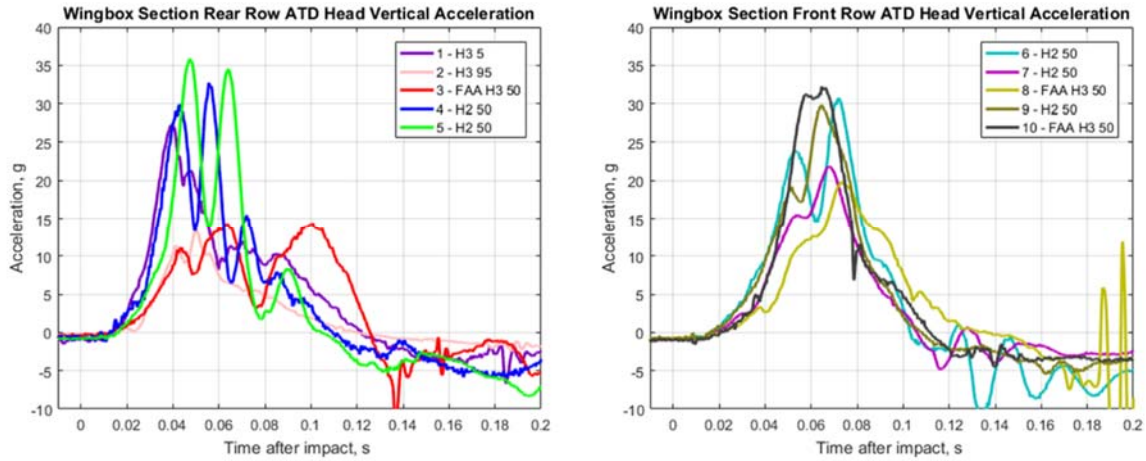

Figure 73 - Wingbox Section ATD head vertical acceleration. Rear row (left) and front row (right)

The head accelerations in the rear row exhibited two distinct types of responses. The first, which occurred in ATDs 1, 4 and 5, consisted of a higher acceleration onset rate, with a higher initial peak occurring earlier than for ATDs 2 and 3. ATDs 1, 4, and 5 had peak acceleration values of 27.3 g, 32.7 g and 35.9 g, respectively. ATDs 2 and 3 exhibited a much slower acceleration onset rate with much lower peak value of acceleration. ATD 2 exhibited a peak value of 13.3 g, while ATD 3 exhibited a peak value of 14.2 g. The response for ATD 3 was explained by the difference in the brace positioning of that ATD, but the response from ATD 2 is at this time unexplained.

For the rear row, the results are similar between all the seats. The onset rate of all accelerations were similar with the exception of ATD 8. ATD 8 experienced the slowest onset rate and the lowest peak acceleration value of 19.7 g. The other ATDs measured peak acceleration values of 30.7 g, 21.9 g, 29.8 g and 32.2 g for 6, 7, 9 and 10, respectively. The horizontal acceleration data were next examined, with results plotted in Figure 74.

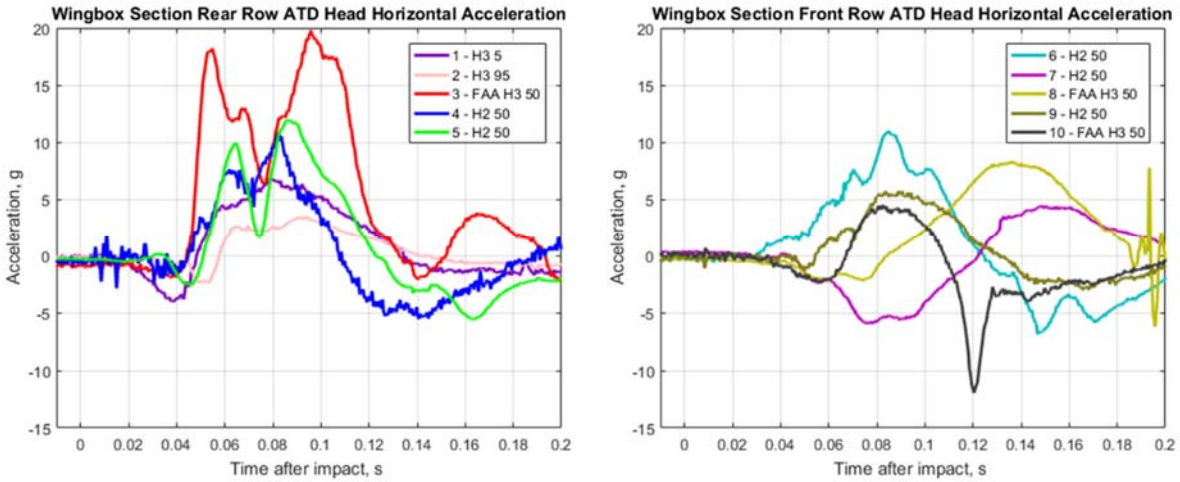

Figure 74 - Wingbox Section ATD head horizontal acceleration. Rear row (left) and front row (right)

The horizontal head accelerations measured by the ATDs varied widely between ATD location, size and type. The most noticeable response was in ATD 3. The response was well above the magnitudes of the accelerations seen in the other ATDs, and again due to the difference in its positioning. In the brace position, its head was oriented mainly in the horizontal direction as opposed to the other ATD heads, which were aligned mainly in the vertical direction. This difference led ATD 3 to measure 19.8 g peak acceleration that occurred 0.096 s after impact. The next highest response was obtained in ATD 5, with a peak acceleration of 11.8 g.

The rear row accelerations for ATDs 3, 4, and 5, which were all 50th percentile ATDs, showed a similar double peak response shape, even though it occurred at different magnitudes. In contrast, the 5th and 95th percentile ATDs showed the lowest acceleration peaks and the longest magnitudes. There was no discernable trend in the responses for the ATDs seated in the front row. Additionally, the response curves for all of the ATDs did not begin until after 0.020 s after impact and didn't end until well after 0.200 s for some of the ATDs located in the front row. The timing offset was indicative that the ATD response lagged that of the airframe.

The head acceleration values were used in the HIC computation, similar to what was done for the Forward Section data. The results of the HIC computation are shown in Table 3.

.

Table 3- Wingbox Section test ATD HIC values

ATD Type - Size	Seat #	HIC Value
H3 – 5	1	48.6*
H3 – 95	2	9.1*
FAA H3 – 50	3	54.4
H2 – 50	4	75.6
H2 – 50	5	107.2
H2 – 50	6	86.9
H2 – 50	7	47.2
FAA H3 – 50	8	32.9
H2 – 50	9	77.9
FAA H3 - 50	10	99.4
*For reference only		

The absence of a high spike in the acceleration time histories indicated that the ATD head did not strike any of the seat back or other surfaces. The low HIC results from ATD 3 were unexpected since the head was resting against the seat 8 seat back, and the expected forward motion would cause a strike into the seat 8 seat back. However, the actual forward motion due to the rotation of the fuselage was not high enough to cause the ATD's head to strike the seat back with any noticeable acceleration. For all seats, all HIC values were well below the established limits, which gave an indication of a low probability of skull fracture.

Finally, pelvic acceleration was examined on each of the ATDs. Figure 75 shows the results from the vertical accelerations both from the rear row ATDs on the left and the front row ATDs on the right.

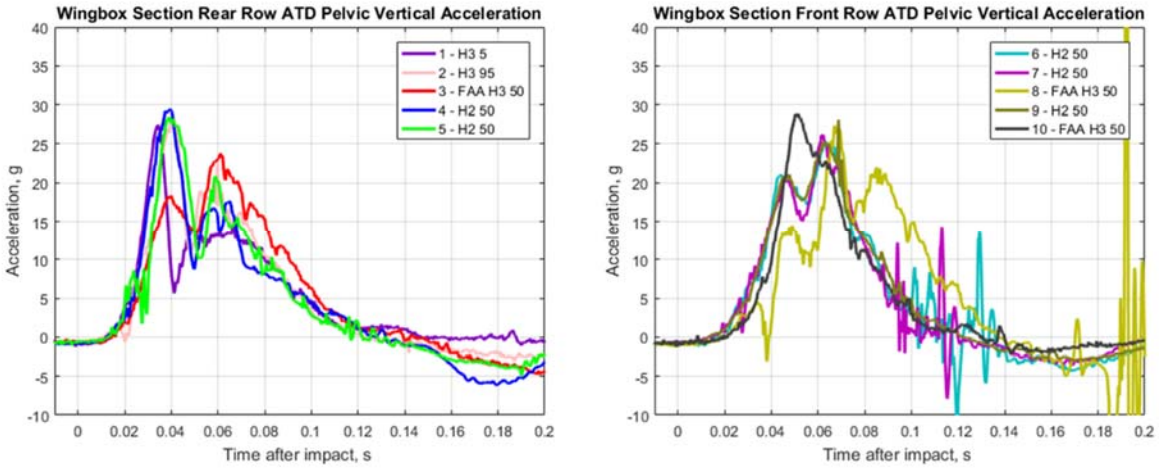

Figure 75 - Wingbox Section ATD pelvic vertical acceleration. Rear row (left) and front row (right)

The pelvic responses were again checked as a backup to the lumbar loading since the accelerometer locations in the pelvis were close to the load cell used for the lumbar load measurement. In the rear row, the responses were all very similar, both in magnitude and in shape for ATDs 1, 2, 4 and 5. ATD 3 exhibited

a different response than the rest, which was expected due to the difference in ATD 3 positioning. The peak pelvic accelerations for ATDs 1, 2, 4, and 5 were 27.4 g, 28.4 g, 29.4 g and 28.3 g, which occurred at 0.034 s, 0.041 s, 0.039 s, and 0.039 s after impact, respectively. ATD 3 measured a peak acceleration of 23.7 g, which occurred at 0.061 s after impact. The general shapes of all of the response curves were similar.

ATDs 6, 7 and 9 also followed similar trends when examining the pelvic vertical acceleration response, while ATDs 8 and 10 showed differences. ATD 10 measured a peak acceleration of 28.8 g, which occurred at 0.051 s after impact, and the ATD 8 measured a peak acceleration of 26.9 g, which occurred 0.067 s after impact. In contrast, the ATDs seated in seats 6, 7 and 9 measured peak accelerations of 25.3 g, 26.1 g, and 25.2 g, which all occurred between 0.062 s and 0.064 s after impact. The horizontal pelvic accelerations measured in the ATDs is shown in Figure 76.

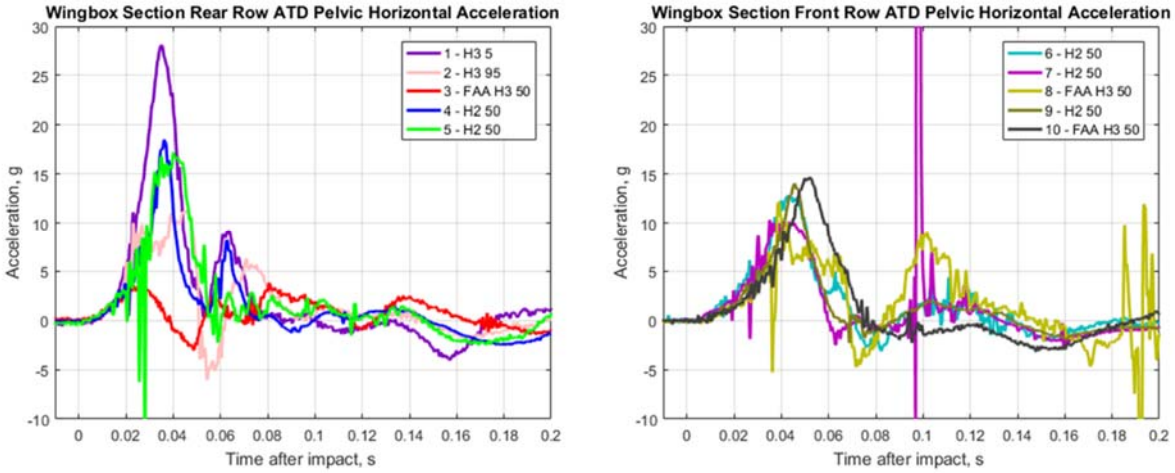

Figure 76 - Wingbox Section ATD pelvic horizontal acceleration. Rear row (left) and front row (right)

The horizontal pelvic responses showed the rear row did not exhibit clear acceleration trends. The 5th sized ATD seated in seat 1 measured the largest acceleration peak of 28.1 g at approximately 0.035 s after impact. The peak could partially be due to the ATD's small size, allowing it to move around in the seat even when fastened into the seat with the seatbelt. The next highest peak accelerations from the rear row ATDs were from seats 4 and 5. ATDs 4 and 5 measured peak acceleration values of 18.5 g and 17.2 g, and generally followed the same post-peak acceleration trend. These results are followed up by the peak acceleration of 11.3 g measured from the 95th sized ATD seated in seat 2. Finally, ATD 3 showed a different response magnitude and shape due to its positioning. This ATD measured a small 3.5 g peak approximately 0.025 s after impact, after which the accelerations reached a maximum negative peak of 3.0 g. It generally hovered around the zero-g mark post-negative peak, with no notable events happening after 0.06 s. The small horizontal accelerations could be due to the lack of horizontal motion the ATD was capable of undergoing, since its head was essentially positioned against the seat back of seat 8, and its pelvis buckled tightly into the seat. There was a possibility that it was wedged into its braced position, unable to move forward or backward during the impact.

In the forward row of seats, the data followed similar trends. The onset rate for all ATDs was similar, and all ATDs reached initial peak values between 0.040 s and 0.055 s after impact. All curves are triangular in

shape with a duration between 0.060 s and 0.080 s. ATD 7 measured a spike at approximately 0.100 s, whose magnitude is 284 g, which is out of the range of Figure 76. The likely cause for this spike was an anomalous electrical signal from the experimental data system used in this ATD. There was no evidence in the video or other test data that the pelvic section in this ATD registered a structural acceleration in this range.

Applicability of Results to Aircraft Crashworthiness Discussion

These two tests were conducted, in part, to collect data for use in the evaluation of transport category aircraft crashworthiness characteristics on two actual aircraft sections. There are numerous metrics that could be used to evaluate crashworthiness of an aircraft, but what is used in this example was borrowed from criteria that have been used in the past for aircraft development. There are four general criteria used when evaluating crashworthiness, and are as follows:

1. Retention of items of mass
2. Maintenance of occupant emergency egress paths
3. Maintenance of acceptable acceleration and loads experienced by the occupants
4. Maintenance of a survivable volume

These metrics have been used to guide aircraft design features for crashworthiness in literature [24-25], and are representative of what a new transport category aircraft crashworthiness rule could entail. One specific criteria used for an aircraft certified by the FAA using a Special Condition (SC) [24] stipulates that crashworthiness must be met on aircraft sections, either through "analysis using validated analytical tools or by direct-test evidence" in conditions of up to 30 ft/s in the vertical direction. Other SCs issued for other new composite aircraft [26] are similar.

Criteria #1 stipulates items such as overhead bins, seats, items in the galley and other items of mass onboard the aircraft must not come loose during an impact. For overhead bins specifically, an attachment failure could lead to a bin detachment, causing a direct strike to an occupant, or the potential of aisle blockage, leading to difficulty in occupant egress. Criterion #2 stipulates the egress paths must be maintained. This criteria relates to mass retention addressed in criteria #1, but also suggests that the floor or floor supporting structures must also remain intact. Criteria #3 addresses the occupant loading levels – specifically limits defined in 14 CFR § 25.562, which are imposed using a 50^{th} percentile Hybrid II (or equivalent) ATD. Criteria #4 addresses the airframe deformation around the occupant with acceptable limits defined such that occupants have the ability for egress.

The four criteria can be addressed using "direct-test evidence" from the data acquired on the two tests conducted. For criteria #1 - In both tests, the overhead items of mass were simulated with aluminum c-channels and ballast, and the attachment fasteners were intentionally oversized to ensure they would not fail. This arrangement means criteria #1 cannot be addressed directly. However, accelerations on the ballast and attachment locations were measured, and a dynamic load factor at the attachment locations is reported. It is hoped that the dynamic load factor provides insight into the actual loading at the attachment locations during a dynamic event, as opposed to an inertial loading conditions like what is stipulated in 14 CFR § 25.561 [27], such that if this were an actual airframe under consideration for certification, the corresponding fasteners and other structure can be sized appropriately. For criteria #2 - The occupant egress

paths can be addressed. The Forward Section showed failures in many of the floor supports; however, it is noted that these floor failures caused the floor panels to bear against the underfloor luggage. Different interpretations can be made whether the egress path was actually maintained, and if this test article were actually undergoing certification, the ultimate decision would be left to the certification expert. In the Wingbox Section, the floor did not fail so the egress path was maintained. In criteria #3, the occupant lumbar loads were exceeded for the majority, but not all, of the ATDs in both tests - with the Wingbox Section results having overall higher values. If using the most conservative case and reporting only the highest loaded ATD as the basis for evaluation, both tests would fail this criterion. However, if a less conservative criteria is used such as the average or the median of the ATD loads, different results can be expected, which could lead to a pass condition depending on interpretation of the data. For criteria #4 – The Forward Section showed 5 inches of maximum dynamic deformation and 1 inch of permanent deformation through the fuselage ovalization, whereas the Wingbox Section produced results that showed negligible deformation. The Wingbox Section definitely passed this criteria, and further evaluations would be necessary to determine whether a maximum of 5 inches of dynamic deformation would intrude into the occupant's survivable volume.

Results obtained using the four criteria are mixed as to whether the sections would exhibit a pass or fail if this aircraft were undergoing actual certification. One consideration needing to be addressed is the size of the F28 sections (and corresponding aircraft) are much smaller than an A350-900 or other wide-body aircraft, and potentially unable to demonstrate adequate crashworthiness at 30 ft/s as stipulated in the referenced SCs. Had the sections been tested at 20 ft/s vertical velocity – representing a reduction of the kinetic impact energy by 44%, all four criteria might have been met. Thus, it is important to propose different limits in the criteria based on aircraft size, weight or other defining factors.

The next item which should be addressed is relative performance of the seats used in these tests. The seats were certified to the most recent FAA guidelines [15], and removed from an in-service aircraft. However, the seats were designed for a different aircraft and modified – mainly in the seat leg spacing – for use in these tests. The modification allowed for the triple aisle seat to be at a large overhang, but potentially out of specification limits for what the seats were originally certified. The low lumbar loads measured in the ATDs seated in the cantilevered triple aisle seats were a result of the large amount of seat support tube deformation that may or may not be representative of the actual certified seat used in the F28.

Additionally, there should be some consideration to determine the applicability for the creation of the double seats used for the port side of the airframes from the modification of a triple seat. There is a difference in weight being supported by the double seats used in the test (approximately 170 lb per 50th percentile ATD for a total of approximately 350 lb) versus what is typically supported by the seats in their unmodified triple configuration - which can be assumed as an additional 170 lb – leading to a 520 lb total weight. If a seat designed for 520 lb of weight is only loaded with 350 lb of weight, the seat design could be too stiff when evaluating the ATD response. However, there is also rationality that suggests triple and double seat designs share common materials and parts, leading to reduced development and certification costs. Taken a step further, the performance of a triple-made-into-a-double seat is identical to the performance of a designed double seat due to the commonality of parts and design. Further conclusions were not made suggesting either viewpoint, with care being taken to ensure that the results for the ATDs seated in the cantilever seats are well documented.

The Wingbox Section test presented an opportunity to configure a test with induced forward motion rather than just repeat a second purely vertical impact condition. The Wingbox Section test article was tipped a small angle forward, which then impacted a sloped surface. The angles were kept relatively small – approximately 2.9 degrees for the test article and 10 degrees for the surface – primarily due to the unknowns of whether the test article would tip over or not. The small chance for a tip over were fully unknown, so precautions were taken and hardware was added to the test article specifically to upright. During the test, the test article experienced a small amount of rotation which briefly induced approximately 9.4 ft/s velocity in the forward direction, but not enough rotation to cause tip over. The forward motion did not significantly affect either the airframe or occupant response. The airframe survived the test with minimal damage, and the ATDs did not show signs of head strike due to the added forward motion. It stands to reason that in order to achieve a noticeable effect in the forward direction, the test article should be tilted to an angle of 20 degrees or more, and if a rotation were to occur at impact, the surface should employ an angle greater than 20 degrees. A 20-degree angle gives a local horizontal velocity of 10.3 ft/s at impact when using a 30 ft/s vertical condition, and the rotation of the test article through the impact would allow for the horizontal velocity to be even higher.

Conclusion

Two tests were conducted on two separate Fokker F28 fuselage sections. The first, named the Forward Section test, was of a forward portion of the F28 fuselage between FS 5305 and FS 7805. There was underfloor space for the addition of 922 lb of luggage, which was added in a loosely stacked four bags wide by four bags deep by three bags high. The test impacted at a nearly zero-degree pitch angle with a impact velocity of 28.9 ft/s. Both tests impacted a bed of soil, and all of the data were successfully collected on the airframe, ATD and CDR sensors. Post-test inspections showed a number of failures in the floor support structure and bottom skin; however, the portion of the fuselage above the floor exhibited little to no deformation. A permanent deformation of approximately 1 inch was observed post-test. The luggage interaction played a large role in the response of the section, with much of the failures of the floor supports caused by a specific bag interaction with the floor structure. The ATDs show mixed results when examining the lumbar loads. Some were above the 1,500 lb limit, while others were below. The two ATDs seated in the overhung seats measured the lowest loads out of all of the ATDs, with the exception of ATD 4, which was affected by the floor failure at its seat base.

A Wingbox Section was used for the second test, which was located between FS 9805 and 12405. This test pitched the test article forward approximately 2.9 degrees onto a 10-degree sloped soil surface. The test article did experience forward motion; however, it was not significant enough to affect the response of the fuselage or the ATDs. The majority of the fuselage deformation occurred in the lower cavity below the wing truss support structure while the rest of the test article appeared to be undamaged. The ATDs measured higher loads than in the Forward Section, which was expected since there was less fuselage deformation. All of the ATDs were over the 1,500 lb limit, with the exception of the ATDs seated in the overhung seats, and ATD 6, which was just slightly under the 1,500 lb limit. The braced positioned ATD 3 showed different response shapes when comparing both its acceleration and lumbar load data with the other ATDs. ATD 10 was consistently on the high end of the responses.

To induce a larger horizontal velocity into the test impact conditions, a larger test article pitch angle onto a larger slope on the impact surface is needed. However, a larger angles pose difficulties in test setup and

conduct due to the additional steps needed to properly zero the measurement sensors, restrain the test article to prevent tip over, and position the ATDs accurately for impact. These hurdles would need to be addressed before such testing could occur.

A series of luggage component tests were conducted to evaluate the luggage response by itself. The luggage showed similar acceleration time histories for both tests conducted using different sets of individual bags at differing impact conditions, which suggested that luggage response is generally consistent and unaffected by bag type, size, or contents to a large degree. Additionally, the data suggest the luggage response can be simulated both physically and computationally using materials having properties that represent either elastic-plastic response, or a linear elastic-constant crush-compaction response. Typically, foams will exhibit the second type of response and an evaluation of various density foams should identify a suitable luggage substitute for future tests.

Three CDRs were used in the tests, both as an evaluation of concept, but also as usable data collection tools. The CDRs used in the luggage from the Forward Section test and in the lower cavity in the Wingbox Section test provided valuable data to quantify the responses at these locations. A second set of CDRs were used as comparisons to the conventional data systems. The results showed very good agreement in the lower ranged CDRs when compared to the ruggedized data systems and give confidence in using the CDRs in tight or otherwise inaccessible spaces not normally available for instrumentation. Since these CDRs are lightweight and portable, they are capable of being used for the collection of these types of data. The only major item learned, as seen in each of the tests, was that the CDR ranges need to be set within the sensor's measurement range, and not within the sensitivity of the sensor.

Finally, a discussion which compares the test data to four crashworthiness metrics is presented. It was not the purpose of the tests and not the purpose of this report to categorize the F28 aircraft as crashworthy. There is applicability; however, in using the data acquired as test cases for an aircraft crashworthiness certification process utilizing the four criteria presented. Results pertaining to each of the four criteria and supporting rationale behind each pass or fail judgement are presented - if a determination could be made. It is hoped that both the data obtained from the tests, along with the lessons learned from the criteria, be used as guides for future work in transport category aircraft crashworthiness.

References

1. Federal Register. Federal Aviation Administration, Aviation Rulemaking Advisory Committee, Transport Airplane and Engine Issues, Vol 80. 2015.

2. Williams, M.S., and Hayduk, R.J. "Vertical Drop Test of a Transport Fuselage Center Section Including the Wheel Wells." NASA-TM-85706. 1983.

3. Fasanella, E.L. and Alfaro-Bou, E. "Vertical Drop Test of a Transport Fuselage Section Located Aft of the Wing." NASA-TM-89025. 1986.

4. Williams, M.S. and Hayduk, R.J. "Vertical Drop Test of a Transport Fuselage Section Located Forward of the Wing." NASA-TM-85679. 1983.

5. Fasanella, E.L., Alfaro-Bou, E. and Hayduk, R.J. "Impact Data from a Transport Aircraft During a Controlled Impact Demonstration." NASA-TP-2589. 1986.

6. Abramowitz, A., Smith, T.G., and Vu, T. "Vertical Drop Test of a Narrow-Body Transport Fuselage Section with a Conformable Auxiliary Fuel Tank Onboard." DOT/FAA/AR-00/56. 2000.

7. Logue, T.V., McGuire, R.J., Reinhardt, J.W., and Vu, T. "Vertical Drop Test of a Narrow-Body Fuselage Section with Overhead Stowage Bins and Auxiliary Fuel Tank System On Board." DOT/FAA/CT-94/116. 1995.

8. Abramowitz, A., Smith, T.G., Vu, T., and Zvanya, J. "Vertical Drop Test of an ATR 42-300 Airplane." DOT/FAA/AR-05/56. 2006.

9. McGuire, R.J., Nissley, W.J., and Newcomb, J.E. "Vertical Drop Test of a Metro III Aircraft." DOT/FAA/CT-93/1. 1993.

10. McGuire, R.J., and Vu, T. "Vertical Drop Test of a Beechcraft 1900C Airliner." DOT/FAA/AR-96/119. 1998.

11. Abramowitz, A., Ingraham, P.A., and McGuire, R.J. "Vertical Drop Test of a Shorts 3-30 Airplane." DOT/FAA/AR-99/87. 1999.

12. Annett, M.S., Littell, J.D., Jackson, K.E., Bark, L.W., DeWeese, R. L., McEntire, B.J., "Evaluation of the First Transport Rotorcraft Airframe Crash Testbed (TRACT 1) Full-Scale Crash Test." NASA-TM-2014-218543. 2014.

13. Littell, J.D. "Crash Tests of Three Cessna 172 Aircraft at NASA Langley Research Center's Landing and Impact Research Facility." NASA-TM-2015-218987. November 2015.

14. Kellas, S., and Jackson, K.E. "Multi-Terrain Vertical Drop Tests of a Composite Fuselage Section." Proceedings from the American Helicopter Society 64th Annual Forum. April 29 – May 1, 2008. Montreal, Canada.

15. Federal Aviation Administration. "Emergency Landing Dynamic Conditions." 14 CFR § 25.562. Amended May 17, 1998.

16. Fokker. "Fokker Fellowship F28 Weight and Balance Manual." Revised January 1, 1999.

17. Gowdy, V., DeWeese, R., Beebe, M., Wade, B., Duncan, J., Kelly, R., and Blaker, J. "A Lumbar Spine Modification to the Hybrid III ATD For Aircraft Seat Tests." SAE TP 1999-01-1609. General, Corporate, and Regional Aviation Meeting and Exposition. Wichita KS. April 20-22, 1999.

18. Society of Automotive Engineering. "J322-1 Instrumentation for Impact Test – Part 1 – Electronic Instrumentation." SAE international, 400 Commonwealth Drive, Warrendale, PA. 1995.

19. Littell, J.D. “Experimental Photogrammetric Techniques used on Five Full-Scale Aircraft Crash Tests.” NASA-TM-2016-219168. 2016.

20. Thomas, M.A., Chitty, D.E., Gildea, M.L., T’Kint, C.M. “Constitute Soil Properties for Unwashed Sand and Kennedy Space Center.” NASA CR-2008-215334. 2008.

21. American Society of Testing and Materials. “Standard Test Method for California Bearing Ratio (CBR) of Laboratory-Compacted Soils.” ASTM D1883. ASTM International, West Conshohocken, PA. 2016.

22. U.S Dept. of Transportation. “Occupant Crash Protection.” Federal Motor Vehicle Safety Standard No. 208.

23. Schmitt, K.-U., Niederer, P. and Walz, F. “Trauma Biomechanics: Introduction to Accidental Injury.” Verlag Berlin Heildelberg New York: Springer, 2004.

24. Federal Register. “Special Conditions: Airbus A350-900 Airplane; Crashworthiness, Emergency Landing Conditions.” Vol 79. No. 143. Friday July 25, 2014.

25. U.S. Army Aviation Systems Command. “Aeronautical Design Standard. Rotary Wing Aircraft Crash Resistance.” ADS-36. May 1, 1987.

26. Federal Register. “Special Conditions: Boeing 787-8 Airplane; Crashworthiness.” Vol 72. No. 186. Wednesday, September 26, 2007.

27. Federal Aviation Administration. “Emergency Landing Conditions: General.” 14 CFR § 25.561. Amended July 29, 1997.

REPORT DOCUMENTATION PAGE

Form Approved
OMB No. 0704-0188

1. REPORT DATE *(DD-MM-YYYY)*	2. REPORT TYPE	3. DATES COVERED *(From - To)*
1-05-2018	Technical Memorandum	

4.

A Summary of Results from Two Full-Scale Fokker F28 Fuselage Section Drop Tests

5a. CONTRACT NUMBER

5b. GRANT NUMBER

5c. PROGRAM ELEMENT NUMBER

6. AUTHOR(S)

Littell, Justin D.

5d. PROJECT NUMBER

5e. TASK NUMBER

5f. WORK UNIT NUMBER

664817.02.07.03.03

7. PERFORMING ORGANIZATION NAME(S) AND ADDRESS(ES)

NASA Langley Research Center
Hampton, VA 23681-2199

8. PERFORMING ORGANIZATION REPORT NUMBER

L-20916

9. SPONSORING/MONITORING AGENCY NAME(S) AND ADDRESS(ES)

National Aeronautics and Space Administration
Washington, DC 20546-0001

10. SPONSOR/MONITOR'S ACRONYM(S)

NASA

11. SPONSOR/MONITOR'S REPORT NUMBER(S)

NASA-TM-2018-219829

12. DISTRIBUTION/AVAILABILITY STATEMENT

Unclassified
Subject Category 39
Availability: NASA STI Program (757) 864-9658

13. SUPPLEMENTARY NOTES

14. ABSTRACT

During 2017, two vertical drop tests were conducted on two partial sections removed from a Fokker F28 MK4000 aircraft as a part of a joint NASA / Federal Aviation Administration (FAA) effort to investigate the crashworthiness characteristics of Transport Category Aircraft, as defined by 14 Code of Federal Regulations, Part 25. The first test was a pure vertical drop test of a relatively uniform forward section, which included an underfloor area for luggage. The second test was a canted drop test onto a sloped surface of a portion of the fuselage representing the wingbox stiffened structure. Instrumentation consisting of accelerometers was installed to measure floor, seat track, luggage, and overhead bin responses in the two airframe sections. In addition, ten Anthropomorphic Test Devices (ATDs, a.k.a. crash test dummies) were included in each test to measure the potential of onboard occupant injury. Self-contained data recorders logging accelerations and rotational rates were also used on the seat tracks and lower structure as evaluations for crash recording devices in potential future tests. Finally, the starboard side of each section was painted with a stochastic black and white speckle pattern for use in full field photogrammetric imaging techniques.

15. SUBJECT TERMS

Impact Testing; airplane testing; full scale crash testing; safety

16. SECURITY CLASSIFICATION OF:			17. LIMITATION OF ABSTRACT	18. NUMBER OF PAGES	19a. NAME OF RESPONSIBLE PERSON
a. REPORT	b. ABSTRACT	c. THIS PAGE			STI Help Desk (email: help@sti.nasa.gov)
U	U	U	UU	80	19b. TELEPHONE NUMBER *(Include area code)* (757) 864-9658